A Fiber-Based Approach for Modeling Beam-Columns under Fire Loading

Ann E. Jeffers

Dissertation submitted to the Faculty of the
Virginia Polytechnic Institute and State University
in partial fulfillment of the requirements for the degree of

Doctor of Philosophy
in
Civil Engineering

APPROVED BY:

Elisa D. Sotelino, Chair
W. Samuel Easterling
Brian Y. Lattimer
Raymond H. Plaut
Amit H. Varma

June 19, 2009
Blacksburg, VA

Keywords: Fire, Steel, Beam-Columns, Finite Element Method, Structural Analysis, Heat Transfer

A Fiber-Based Approach for Modeling Beam-Columns under Fire Loading

Ann E. Jeffers

Abstract

The work described herein emphasizes a new fiber-based approach to modeling the response of structural frames subjected to realistic fire conditions. The proposed approach involves the development and validation of two finite elements that can be used collectively to simulate the thermal and mechanical response of structural frames at elevated temperatures. To model the thermal response, a special-purpose fiber heat transfer element is introduced. The first of its kind, the fiber heat transfer element uses a combination of finite element and finite difference methods to provide an accurate and highly efficient solution to the three-dimensional thermal problem. To simulate the mechanical response, a flexibility-based fiber beam-column element is used. The element presented here extends the formulation of Taucer et al. (1991) to include thermal effects, geometric nonlinearities, and residual stresses.

Both fiber elements are implemented in ABAQUS (2007) using the user-defined element (UEL) subroutine. The element formulations are verified by analyses of benchmark experimental tests and comparisons with traditional finite elements. Results indicate that both elements offer superior accuracy and computational efficiency when compared to traditional methods of analysis. Analyses of structures subjected to non-uniform heating emphasize the advantages of the fiber-based approach.

To demonstrate a realistic application of the proposed approach, the work concludes with an investigation of the response of unprotected steel beams subjected to localized fires. Because realistic fires are considered, the treatment of strain reversal upon cooling is also addressed. The analyses are used to demonstrate that the standard fire test is generally unconservative at predicting the time at failure of a structure subjected to realistic fire conditions, since failure depends more on the evolution of temperatures within the steel beams than the duration of fire exposure. The analyses also show that

critical temperatures from the standard fire test are conservative and thus offer a better means for predicting failure in steel structures within the scope of the standard fire test.

Dedication

This work is dedicated to Susan,
for giving me the confidence, motivation, and support
to succeed in this endeavor.

Acknowledgements

I would like to thank everyone at Virginia Tech who has contributed to my education and to this research. In particular, I would like to thank the members of my advisory committee, Dr. Elisa Sotelino, Dr. Samuel Easterling, Dr. Brian Lattimer, and Dr. Raymond Plaut from Virginia Tech, and Dr. Amit Varma from Purdue University, for their commitment and their helpful comments and suggestions. I am especially grateful to Dr. Sotelino, who has been a great advisor, mentor, and friend over the past few years. She gave me the opportunity to pursue a research topic that was both challenging and interesting, and I am thankful for her advice and continuous support throughout my doctoral education. I would also like to acknowledge the Charles E. Via Fellowship Program at Virginia Tech for funding my education.

Table of Contents

List of Figures

List of Tables

Chapter 1: Introduction

Structural design for fire has traditionally followed a prescriptive approach, in which fire resistance is determined from the standard fire test (e.g., ASTM E119). While the current prescriptive codes ensure at least a minimum level of safety, the prescriptive approach to structural fire design has come under much criticism in recent years because it offers little flexibility for developing alternative design solutions. As the profession seeks to develop more rational approaches to structural fire design, we are inhibited by our lack of knowledge on the subject, as most of the work to date is based largely on the standard fire test. Consequently, there is a great interest in broadening our understanding of structural response under realistic fire conditions. This is the motivation behind much of the work being conducted in the area of structural fire engineering in the United States and abroad.

The work described herein is meant to contribute to this widespread effort to develop a fundamental understanding of structural response under fire. Because this project was exploratory in nature, the scope of this research was very loosely defined from the start. Consequently, many of the ideas that are developed here were motivated simply by curiosity and a desire to understand this complex and interdisciplinary field of study. While this dissertation covers a wide array of topics, a central theme emerges. That is, this research seeks to develop improved methods for analyzing structural response under realistic fire conditions. Under this heading, we see the development of the proposed fiber-based approach and its application.

The first section of this chapter provides an overview of the fiber-based approach and defines the scope of the project. The organizational structure of the dissertation is described in the second section.

1.1 Overview and Scope of the Project

The proposed fiber-based approach involves the development and validation of two finite elements for simulating the thermal and mechanical response of structural frames subjected to fire. To model the thermal response, a fiber heat transfer element is

developed. The fiber heat transfer element uses a combination of finite element and finite difference methods to provide an accurate and highly efficient approximation of the three-dimensional temperature field in a structural frame subjected to any type of thermal loads. To model the force-deformation response, a flexibility-based fiber beam-column element is used. The element presented here extends the original formulation by Taucer et al. (1991) to account for thermal effects, geometric nonlinearities, and residual stresses.

The fiber-based elements are implemented in ABAQUS (2007) using user-defined element (UEL) subroutines. This approach allows us to explore new element formulations without having to develop an entire standalone finite element analysis program. Although there were some limitations to working within the rigid structure of ABAQUS (e.g., the maximum number of temperature degrees of freedom allowed per element), we found that implementing the two fiber elements as user-defined elements in ABAQUS worked reasonably well for the analyses carried out here.

Both fiber elements are validated through comparisons with traditional finite elements and analyses of benchmark experimental tests. The accuracy and efficiency of the fiber heat transfer element is demonstrated through comparisons with 1D, 2D, and 3D solid heat transfer elements in ABAQUS. Similarly, the capabilities of the flexibility-based fiber beam-column element are shown by comparison with a distributed plasticity frame finite element in ABAQUS. The benchmark experimental tests considered here include uniformly heated steel beams and frames (Rubert, 1984; Rubert and Schaumann, 1985, 1986), steel columns with blocked-in webs (Wainman and Kirby, 1988), and steel beams supporting non-composite concrete slabs (Wainman and Kirby, 1988, 1989).

To demonstrate the fiber-based approach in a real-world application, this research culminates with a series of analyses on unprotected steel beams subjected to localized fires. While the fiber-based approach is ultimately intended to be used in simulations of large-scale structural systems, it was decided that an investigation involving realistic fire behavior should be pursued first, because the fiber heat transfer element gives us an opportunity to investigate structural response under non-uniform thermal loads. Thus, the last section of this dissertation investigates the effects of different types of localized fire behavior on the response of unprotected steel beams supporting non-composite concrete slabs. Because the analyses involve realistic fire behavior, the treatment of strain reversal

upon cooling is also addressed. The analyses are used to evaluate the standard fire test in terms of its ability to ensure structural integrity under natural fire conditions. It is found that the concept of "fire resistance" (i.e., the time period during which a member is able to withstand the standard fire) is unconservative at predicting the failure of steel beams under realistic fire conditions and that the critical temperature (i.e., the maximum temperature in the member at failure) obtained from the standard fire test may be a better indicator of the overall performance in fire. Note that these conclusions are drawn from comparisons to standard fire tests conducted in Europe, in which the structures were loaded and heated until failure according to the ISO 834 standard.

1.2 Organization

The organizational structure of this dissertation follows the manuscript format, in which the standard dissertation chapters are replaced by manuscripts that will be submitted or have already been accepted for publication in refereed scholarly journals. To orient the reader, Chapter 2 provides an overview of the current state of the practice and a review of fundamental concepts related to the theoretical developments in the remainder of the dissertation. Chapter 3 offers a review of literature pertaining directly to the analysis of structural frames in fire and the response of structures subjected to non-uniform heating. The subsequent three chapters consist of manuscripts containing the major theoretical developments of this research. Chapter 4 is a manuscript entitled "A Fiber Heat Transfer Element for Modeling the Thermal Response of Structures in Fire," which has been accepted for publication in the *Journal of Structural Engineering*. The chapter focuses primarily on the development and validation of the fiber heat transfer element. Chapter 5 is a manuscript entitled "Modeling Structural Response in Fire using a Fiber-Based Approach," in which the flexibility-based fiber beam-column is introduced. In addition to introducing the flexibility-based element, Chapter 5 highlights the fiber-based approach, in which the fiber heat transfer element is used with the flexibility-based fiber beam-column element to simulate the response of structures subjected to non-uniform thermal loads. Chapter 6 is a manuscript entitled "Analysis of Unprotected Steel Beams Subjected to Localized Fires," in which the fiber-based approach is utilized to investigate the response of steel beams subjected to localized fires. Lastly, Chapter 7

summarizes the findings of this research and discusses directions for future work. An extensive list of references is provided after Chapter 7.

Chapter 2: The Current State of the Practice and a Review of Fundamental Concepts

This chapter provides an overview of the current state of the practice and an introduction to key concepts related to the theoretical developments in the remaining chapters of this dissertation. The first section in this chapter discusses the shift in design philosophy from the current prescriptive approach to the performance-based approach that is occurring in the United States and abroad. The second section in this chapter provides an overview of analytical methods for evaluating structural performance in fire and highlights topics such as fire behavior, fundamentals of heat transfer analysis, and the response of structures at elevated temperatures. The purpose of this chapter is to provide a context and motivation for the work described in subsequent chapters.

2.1 Structural Design for Fire Resistance

There are currently two acceptable approaches to designing structures for fire: (1) the prescriptive approach, and (2) the performance-based approach. While current building codes emphasize the prescriptive approach to designing structures for fire, engineers realize the need for performance-based methods that take into account the fundamental response of structures subjected to elevated temperatures. These two approaches to structural fire design are described in the following sections.

2.1.1 Prescriptive Approach

Traditional methods for designing structures for fire resistance are based on a prescriptive approach, in which

1. Building codes (e.g., IBC, 2003) prescribe fire resistance ratings for structures based on building occupancy and type of construction, and
2. Structural components and fire protection materials are selected based on the minimum required fire resistance.

Fire resistance is determined from a standard fire test (e.g., ASTM E119), and is defined as the time during which a structural component meets certain performance criteria when

subjected to the standard fire. The standard fire test allows structural components to be tested with or without load, and failure is defined as the time at which the member fails to carry the test load or the time at which the temperature in the specimen exceeds a maximum allowable temperature.

The prescriptive approach generally translates into simple design requirements, which often require little to no consideration by the structural engineer. For structural steel members, it is not uncommon for external fire protection (e.g., sprays, boards, and intumescent coatings) to be "blindly" applied to all exposed steel to satisfy the minimum fire resistance criteria (Bailey, 2006). For reinforced concrete members, fire resistance is implicitly taken into account in the design specifications, i.e., in the initial sizing of members and in the minimum cover requirements (Bailey, 2004). The idea is that fire is not considered a structural load in the same way that other natural phenomena, such as wind and earthquakes, are, and so the responsibility of ensuring that buildings are adequately designed for fire resistance falls outside of the obligations of the structural engineer (Johann et al., 2006).

While the prescriptive approach is easily understood by design engineers and has proven to be adequate in ensuring a minimum level of safety in buildings subjected to fire loading, it falls drastically short in giving engineers a fundamental understanding of how structures behave under realistic fire loading. The standard fire test does not require consideration of the evolution of forces and deformations in structural members at elevated temperatures, nor does it account for interactions between structural members, which have been shown (Newman, 1999; Bailey, 2004a, 2004b; Wald et al., 2006) to have a significant effect on the response of structural systems subjected to fire. Dating back to the early 1900s, the standard fire test was developed at a time when methods of design and construction were significantly different from today's practice (Bailey, 2004b) and the profession had a different understanding of fire behavior (Bukowski, 2003). Furthermore, the temperature-time curve for the standard fire, as shown in Fig. 2-1, is not representative of a realistic fire, meaning that the results from the standard fire test give no indication of how a structure will respond in an actual fire (Bukowski, 2003). Because of shortcomings in the prescriptive approach, the profession is currently trying to develop a performance-based approach to fire safety design, as described in the following section.

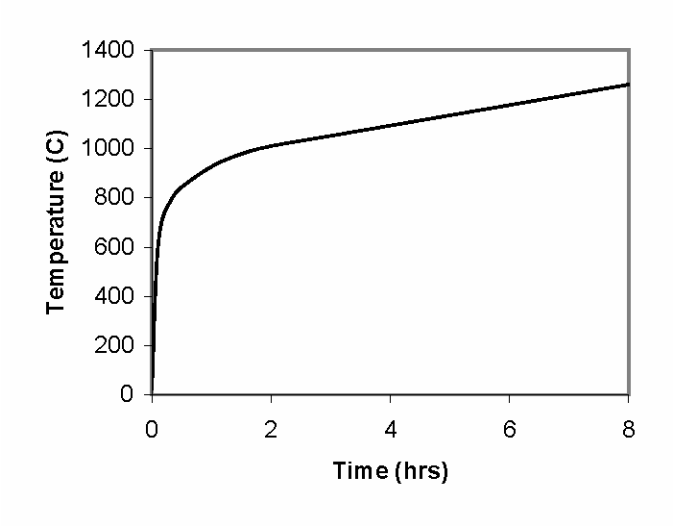

Fig. 2-1. Temperature-time curve for the standard ASTM E119 fire (ASTM, 1999)

2.1.2 Performance-Based Approach

Performance-based design can be broadly defined as a process of engineering a solution to meet certain levels of performance for a given design event (Thompson and Bank, 2007). A performance-based code requires that design engineers (1) specify target levels of performance, (2) state the conditions under which the desired levels of performance are to be met, and (3) prove that the performance objectives are met in final engineering designs (Meacham et al., 1998). While the prescriptive codes solely enforce minimum levels of safety, performance-based design allows alternative performance factors, such as property loss and interruption of business, to be considered. Furthermore, performance-based design allows the consideration of more realistic design events which can be selected on the basis of a probability of occurrence. While considerably more involved than the prescriptive methods, the performance-based approach allows greater flexibility in balancing cost and risk in structural design and results in solutions that are grounded in engineering principles. The United States has already implemented performance-based methods in the design of structures for other types of loads, such as gravity, wind, and seismic loads, and several countries, including the United States, have developed or are in the process of developing performance-based codes for structural fire design (Thompson and Bank, 2007).

Meacham et al. (1998) provide a detailed framework for a performance-based approach to fire safety design. In this reference, the authors present a seven-step method for conducting a performance-based fire safety design. The seven steps are as follows:

1. Identification of site or project information,
2. Identification of fire safety goals and objectives,
3. Development of performance criteria and design criteria,
4. Development of fire scenarios,
5. Development of design fires,
6. Development and evaluation of candidate (trial) designs, and
7. Development of final documentation (Meacham et al., 1998).

While the process is relatively straightforward, there are a number of issues that arise when the design process is applied to a realistic problem. For example, the development of design fires requires an understanding of fire behavior, an ability to simplify that behavior into a useful model, and a probabilistic method for determining the fire intensity that can be expected in a given building structure. Because fire behavior is extremely unpredictable, there is a need for analytical tools that allow designers to approximate fire behavior based on the characteristics of a given building.

Another important issue that arises from the performance-based approach is that, given a design fire, the performance of the building must be evaluated. In terms of structural performance, the engineer must be able to assess the force-deformation response of the structure at elevated temperatures. While there are a number of existing methods for evaluating the thermal and mechanical response of structures at elevated temperatures, there is a question as to the level of detail required in these analyses. Simplistic approaches may fail to capture important aspects of the response, while detailed methods of analysis can be computationally expensive. Furthermore, there is a shortage of reliable data that is needed to develop and validate tools for carrying out performance-based design because most experimental fire tests are based on the standard fire test (Beyler et al., 2007). Current research efforts, including the work proposed herein, seek to address these issues.

2.2 Analysis of Structures Subjected to Fire Loading

Analyzing a structure subjected to fire loading involves three components: (1) estimation of the fire behavior, (2) analysis of the thermal response of the structure, and

(3) analysis of the mechanical response of the structure. In building structures made of steel and concrete, these three analyses are typically assumed to be sequentially-coupled. That is, the fire behavior will govern the thermal response of the structure, but the thermal response is assumed to have little effect on the fire behavior. Similarly, the thermal response will govern the force-deformation response of the structure, but changes in geometry and cross-sectional properties are assumed to be relatively small and have little effect on the thermal response of the structure. Thus, a fire analysis results in time-dependent characteristics (e.g., temperatures or surface fluxes) that constitute the input for the thermal analysis. A thermal analysis yields time-dependent temperature profiles within the structure that are specified as the input in the mechanical analysis.

The three components of structural fire analysis are described in the following sections. Each section provides a brief explanation of the underlying physics associated with the behavior or response being considered. Common assumptions and analysis techniques are discussed where appropriate. It is important to note that each step of the analysis involves important decisions that can significantly affect the accuracy and worth of the overall results. For example, if one assumes the fire to behave according to the standard fire, the results will give no information about the way in which a given structure will respond to a realistic fire.

2.2.1 Fire Behavior

At the start of a fire, combustible materials are heated by a variety of combustion processes, such as smoldering and flaming. Once ignited, the fire undergoes a period of steady growth in which temperatures increase significantly as the fire spreads. If the conditions are right, a developing fire may reach the point of flashover, which is a short period marked by rapid growth associated with the nearly simultaneous ignition of all combustible material in a compartment (Gewain et al., 2003). Beyond flashover, the contents of a compartment burn steadily at extreme temperatures, until the fuel eventually runs out and the fire begins to decay. It is important to note that most fires do not reach flashover because the conditions are not right, e.g., the ventilation may be poor or fire suppression systems (e.g., sprinkler systems) may prevent the fire from growing (Gewain et al., 2003).

While the characteristics of an actual fire depend on a number of factors including compartment size, ventilation conditions, and the type and distribution of combustible material, the development of a fire can be described in three fundamental stages: (1) growth, (2) steady burning, and (3) decay (Bailey, 2004b). A generic model illustrating the temperature-time curve associated with these stages of fire development is shown in Fig. 2-2. Note that the actual temperature-time curve for a realistic fire may differ significantly from the generic model shown in Fig. 2-2. For example, a compartment with good ventilation would result in a fast-burning fire with extremely high temperatures. If we consider an identical compartment that, instead, has poor ventilation characteristics, the compartment fire would burn for a longer duration at lower temperatures. It is evident that these two types of fires (often called short-duration high-temperature fires and long-duration low-temperature fires, respectively) have drastically different characteristics.

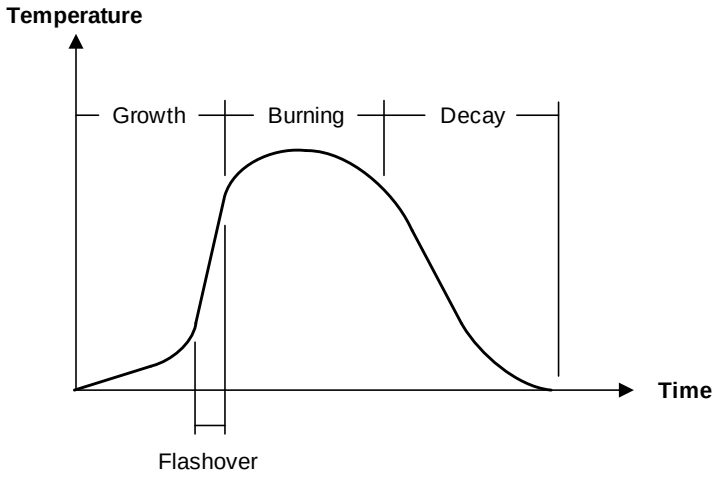

Fig. 2-2. Stages of fire development (adapted from Gewain et al., 2003)

Because fire behavior is highly unpredictable, it is difficult to develop design tools that are simple enough to be used in design yet capture the fundamental characteristics of a realistic fire. Current methods of fire analysis range in complexity from simple calculation methods to advanced numerical simulations. For pre-flashover fires, zone models and field models are most commonly used (Buchanan, 2001). Other models have been developed specifically for localized fire plumes (SFPE, 2004). For fully-developed compartment fires, a number of parametric fire curves are available for

estimating the temperature-time response based on factors such as ventilation and fuel load. Parametric fire curves are commonly used for modeling structural response in fire since they are relatively straightforward and provide a reasonable approximation of compartment fire behavior. Commonly referenced parametric fire curves include the Swedish fire curves (Magnusson and Thelandersson, 1970) and the Eurocode parametric fire curves (*EN 1991-2.2*). A complete review of existing models for compartment fires and localized fire plumes can be found in SFPE (2004).

2.2.2 Thermal Response of Structures Subjected to Fire Loading

During combustion, energy is released primarily in the form of heat. Heat released by a fire is transferred throughout the compartment by means of conduction, convection, and radiation. This process of heat transfer is governed by the first law of thermodynamics, which states that energy can be neither created nor destroyed. By enforcing conservation of energy, the evolution of temperatures within a control volume can be described in terms of the fundamental modes of heat transfer: conduction, convection, and radiation. In this section, we will look at the three modes of heat transfer, which are illustrated in Fig. 2-3, and see how the principle of conservation of energy can be used to derive a relationship that describes thermal response of a structure subjected to fire loading.

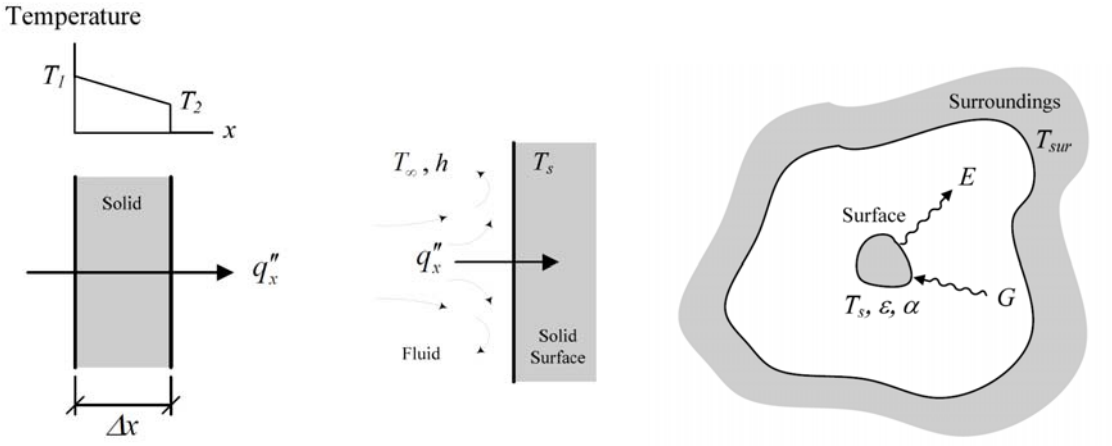

(a) (b) (c)

Fig. 2-3. Modes of heat transfer: (a) conduction through a solid, (b) convection at the boundary between a solid and a fluid, and (c) radiation exchange between a surface and its surroundings.

a. *Conduction:* Conduction, illustrated in Fig. 2-3(a), is the transport of thermal energy in a stationary medium and is the primary means by which heat flows through a solid. Conduction is governed by Fourier's law, which states that the rate of heat transfer per unit area (stated as a flux q_n'') in an arbitrary direction *n* is proportional to the temperature gradient $\frac{\partial T}{\partial n}$ in that direction, i.e.,

$$q_n'' = -k\frac{\partial T}{\partial n}, \tag{1}$$

where *k* is the thermal conductivity of the material (Incropera and DeWitt, 2002). The minus sign in Eqn. (1) simply indicates that heat flows from higher temperature regions to lower temperature regions, as shown in Fig. 2-3(a).

b. *Convection:* Convection is the transport of thermal energy in a fluid. When considering the thermal response of structures subjected to fire, we are primarily interested in the convection heat transfer that occurs at the boundary between the solid surface of the structure and the surrounding fluid, as illustrated in Fig. 2-3(b). While convection is an extremely complex process, the convective flux at such a boundary can be described by Newton's law of cooling. Essentially, the convective flux q_n'' normal to the bounding surface is given by

$$q_n'' = h(T_s - T_\infty), \tag{2}$$

where *h* is the convection heat transfer coefficient, T_s is the surface temperature of the solid, and T_∞ is the fluid temperature at the boundary (Incropera and DeWitt, 2002). While Eqn. (2) appears to be relatively straightforward, some difficulties arise in predicting the heat transfer coefficient *h*, since it depends on a number of factors including the surface geometry and the characteristics of the fluid motion.

c. *Radiation:* Radiation is thermal energy emitted by matter in the form of electromagnetic waves. All surfaces have the potential to emit and absorb thermal radiation, and the amount of energy emitted or absorbed depends on the radiative properties (i.e., emissivity ε and absorptivity α) of a given surface. The heat flux

emitted by a surface at temperature T_s is governed by the Stefan-Boltzmann law. Essentially, the energy released per unit area (also called the emissive power E) for any surface is given by

$$E = \varepsilon \sigma T_s^{\,4}, \tag{3}$$

where ε is the emissivity of the surface, σ is the Stefan-Boltzmann constant ($\sigma = 5.67 \times 10^{-8}$ W/m$^2 \cdot$K^4), and T_s is the surface temperature (Incropera and DeWitt, 2002). The emissivity of a surface is a number between zero and one, with an ideal radiator (i.e., a blackbody) having an emissivity of one.

Some of the radiation that is incident on a surface (also called irradiation G) is absorbed by the surface. The amount of irradiation absorbed by a surface depends on the absorptivity α of the surface. Similar to emissivity, absorptivity is a number between zero and one. Absorptivity for a given surface depends on the nature of the irradiation as well as the properties of the surface. The amount of irradiation absorbed by a surface G_{abs} is equal to the radiation G incident on the surface multiplied by the absorptivity α of the surface (Incropera and DeWitt, 2002), i.e.,

$$G_{abs} = \alpha G. \tag{2.4}$$

Depending on the nature of the surface, portions of irradiation may be reflected.

Oftentimes, we need to determine the radiation exchanged between a small surface and a much larger surface or enclosure, as shown in Fig. 2-3(c). Such examples include the radiation transmitted from the walls of a furnace to a test specimen or the radiation transmitted between a compartment fire and the walls of the compartment. In such cases, it is common to assume that the irradiation G from the surroundings can be approximated by the emission of a blackbody (i.e., $G = \sigma T_{sur}^{\,4}$) and that the emissivity and absorptivity of the smaller surface are equal (i.e., the smaller surface is considered to be a "gray surface"), (Incropera and DeWitt, 2002). These assumptions lead to a net rate of radiation heat transfer of

$$q''_{rad} = \varepsilon \sigma (T_s^{\,4} - T_{sur}^{\,4}), \tag{5}$$

where q''_{rad} is the net heat flux due to radiation. In the case of a compartment fire, the emissivity of the fire, the gas temperature, and the temperature of the surrounding enclosure are substituted into Eq. (5) for ε, T_s, and T_{sur}, respectively. The radiative heat flux given in Eq. (5) may be sufficient for approximate analyses of structures subjected to fire. However, more accurate models (e.g., Ghojel, 1998; Prasad and Baum, 2005) for the radiation heat transfer associated with fire are recommended for more realistic analyses.

Understanding the modes of heat transfer, we can use the principle of conservation of energy to establish a relationship that describes the thermal response within a specified region. To do this, we will consider energy flow through a control volume, as shown in Fig. 2-4. Energy flows into and out of the control volume by one or more of the fundamental modes of heat transfer. In addition, some amount of energy is generated within the control volume due to, for example, a chemical reaction. To satisfy the principle of conservation of energy, the change in internal energy $\frac{dE}{dt}$ at any time t must be equal to the net energy flow through the control volume. Mathematically, this relationship can be expressed as

$$\frac{dE}{dt} = \dot{E}_{in} - \dot{E}_{out} + \dot{E}_{gen}, \tag{6}$$

where $\dot{E}_{in}$ is the rate of energy flowing into the control volume, $\dot{E}_{out}$ is the rate of energy flowing out of the control volume, and $\dot{E}_{gen}$ is the rate of energy generation within the control volume (Incropera and DeWitt, 2002).

Fig. 2-4. Energy flow through a control volume

For heat transfer in a solid, thermal energy due to convection and radiation appears as a surface flux on the exterior boundary of the solid, as illustrated in Fig. 2-5(a). Heat is transferred to interior points within the solid by conduction. To derive the equation governing conduction heat transfer, consider a differential control volume having dimensions *dx*, *dy*, and *dz*, as shown in Fig. 2-5(a). Fig. 2-5(b) shows the energy flow through the differential control volume. In this diagram, the terms q_x, q_y, and q_z represent the energy flowing into the control volume in the *x*, *y*, and *z* directions, respectively, and the terms q_{x+dx}, q_{y+dy}, and q_{z+dz} represent the energy flowing out of the control volume in the *x*, *y*, and *z* directions, respectively. Because we are considering a differential element of volume, the terms q_{x+dx}, q_{y+dy}, and q_{z+dz} can be approximated by the following relationships:

$$q_{x+dx} \approx q_x + \frac{\partial q_x}{\partial x} dx, \qquad q_{y+dy} \approx q_y + \frac{\partial q_y}{\partial y} dy, \qquad q_{z+dz} \approx q_z + \frac{\partial q_z}{\partial z} dz. \tag{7}$$

Energy flow (e.g., q_x) across a surface is equal to the flux incident on the surface multiplied by the perpendicular area. For example,

$$q_x = q_x'' A_x, \tag{8}$$

where q_x'' is the flux acting in the *x* direction and A_x is the area of the surface normal to q_x'' (i.e., $A_x = dy\, dz$). Similar relationships can be developed for the remaining energy flow terms in Fig. 2-5(b). Since heat is transferred only by conduction in the control volume shown, heat flux is given by Eq. (1). Thus, terms q_x, q_y, and q_z are given by the following relationships:

$$q_x = -k \frac{\partial T}{\partial x} dy\, dz, \qquad q_y = -k \frac{\partial T}{\partial y} dx\, dz, \qquad q_z = -k \frac{\partial T}{\partial z} dx\, dy. \tag{9}$$

Note that the thermal conductivity *k* is assumed to be independent of material orientation in Eq. (9).

If some amount of heat is generated internally within the control volume, the net energy flow through the control volume (i.e., the terms on the right-hand side of Eq. (6)) can be expressed as

$$\dot{E}_{in} - \dot{E}_{out} + \dot{E}_{gen} = (q_x + q_y + q_z) - (q_{x+dx} + q_{y+dy} + q_{z+dz}) + Q\,dV\,, \tag{10}$$

where Q is the amount of heat generated internally per unit volume and dV is the volume of the differential control volume. Substituting Eqs. (7) and (9) into Eq. (10) and rearranging terms gives

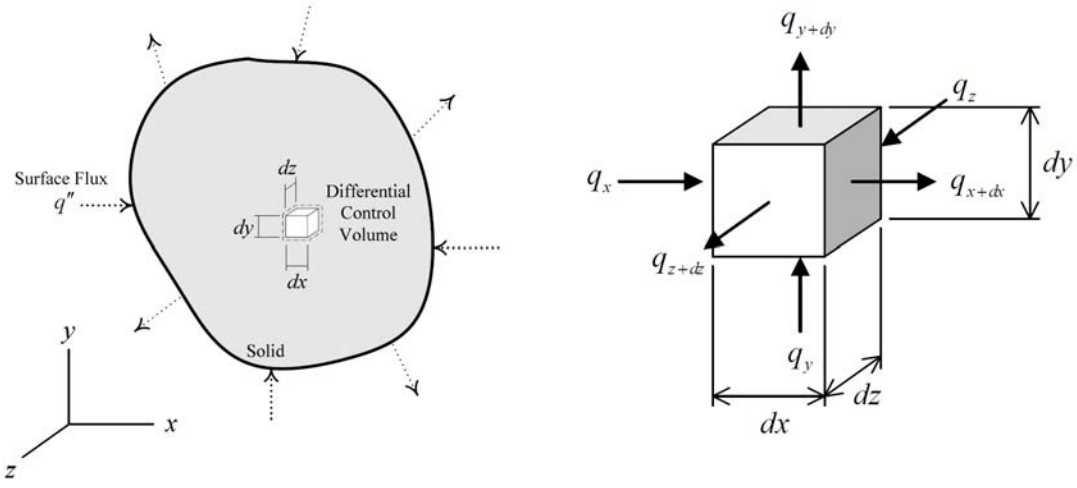

(a) (b)

Fig. 2-5. Heat transfer in a solid body: (a) differential control volume, (b) energy flow through a differential control volume

$$\dot{E}_{in} - \dot{E}_{out} + \dot{E}_{gen} = \frac{\partial}{\partial x}\left(k\frac{\partial T}{\partial x}\right)dV + \frac{\partial}{\partial y}\left(k\frac{\partial T}{\partial y}\right)dV + \frac{\partial}{\partial z}\left(k\frac{\partial T}{\partial z}\right)dV + Q\,dV\,. \tag{11}$$

Lastly, a relationship describing the change in internal energy $\frac{dE}{dt}$ needs to be defined. In most cases, the change in internal energy is based on the energy associated with the random excitation of molecules and the latent energy associated with a phase change (Incropera and DeWitt, 2002). If no phase change occurs, the rate of energy storage in a differential volume dV can be expressed as

$$\frac{dE}{dt} = \rho C\frac{\partial T}{\partial t}dV\,, \tag{12}$$

where ρ is the density, C is the specific heat, and T is the temperature. Eqs. (11) and (12) can be substituted into Eq. (6) to give the differential equation governing transient diffusion in a three-dimensional space, i.e.,

$$\rho C \frac{\partial T}{\partial t} = \frac{\partial}{\partial x}\left(k \frac{\partial T}{\partial x} \right) + \frac{\partial}{\partial y}\left(k \frac{\partial T}{\partial y} \right) + \frac{\partial}{\partial z}\left(k \frac{\partial T}{\partial z} \right) + Q \,. \tag{13}$$

Note that Eq. (13) can be solved for the three-dimensional temperature distribution T as a function of time. Solving this equation requires the specification of thermal boundary conditions (i.e., prescribed temperatures or surface heat fluxes) along the exterior surface of the body as well as initial temperatures at all points within the boundary.

Depending on the complexity of a given problem, an exact solution to Eq. (13) is often difficult (if not impossible) to obtain, and so a numerical solution method is generally employed. Traditional techniques for solving conduction heat transfer problems are described in a number of texts (e.g., Incropera and DeWitt, 2002; Jaluria and Torrance, 2003). Commonly used methods include the finite difference and finite element methods. There are also a number of spectral methods (e.g., Green's functions, Fourier transforms) that are suitable for solving heat transfer problems. These traditional approaches are well-established and can yield excellent results for a multitude of heat transfer problems.

When analyzing the response of a building structure subjected to fire, the size of the problem can be extremely large, and it can be costly to perform full three-dimensional heat transfer analyses for all members within a given compartment. In such cases, it is common to make simplifying assumptions about the thermal response of structural members. For example, one approach is to neglect temperature variations along the length of a member and perform a two-dimensional heat transfer analysis of the cross-section using one of the classical methods of heat transfer analysis. In addition, for members with high thermal conductivity (e.g., members made of steel), it is commonly assumed that the temperature of the cross-section can be approximated by a constant or linear temperature function.

2.2.3 Mechanical Response of Structures Subjected to Fire Loading

The event of a structural fire can be extremely damaging to a structural assembly. During a fire, the structure can be subjected to extreme temperatures, resulting in material degradation, large deformations, load redistribution, and instabilities, which can ultimately lead to collapse. The temperature increase associated with fire causes materials to expand, producing thermal strains within the structure. For a member restrained against thermal expansion, the additional stresses associated with heating can greatly reduce the capacity of the member (Cabrita Neves et al., 2002). In addition, fires can generate non-uniform temperature profiles within structural members, resulting in non-uniform thermal expansion. A column heated on one side, for example, experiences thermal bowing due to the temperature differential across its cross-section; this thermal bowing can lead to a reduction in capacity due to second-order effects (Ossenbruggen et al., 1973).

A significant amount of research has shown that extreme temperatures associated with fire can significantly reduce the stiffness and strength of materials. When subjected to fire, certain types of materials may also experience creep, phase change, decomposition, loss of moisture, and loss of material (Milke, 1999). Localized effects (e.g., local buckling in steel, and cracking and spalling in reinforced concrete) play an important role in the overall response of structures subjected to fire loading. Thus, accurate modeling of structures subjected to fire requires sufficient understanding of material behavior at elevated temperatures. Estimating material properties at elevated temperatures can be difficult and, while a number of material models are available for common building materials (e.g., steel, reinforced concrete), material behavior under these extreme conditions is still an important and active field of research.

A substantial amount of knowledge regarding the mechanical response of structures subjected to fire has resulted from significant experimental and analytical research efforts over the past several decades. Because traditional methods for designing structures for fire are based entirely on the standard fire test, much of the research to date has focused on the response of *isolated members* (e.g., columns and beams) subjected to elevated temperatures. While tests conducted on individual structural components can yield important information about the way in which structures respond to fire, large-scale experimental tests (e.g., the Cardington fire tests) have demonstrated that a number of

behaviors observed in structural frames under fire were virtually absent in isolated member tests. Thus, research focus has shifted in recent years toward developing an understanding of how *structural systems* (e.g., frames and subassemblies) respond to fire loading.

Chapter 3: Literature Review

There is an overwhelming amount of literature pertaining to the response of building structures subjected to fire loading. Major research topics within the field of structural fire engineering include:

- Development and implementation of performance-based standards for structural fire design;
- Understanding fire behavior and developing suitable fire models to be used in research and in design;
- Evaluation of the thermal response of structures subjected to various kinds of heating;
- Determining material properties at elevated temperatures and developing appropriate material models; and
- Experimental testing and analysis of structural elements and structural systems subjected to various kinds of heating.

This chapter contains a survey of literature directly related to the present dissertation. Topics addressed in this chapter include (1) the effects of non-uniform heating on the mechanical response of structures, and (2) methods for evaluating the mechanical response of structural frames subjected to fire.

3.1 Non-Uniform Heating in Structures

Because 3D heat transfer analyses are computationally expensive, analysis of the thermal response of frame structures subjected to fire usually involves a simplification of the actual thermal problem (e.g., longitudinal temperature variations are often neglected, or the temperature field across a member's cross-section is approximated as constant or linear). These simplifications are based on the assumption that the temperature within a compartment is uniform. However, there are many instances in which the temperature distribution within a compartment may be non-uniform. For example, in the initial stages of fire development, a fire is localized within the compartment before it becomes fully developed (Franssen et al., 2007). In other cases, the fuel may be concentrated within a

region of the compartment and so the heating is again localized to a particular region in the compartment (SFPE, 2004). Even during a standard fire test, temperature distributions within a given furnace will be non-uniform to some extent depending on the characteristics of the furnace (Witteveen and Twilt, 1981/82).

In addition to non-uniform heating, temperature variations may develop within structures due to the inherent continuity in structural frames. For example, cooler adjacent floors in a building will act as heat sinks during fire, thus affecting the longitudinal temperature distributions within structural columns (Becker, 2002a). In composite floor systems, temperature differences of more than 100^{o}C can develop across the cross-section of the beam because of continuity between the beam and concrete slab (Franssen et al., 1995). Complex thermal behavior at structural joints can also be a source of non-uniform temperature distributions within structural frames; however, analyses have shown that the effects at the joints are highly localized and have little influence on the overall structural response (Franssen, 2007).

Because the mechanical response is directly affected by the thermal response, simplifications of the thermal response may lead to loss of accuracy during an analysis. Several researchers have investigated the effects of non-uniform heating on the mechanical response of structural members. The following is a survey of literature related to non-uniform heating in structures.

- Culver (1972) studied the effects of longitudinal temperature variations on the buckling resistance of steel columns using a finite difference approach. It was found that non-uniform heating along column length can significantly affect the stability of steel columns.
- Ossenbruggen et al. (1973) investigated the influence of transverse temperature gradients on the buckling load of steel columns. Thermal bowing resulted in second-order effects which greatly reduced the capacity of the columns considered.
- Kruppa (1981/1982) described a series of experimental tests on external steel columns involving non-uniform heating along the length and across the cross-section. It was found that temperatures in the flanges of steel columns heated on one side can differ by more than 200^{o}C, indicating that it may be inadequate to

- Witteveen and Twilt (1981/82) conducted a series of parametric analyses to determine factors affecting the reproducibility of results in standard fire tests of steel columns. Using a simple calculation method, they found that the critical temperature from a standard fire test can be significantly underestimated by assuming heating is uniform along the member length.
- Cooke and Latham (1987) performed an experimental test on a steel frame subjected to natural fire. The test frame was subsequently analyzed by Franssen et al. (1995). It was found that the response was governed largely by thermal bowing in the columns and beam resulting from non-uniform heating over the cross-section of the members. In addition, these studies concluded that the response of the structural system was significantly different from that of the individual members acting alone.
- Becker (2002a) analyzed the effects of heat sinks on the longitudinal temperature distributions in steel columns and, in a subsequent paper (Becker, 2002b), studied the effects of heat sinks on the mechanical response of steel frames. It was found that the presence of heat sinks significantly delayed the time of failure for structural systems subjected to fire and affected the formation of plastic hinges in columns and beams.
- Tan and Yuan (2008) studied the combined effects of longitudinally non-uniform heating and thermal restraint on the stability of steel columns. It was found that the buckling load for a column is significantly underestimated by assuming uniform heating along the column's length.

While non-uniform heating has been shown to have a significant effect on the mechanical response of structures, few researchers have attempted to develop efficient methods for incorporating 3D temperature distributions in structural members. The following are simplified approaches that have been considered for incorporating 3D

temperature distributions in structural members. Both methods reduce the 3D thermal problem to a series of 2D analyses.

- In an analysis of the Cooke and Latham (1987) test frame, Franssen et al. (1995) incorporated 3D temperature distributions by performing a 2D analysis of the structure and then multiplying the 2D temperature field by a reduction function based on experimental temperature measurements. This method yielded sufficiently accurate approximations of the temperature field, but relies on the availability of experimental measurements of temperatures.
- Franssen et al. (2007) used an example of a non-uniformly heated steel bar to illustrate that the 3D thermal response can be approximated by a series of uncoupled 2D heat transfer analyses performed along the member's length.

The fiber heat transfer element developed in this work and described in Chapter 4 differs from existing methods in that it provides a fully coupled solution to the 3D thermal problem. The element uses a combination of finite element and finite difference methods to balance accuracy and computational efficiency in modeling the thermal response. In addition, the fiber heat transfer element offers a significant advantage in the transfer of data from the heat transfer analysis to the structural analysis, since it has a fiber mesh that is compatible with any fiber-based (i.e., distributed plasticity) frame finite element. Consequently, the temperature data is calculated and transferred directly to the integration points for the structural element. These advantages make the fiber heat transfer element a valuable tool for modeling structural response under non-uniform thermal conditions, as is made evident in the analyses described in Chapters 4-6.

3.2 Evaluating the Mechanical Response of Frames Subjected to Fire

A number of simple calculation methods for isolated members have been developed based on fundamental principles of mechanics and experimental tests. For example, Huang and Tan (2003) presented a Rankine approach for analyzing the critical temperature in steel columns with axial restraint and creep effects. Such simple calculation methods are generally developed with the intent of being used in a design

setting. For research purposes, however, advanced numerical models are often required to provide an in-depth understanding of structural response in fire. Hence, this section focuses on more advanced computational methods that have been developed to simulate the response of structures in fire.

The finite element method is a common approach to analyzing structures subjected to fire loading. A number of finite element codes have been developed specifically for the purpose of modeling steel and/or concrete structures subjected to fire. Examples of such programs include SAFIR (Franssen, 2005) and VULCAN (Huang et al., 2000). Alternatively, finite element analyses can be carried out using commercially available finite element programs such as ABAQUS (2007).

Because structural fire problems are extremely complex, researchers have sought methods that are more efficient than the traditional finite element method. Examples of such approaches include the plastic hinge method and the plastic zone method (also called the spread-of-plasticity or distributed plasticity approach). Both of these methods use frame elements to represent beams and columns. However, the two methods differ in how yielding is incorporated in the analysis. In the plastic hinge method, yielding is lumped in a plastic region of zero length. To account for gradual yielding of the cross-section, the plastic hinge is given a stiffness based on an approximation of the response beyond yield. In the plastic zone method, yielding is modeled by dividing the cross-section into a series of fibers and tracking the stresses within these fibers at specific locations within the beam or column. While the plastic zone method gives a more realistic representation of the structural response, the plastic hinge method is more computationally efficient.

Adaptations of the plastic hinge method have been successfully used by a number of researchers, including Chan and Chan (2001), Toh et al. (2001), Wong (2001a, 2001b), Iu and Chan (2004), Landesmann et al. (2005), Iu et al. (2007), and Souza Junior and Creus (2007), to model the response of steel structures subjected to uniform fire conditions. Based on the plastic hinge approach, Liew et al. (1998) developed an elastoplastic beam-column finite element for modeling steel frames subjected to fire. The plastic hinge method, however, is limited in that it is unable to capture more complex

types of behavior due to flexural-torsional buckling, local buckling, and yielding under combined bending and axial load (Jiang et al., 2002).

The distributed plasticity approach has proven to be more accurate than the plastic hinge method. The following is a review of distributed plasticity (i.e., fiber-based) elements that have been developed for analyzing structural frames under fire.

- Saab and Nethercot (1991) developed a 2D distributed plasticity beam-column element for modeling steel frames subjected to fire. Najjar and Burgess (1996) extended the 2D element formulation and developed a 3D beam-column finite element based on the spread-of-plasticity approach. The element incorporated non-uniform temperature distributions across the section and accounted for biaxial bending. Bailey (1998) extended the model by including rotational springs to model semi-rigid connections. Huang et al. (2000) used the beam-column element along with shell elements to model composite beams subjected to fire. Cai et al. (2002) further extended the 3D beam-column element to allow for steel members with asymmetric cross-sections. The generalized beam-column element formulation was presented by Cai et al. (2003), in which the element's full capabilities for modeling steel and concrete structures subjected to fire were described in detail.
- Poh and Bennetts (1995) developed a fiber-based numerical model for beam-columns subjected to fire. The model uses an iterative approach to satisfy equilibrium, compatibility, and constitutive relationships at the section and element levels.
- Song et al. (2000) and Izzuddin et al. (2000) used an adaptive analysis technique to model the response of structures subjected to blast immediately followed by fire. The procedure starts by using a coarse mesh of elastic elements to model frame members. At each step of the analysis, the program checks specified regions to see if yielding is about to occur. In regions where yielding occurs, the program refines the mesh and replaces linear elements with fiber elements to allow for gradual yielding of the members. The process minimizes the use of the computationally expensive fiber elements.

- Tan et al. (2002) developed a 2D beam-column element for modeling steel frames subjected to fire, which is based on the spread-of-plasticity approach. The element's cross-section is subdivided into a number of horizontal slices, and a uniaxial stress-strain relationship is employed.
- Liew and Chen (2004) used a fiber beam-column element to model the response of steel structures subjected to explosion and fire loading. To reduce computation time, fiber elements were used in regions directly affected by blast and fire, and plastic hinge elements were used for the remainder of the structure.
- Di Capua and Mari (2007) presented a fiber element based on an arc-length method which can be used to model the response of reinforced concrete members subjected to fire loading. Because the element formulation is developed at the section level, the authors stated that the current element can only be used to analyze statically determinate structures.
- Kodur and Dwaikat (2008) presented a fiber element used to model the response of reinforced concrete beams subjected to fire. Throughout the analysis, relationships between moment and curvature were tracked for longitudinal segments of the member. Effects due to axial force and shear were neglected.

These models have only considered structures that are heated uniformly along the length. For cases in which temperatures vary over the cross-section, either 2D heat transfer analyses are conducted using solid elements or the temperatures are assumed over the cross-section.

In addition to the plastic hinge and plastic zone approaches, other types of analyses have been explored by researchers. For example, Burgess et al. (1990) and El-Rimawi et al. (1995) used secant stiffness (rather than tangent stiffness) approaches to model the response of structures subjected to fire. Hozjan et al. (2007) explored the use of artificial neural networks for predicting the response of steel structures subjected to fire.

Existing elements for modeling structural response in fire are currently limited to the stiffness method of analysis in which the element formulations are based on an assumed deformed configuration. Such displacement-based elements often experience loss of accuracy in highly nonlinear problems since the equations of equilibrium can be

violated. Consequently, a significant amount of research (e.g., Spaconi et al., 1996; Petrangeli and Ciampi, 1997; Neuenhofer and Filippou, 1997; Nukala and White, 2004; Adessi and Ciampi, 2007) on the analysis of structures at ambient temperatures has focused on the development of flexibility-based and mixed formulation elements. Such elements tend to offer greater accuracy and computational efficiency because equilibrium is strictly enforced within the element.

Because flexibility-based and mixed formulations offer significant advantages in the analysis of structures at room temperature, the work described in Chapter 5 focuses on the development of a flexibility-based element for modeling structural response under fire conditions. Based on an element developed by Taucer et al. (1991), the proposed flexibility-based fiber beam-column contains an iterative loop at the element level that enforces equilibrium, compatibility, and the material constitutive law within a prescribed tolerance. The original formulation is extended to account for thermal effects, geometric nonlinearities, and residual stresses. In Chapter 5, the fiber beam-column element is validated against benchmark experimental tests and compared to a stiffness-based element in ABAQUS (2007).

Chapter 4: "A Fiber Heat Transfer Element for Modeling the Thermal Response of Structures in Fire"

A. E. Jeffers, S.M.ASCE[1]; and E. D. Sotelino, M.ASCE[2]

[To appear in the *Journal of Structural Engineering*]

Abstract

This paper introduces a novel type of heat transfer finite element that can be used to model the three-dimensional thermal response of structural beams and columns subjected to elevated temperatures associated with fire. The element is a 3-node heat transfer element that uses a fiber discretization to account for both transverse and longitudinal temperature variations in a structural member. This fiber heat transfer element is purposely formulated to be compatible with any fiber beam-column finite element in a sequentially-coupled thermal-mechanical analysis of structural frames subjected to fire. The element is implemented in ABAQUS (2007) using a user-defined element (UEL) subroutine. To demonstrate the capabilities of the fiber heat transfer element, analyses are performed on members with various types of thermal boundary conditions. Results indicate that the fiber heat transfer element offers excellent accuracy with minimal computational expense, making the fiber heat transfer element a valuable tool for modeling the behavior of frame structures in fire.

CE Database subject headings

Heat transfer; Fire resistance; Finite element method; Frames; Temperature

4.1 Introduction

Because of costs and limitations associated with experimental tests, a substantial amount of research has focused on the development of analytical methods for understanding the behavior of building structures in fire. In terms of understanding the

[1] Graduate Research Assistant, The Charles E. Via, Jr. Dept. of Civil and Environmental Engineering, Virginia Polytechnic Institute and State Univ., Blacksburg, VA 24061.
[2] Professor, The Charles E. Via, Jr. Dept. of Civil and Environmental Engineering, Virginia Polytechnic Institute and State Univ., Blacksburg, VA 24061.

mechanical aspects of the response, emphasis is placed on numerical methods that balance solution accuracy and computational efficiency. Examples of such methods include the plastic hinge and plastic zone methods, both of which have been shown to yield accurate predictions of nonlinear structural response in fire. For modeling the thermal response, however, researchers generally resort to one of the traditional methods of heat transfer analysis (e.g., the finite difference or finite element methods). While such methods are well-established and yield accurate results for a multitude of problems, they can be costly, particularly when the problem size is quite large, as is often the case when building fires are considered. To overcome the costliness of full-blown three-dimensional (3D) heat transfer analyses, researchers often make simplifying assumptions about the thermal response of structural members. For example, longitudinal temperature variations are often neglected, or the temperature field over a member's cross-section is approximated as constant or linear.

While these simplifications greatly reduce the amount of calculations required, important aspects of the response may be lost in the analysis or there may be instances in which these assumptions are invalid. For example, it may be necessary to account for non-uniform temperatures within a compartment, e.g., during the initial stages of fire development (Franssen et al., 2007) or when the fuel is concentrated within a particular region of the compartment (SFPE, 2004). Alternatively, it may be necessary to account for temperature variations within structural members due to the inherent continuity provided by structural frames. For example, temperatures within composite steel beams may be significantly affected by the adjoining concrete slab (Franssen et el., 1995), or cooler adjacent floors in a building may act as heat sinks, thereby affecting longitudinal temperatures within structural columns (Becker, 2002a).

Although non-uniform heating in structural members has been shown to have a significant effect on the mechanical response of structures (such evidence can be found in Culver, 1972; Ossenbruggen et al., 1973; Kruppa, 1981/82; Witteveen and Twilt, 1981/82; Becker, 2002b; Tan and Yuan, 2008; among others), few have attempted to develop efficient methods for incorporating 3D temperature distributions in structural members when modeling the response of structures in fire. Exceptions include Franssen et al. (1995), in which a 3D approximation of the temperature field was obtained by

multiplying results from a 2D analysis by a reduction function based on experimental measurements of temperatures, and Franssen et al. (2007), in which the 3D thermal response was approximated by a series of uncoupled 2D heat transfer analyses along the member's length.

The work described herein takes a different approach to modeling the thermal response of structural frames subjected to fire. Rather than reduce the heat transfer problem to a 2D analysis, a new type of heat transfer finite element is introduced that can fully capture the 3D thermal response in structural beams and columns. By using both finite element and finite difference approximations of the governing heat transfer equation, the proposed fiber heat transfer element provides an accurate and efficient means for obtaining the transient temperature distributions within structural frames. Furthermore, the fiber heat transfer element is specifically designed to be compatible with any fiber-based (i.e., spread-of-plasticity) beam-column finite element in a sequentially-coupled thermal-mechanical analysis of frame structures in fire. Because the fiber element (i.e., spread-of-plasticity) approach has proven to be particularly effective at modeling the mechanical response of structural frames in fire, a number of these beam-column elements have already been developed (Poh and Bennetts, 1995; Song et al., 2000; Tan et al., 2002; Cai et al., 2003; Liew and Chen, 2004; Di Capua and Mari, 2005; and Kodur and Dwaikat, 2008; among others). Thus, the fiber heat transfer element offers a great simplification in the modeling of structures in fire, while providing an accurate and efficient solution to the thermal problem.

4.1 Element Formulation

Shown in Fig. 4-1, the fiber heat transfer element is a 1D finite element with a fiber discretization over the member's cross-section. The use of longitudinal fibers results in a finite element mesh that is compatible with any fiber beam-column element in a sequentially-coupled thermal-mechanical analysis of frames. In addition, the fiber discretization allows for varying material properties across the section; thus, the fiber heat transfer element can be used to model members made of multiple materials (e.g., steel-concrete composite members) as well as members with temperature-dependent material properties.

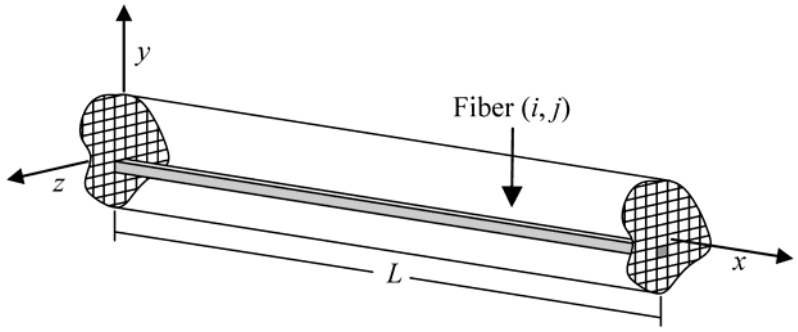

Fig. 4-1. The fiber heat transfer element

The general procedure adopted in the formulation of the fiber heat transfer element is described as follows. Because the cross-sectional area of a given fiber is relatively small, temperatures are assumed to vary only along the length of the given fiber. Each fiber can subsequently be treated as a 1D heat transfer finite element; in this paper, fiber temperatures are approximated by quadratic shape functions. To account for temperature variations over the cross-section of the structural member, a set of finite difference equations are then written at the member's cross-section that account for heat flow over the fiber boundaries. When the fiber equations are assembled into the element degrees of freedom, the resulting element equations are written in the form

$$[c]\{\dot{T}\} + [k]\{T\} = \{r\}, \tag{1}$$

where $[c]$ is the heat capacity matrix, $\{\dot{T}\}$ is an array containing the first derivatives of the nodal temperatures with respect to time (for transient analysis), $[k]$ is the conductivity matrix, $\{T\}$ is an array of nodal temperatures, and $\{r\}$ is an array of thermal loads. The element can then be implemented into an existing finite element code and the thermal response of structural frames can be analyzed.

To derive the element equations, consider a member (i.e., a beam or column) of length L with arbitrary cross-section, as depicted in Fig. 4-1. The member has local xyz coordinate axes, which are also shown in Fig. 4-1, and it is discretized into a series of longitudinal fibers. As illustrated in Fig. 4-2, these fibers are arranged in a rectangular grid over the cross-section. Integers i and j indicate the position of fiber (i, j) with respect to the local y and z coordinate axes, respectively. Fiber (i, j) has dimensions Δy and Δz,

and area *A*. Note that not all fibers need to have the same dimensions, as will be illustrated in a later example.

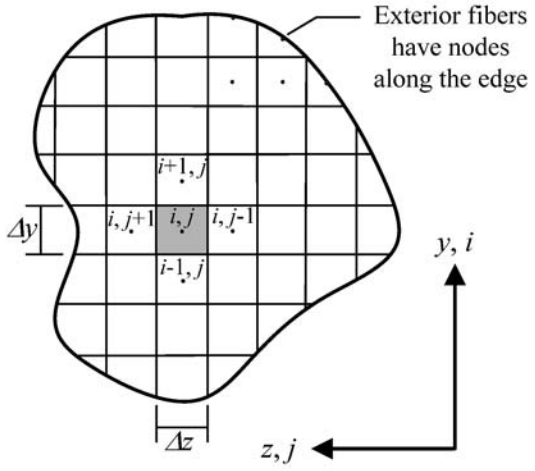

Fig. 4-2. Fiber grid

Each fiber is treated as a separate control volume. Based on the principle of conservation of energy, the equation governing the 3D transient heat conduction in fiber (*i*, *j*) is given by

$$\rho C \frac{\partial T}{\partial t} = \frac{\partial}{\partial x}\left(k \frac{\partial T}{\partial x} \right) + \frac{\partial}{\partial y}\left(k \frac{\partial T}{\partial y} \right) + \frac{\partial}{\partial z}\left(k \frac{\partial T}{\partial z} \right) + Q , \tag{2}$$

where ρ is the mass density, *C* is the specific heat, *k* is the thermal conductivity, *T* is temperature, *t* is time, and *Q* is the internal heat generation per unit volume (Incropera and Dewitt, 2002). Because a combination of finite element and control volume methods will be used to approximate the temperature field in the fiber heat transfer element, the integral form of the governing equation must be stated (Jaluria and Torrance, 2003). By integrating over the fiber's volume *V*, the integral form of Eq. (2) is

$$\int_V \left[\rho C \frac{\partial T}{\partial t} - \frac{\partial}{\partial x}\left(k \frac{\partial T}{\partial x} \right) - \frac{\partial}{\partial y}\left(k \frac{\partial T}{\partial y} \right) - \frac{\partial}{\partial z}\left(k \frac{\partial T}{\partial z} \right) - Q \right] dV = 0 . \tag{3}$$

If the area of fiber (*i*, *j*) is relatively small, the temperature variations over the fiber's cross-section can be neglected and the fiber's temperature can be assumed to vary only along its length. Thus, the temperature $T \equiv T(x, y, z, t)$ in Eq. (3) can be replaced by the fiber temperature $T_{i,j} \equiv T_{i,j}(x, t)$. To satisfy the energy balance, however, additional

terms are introduced in the governing equation to account for energy flowing into the fiber at the boundaries, i.e., at grid locations $i \pm ½$ and $j \pm ½$. Thus, the governing equation becomes

$$\int_V \left[\rho C \frac{\partial T_{i,j}}{\partial t} - \frac{\partial}{\partial x}\left(k \frac{\partial T_{i,j}}{\partial x} \right) - Q \right] dV + \int_L \left[\left(k \frac{\partial T}{\partial y} \right)\Big|_{i^-} \Delta z \right] dx$$
$$- \int_L \left[\left(k \frac{\partial T}{\partial y} \right)\Big|_{i^+} \Delta z \right] dx + \int_L \left[\left(k \frac{\partial T}{\partial z} \right)\Big|_{j^-} \Delta y \right] dx - \int_L \left[\left(k \frac{\partial T}{\partial z} \right)\Big|_{j^+} \Delta y \right] dx = 0. \tag{4}$$

The first term in Eq. (4) is obtained by substituting $T_{i,j}$ in place of T in Eq. (3), while the additional four terms represent heat flow at the fiber boundaries. Symbols i^+ and i^- are used to denote fiber boundaries between grid points in the *y*-direction (i.e., $i \pm ½$), while symbols j^+ and j^- are used to denote fiber boundaries between grid points in the *z*-direction (i.e., $j \pm ½$).

4.1.1 Finite Difference Approximation of the Boundary Terms

Because fiber cross-sectional temperatures are assumed constant, the calculation of temperatures over the element's cross-section is best accomplished using a finite difference scheme. As illustrated in Fig. 4-2, nodes are assigned to the fibers to indicate discrete locations at which the cross-sectional temperatures will be calculated. Note that exterior fibers have nodes along the edge; this is done to provide greater accuracy in accounting for thermal boundary conditions (Jaluria and Torrance, 2003). The mesh shown in Fig. 4-2 is used to generate finite difference approximations of the flux terms $\left(k \cdot \partial T / \partial y\right)\big|_{i^\pm}$ and $\left(k \cdot \partial T / \partial z\right)\big|_{j^\pm}$ in Eq. (4).

For an interior edge (i.e., an edge bordering an adjacent fiber), the boundary flux can be written as an effective conductivity $k_{i^\pm}$ or $k_{j^\pm}$ at the interface multiplied by a finite difference approximation of $\left(\partial T / \partial y\right)\big|_{i^\pm}$ or $\left(\partial T / \partial z\right)\big|_{j^\pm}$. Using a first-order finite difference scheme, the boundary fluxes for interior edges are

$$\left(k \frac{\partial T}{\partial y} \right)\Big|_{i^-} = k_{i^-} \left(\frac{T_{i,j} - T_{i-1,j}}{y_{i,j} - y_{i-1,j}} \right), \qquad \left(k \frac{\partial T}{\partial y} \right)\Big|_{i^+} = k_{i^+} \left(\frac{T_{i+1,j} - T_{i,j}}{y_{i+1,j} - y_{i,j}} \right), \tag{5}$$

$$\left(k\frac{\partial T}{\partial z}\right)\Bigg|_{j^-} = k_{j^-}\left(\frac{T_{i,j}-T_{i,j-1}}{z_{i,j}-z_{i,j-1}}\right), \qquad \left(k\frac{\partial T}{\partial z}\right)\Bigg|_{j^+} = k_{j^+}\left(\frac{T_{i,j+1}-T_{i,j}}{z_{i,j+1}-z_{i,j}}\right).$$

Note that $T_{m,n}$ is the temperature of fiber (m, n), which is a function of x and t. Coordinates $y_{m,n}$ and $z_{m,n}$ represent the location where temperatures are computed for fiber (m, n).

The effective conductivities $k_{i^\pm}$ and $k_{j^\pm}$ in Eq. (5) are obtained by averaging the thermal resistances of the grid points on either side of the interface (Jaluria and Torrance, 2003). For example, if the interface is midway between two grid points, the effective conductivity k_{eff} would be

$$k_{eff} = \frac{2k_a k_b}{k_a + k_b}, \tag{6}$$

where k_a is the conductivity of fiber (i, j) and k_b is the conductivity of the adjacent fiber.

For an exterior edge (i.e., an edge that coincides with the boundary of the structural member), the boundary flux in Eq. (4) depends on the type of condition specified at the boundary. If a temperature T_s is specified on the surface, then

$$T_{i,j} = T_s, \tag{7}$$

and the flux at the boundary is unknown. If a surface heat flux q_b'' is prescribed on the surface $i^\pm$ or $j^\pm$, then

$$\left(k\frac{\partial T}{\partial y}\right)\Bigg|_{i^\pm} = q_b'' \quad \text{or} \quad \left(k\frac{\partial T}{\partial z}\right)\Bigg|_{j^\pm} = q_b''. \tag{8}$$

If a convective condition exists on the surface $i^\pm$ or $j^\pm$, then

$$\left(k\frac{\partial T}{\partial y}\right)\Bigg|_{i^\pm} = h(T_\infty - T_{i,j}) \quad \text{or} \quad \left(k\frac{\partial T}{\partial z}\right)\Bigg|_{j^\pm} = h(T_\infty - T_{i,j}), \tag{9}$$

where h is the heat transfer coefficient and T_∞ is the fluid temperature.

For radiation exchange between a surface and its surroundings, the radiative flux q_{rad}'' is often stated as

$$q_{rad}'' = \varepsilon\sigma(T_s^{\,4} - T_{sur}^{\,4}), \tag{10}$$

where ε is the emissivity, σ is the Stefan-Boltzmann constant (5.67×10^{-8} W/m$^2\cdot$K^4), T_s is the surface temperature, and T_{sur} is the temperature of the surroundings (Incropera and DeWitt, 2005). Equation (10) will be linearized so that the flux due to radiation is linear in temperature. Thus, a radiation boundary condition on surface $i^{\pm}$ or $j^{\pm}$ is given by

$$\left(k\frac{\partial T}{\partial y}\right)\Big|_{i^{\pm}} = h_r(T_{sur}-T_{i,j}) \quad \text{or} \quad \left(k\frac{\partial T}{\partial z}\right)\Big|_{j^{\pm}} = h_r(T_{sur}-T_{i,j}), \tag{11}$$

where the radiation heat transfer coefficient h_r is given by

$$h_r = \varepsilon\sigma(T_{i,j}+T_{sur})(T_{i,j}{}^2+T_{sur}{}^2) \tag{12}$$

(Incropera and DeWitt, 2005). Note that h_r is highly dependent on temperature.

4.1.2 Application of the Finite Element Method

Fiber (i, j) is subsequently treated as a 1D finite element with n nodes. The temperature $T_{i,j}$ in fiber (i, j) is interpolated from the fiber's nodal temperatures $\{T_{i,j}\}$ using the fiber's shape function matrix [N], i.e.,

$$T_{i,j}(x,t) \approx [N]\{T_{i,j}\}. \tag{13}$$

Because the longitudinal temperature is generally nonlinear, a 3-node quadratic element, as shown in Fig. 4-3, is used to approximate the temperature field in fiber (i, j). Thus, the shape function matrix for the fiber is

$$[N] = \left[\frac{(x_2-x)(x_3-x)}{(x_2-x_1)(x_3-x_1)} \quad \frac{(x_1-x)(x_3-x)}{(x_1-x_2)(x_3-x_2)} \quad \frac{(x_1-x)(x_2-x)}{(x_1-x_3)(x_2-x_3)}\right], \tag{14}$$

where x_1, x_2, and x_3 are the locations of nodes 1, 2, and 3 with respect to the element's local coordinate system (Cook et al., 1989).

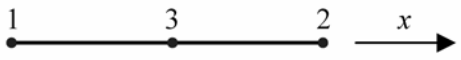

Fig. 4-3. 3-Node quadratic element

The Galerkin finite element method is now applied to Eq. (4). First, the terms inside the integrals in Eq. (4) are pre-multiplied by the individual shape functions. Then,

the diffusion term is simplified using integration by parts. The resulting boundary term is converted from a volume integral to a surface integral using Gauss's theorem (Jaluria and Torrance, 2003). Thus, the governing equation becomes

$$\int_V \left([N]^T \rho C \frac{\partial T_{i,j}}{\partial t} \right) dV + \int_V \left([B]^T k \frac{\partial T_{i,j}}{\partial x} \right) dV - \int_V [N]^T Q \, dV - \int_S \left([N]^T k \frac{\partial T_{i,j}}{\partial x} \right) \cdot \bar{n} \, dS + \int_L \left[[N]^T \left(k \frac{\partial T}{\partial y} \right)\Big|_{i^-} \Delta z \right] dx - \int_L \left[[N]^T \left(k \frac{\partial T}{\partial y} \right)\Big|_{i^+} \Delta z \right] dx + \int_L \left[[N]^T \left(k \frac{\partial T}{\partial z} \right)\Big|_{j^-} \Delta y \right] dx - \int_L \left[[N]^T \left(k \frac{\partial T}{\partial z} \right)\Big|_{j^+} \Delta y \right] dx = 0, \tag{15}$$

where $[B] = \partial [N] / \partial x$, $\bar{n}$ is a unit vector which is normal to the bounding surface *S*, and $k \cdot \partial T_{i,j} / \partial x$ is the flux acting on the boundary *S*. Note that *S* is the remaining part of the fiber's boundary that was not accounted for in Eq. (4).

The flux acting on boundary *S* depends on the conditions specified at that boundary. For a prescribed flux q_b'', it becomes

$$k \frac{\partial T_{i,j}}{\partial x} = q_b'', \tag{16}$$

while for a convective boundary condition, it is given by

$$k \frac{\partial T_{i,j}}{\partial x} = h(T_\infty - T_{i,j}), \tag{17}$$

and for a radiation boundary condition, it turns out to be

$$k \frac{\partial T_{i,j}}{\partial x} = h_r (T_{sur} - T_{i,j}) \tag{18}$$

where the radiation heat transfer coefficient h_r is given by Eq. (12).

The final step of the formulation consists of substituting the finite element approximation of the fiber's temperature, given by Eq. (13), into the governing equation. For a typical interior fiber, Eqs. (5) are substituted into Eq. (15). All three types of boundary conditions in Eqs. (16)-(18) are also substituted into Eq. (15). Boundary terms in Eqs. (8), (9), and (11) for exterior fibers are handled separately. All fiber temperatures are then replaced with the finite element approximation in Eq. (13). Thus, for a typical interior fiber, Eq. (15) becomes

$$\int_V \left([N]^T\ \rho C[N]\{\dot{T}_{i,j}\}\right)dV + \int_V \left([B]^T k[B]\{T_{i,j}\}\right)dV - \int_V [N]^T Q dV - \int_S [N]^T (q_s'' + hT_\infty)\, dS$$
$$+ \int_S [N]^T h[N]\{T_{i,j}\}\, dS + \int_L \left([N]^T \frac{\Delta z\, k_{i^-}}{y_{i,j} - y_{i-1,j}} [N] \right) [\{T_{i,j}\} - \{T_{i-1,j}\}] dx$$
$$- \int_L \left([N]^T \frac{\Delta z\, k_{i^+}}{y_{i+1,j} - y_{i,j}} [N] \right) [\{T_{i+1,j}\} - \{T_{i,j}\}] dx + \int_L \left([N]^T \frac{\Delta y\, k_{j^-}}{z_{i,j} - z_{i,j-1}} [N] \right) [\{T_{i,j}\} - \{T_{i,j-1}\}] dx$$
$$- \int_L \left([N]^T \frac{\Delta y\, k_{j^+}}{z_{i,j+1} - z_{i,j}} [N] \right) [\{T_{i,j+1}\} - \{T_{i,j}\}] dx = 0. \tag{19}$$

Eq. (19) can be written in the following simplified form:

$$[c_{i,j}]\{\dot{T}_{i,j}\} + [k_{i,j}]\{T_{i,j}\} + \left([k_{i^-}]\{T_{i-1,j}\} + [k_{i^+}]\{T_{i+1,j}\} + [k_{j^-}]\{T_{i,j-1}\} + [k_{j^+}]\{T_{i,j+1}\}\right) = \{r_{i,j}\}, \tag{20}$$

where

$$[c_{i,j}] = \int_L [N]^T\ \rho CA[N] dx, \tag{21}$$

$$[k_{i,j}] = \int_L [B]^T kA[B] dx + [k_{i^-}] + [k_{i^+}] + [k_{j^-}] + [k_{j^+}] + [h_{i,j}], \tag{22}$$

$$[k_{i^-}] = \int_L [N]^T \frac{\Delta z\, k_{i^-}}{y_{i,j} - y_{i-1,j}} [N] dx, \tag{23}$$

$$[k_{i^+}] = \int_L [N]^T \frac{\Delta z\, k_{i^+}}{y_{i+1,j} - y_{i,j}} [N] dx, \tag{24}$$

$$[k_{j^-}] = \int_L [N]^T \frac{\Delta y\, k_{j^-}}{z_{i,j} - z_{i,j-1}} [N] dx, \tag{25}$$

$$[k_{j^+}] = \int_L [N]^T \frac{\Delta y\, k_{j^+}}{z_{i,j+1} - z_{i,j}} [N] dx, \tag{26}$$

$$[h_{i,j}] = \int_S [N]^T h[N]\, dS + \int_S [N]^T h_r [N]\, dS, \tag{27}$$

$$\{r_{i,j}\} = \{r_Q\} + \{r_q\} + \{r_h\}, \tag{28}$$

$$\{r_Q\} = \int_L [N]^T QA dx, \tag{29}$$

$$\{r_q\} = \int_S [N]^T q_s''\, dS, \tag{30}$$

$$\{r_h\} = \int_S [N]^T h T_\infty \, dS + \int_S [N]^T h_r T_{sur} \, dS \,. \tag{31}$$

In Eqs. (20)-(31), $[c_{i,j}]$ is the heat capacity matrix for fiber (i, j); $[k_{i,j}]$ is the conductivity matrix for fiber (i, j); $[k_{i^-}]$, $[k_{i^+}]$, $[k_{j^-}]$, and $[k_{j^+}]$ are the adjacent fiber conductivity (AFC) matrices for fiber (i, j); $[h_{i,j}]$ is the convection heat transfer matrix for fiber (i, j), which includes any contributions due to radiation; and $\{r_{i,j}\}$ is the array of thermal loads for fiber (i, j), which is made up of thermal loads due to convective and radiation boundary conditions $\{r_h\}$, prescribed fluxes $\{r_q\}$, and internal heat generation $\{r_Q\}$.

For exterior fibers, Eq. (20) is modified to incorporate the appropriate boundary conditions. For a prescribed flux, the following term is added to $\{r_{i,j}\}$:

$$\{r_{qb}\} = \int_L [N]^T q_b'' \, b_{fib} \, dx \,, \tag{32}$$

where b_{fib} is the appropriate fiber width (i.e., $b_{fib} = \Delta z$ if the boundary condition exists on surface i^+ or i^-, and $b_{fib} = \Delta y$ for surface j^+ or j^-). For a convective condition, the following terms are added to $[k_{i,j}]$ and $\{r_{i,j}\}$, respectively:

$$[h_b] = \int_L [N]^T h b_{fib} [N] dx \,, \qquad \{r_{hb}\} = \int_L [N]^T h T_\infty b_{fib} dx \,. \tag{33}$$

For a radiation condition, the following terms are added to $[k_{i,j}]$ and $\{r_{i,j}\}$, respectively:

$$[h_{rb}] = \int_L [N]^T h_r b_{fib} [N] dx \,, \qquad \{r_{hrb}\} = \int_L [N]^T h_r T_{sur} b_{fib} \, dx \,. \tag{34}$$

4.1.3 Assembling the Fibers

Because the temperature in fiber (i, j) is dependent on the temperatures of adjacent fibers, it is now convenient to define a set of "global" degrees of freedom for the element so that the fiber equations can readily be assembled into a system of element equations. The fiber heat transfer element is subdivided into n_{fib} fibers, each of which has three nodes and, therefore, three degrees of freedom. Thus, the fiber heat transfer element has a total of $3n_{fib}$ degrees of freedom. These degrees of freedom are numbered by considering all fiber temperatures at node 1, then all fiber temperatures at node 2, and finally all fiber temperatures at node 3. Thus,

$$\{T\} = \begin{Bmatrix} \{T_1\} \\ \{T_2\} \\ \{T_3\} \end{Bmatrix} \tag{35}$$

where $\{T_j\}$ is a vector containing the fiber temperatures at node j, i.e.,

$$\{T_j\}^T = \left\{ (T_1)_j, \quad \ldots, \quad (T_{ifib})_j, \quad \ldots, \quad (T_{nfib})_j \right\}. \tag{36}$$

Here, $(T_{ifib})_j$ is the temperature of fiber i_{fib} at node j. Note that fibers are now identified by a single subscript i_{fib}, which ranges from 1 to n_{fib}. By assembling Eq. (20) for all fibers into this system, the element equations given in Eq. (1) are obtained. Note that matrices $[c]$ and $[k]$ have dimensions $3n_{fib}$ x $3n_{fib}$, and $\{r\}$ is a vector with $3n_{fib}$ quantities.

4.2 Verification

The value of the proposed fiber heat transfer element depends on its ability to accurately and efficiently capture the thermal response of frame members subjected to any type of thermal conditions, including non-uniform heating over the cross-section and along the length. Thus, to verify the element formulation, a series of analyses is carried out on the rectangular steel bar shown in Fig. 4-4. In the following examples, the steel bar is subjected to various types of heating, and the transient temperature distributions are calculated using the fiber heat transfer element. Results are compared to finite element analyses conducted in ABAQUS (2007) using traditional solid finite elements. Material properties for steel are assumed constant and independent of temperature. In the following analyses, the fiber heat transfer element is implemented in ABAQUS as a user-defined element (UEL).

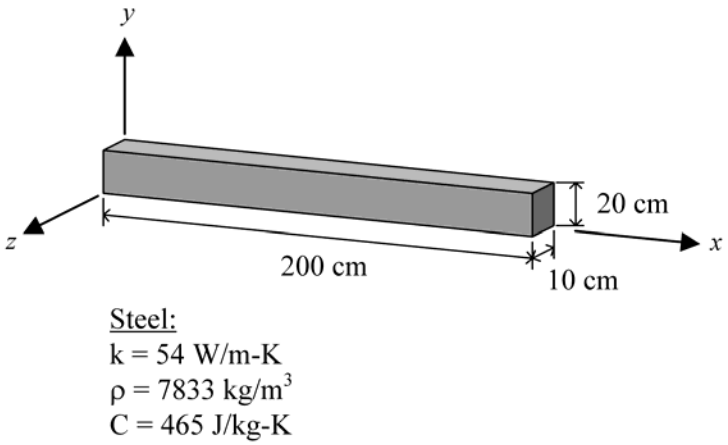

Fig. 4-4. Rectangular steel bar

4.2.1 1D Heat Transfer over the Member's Cross-section

To demonstrate the element's ability to model 1D heat transfer over the member's cross-section, the heating schemes depicted in Fig. 4-5 are considered. The bar is insulated at the ends and heated uniformly along the length so that temperatures only vary over the member's cross-section. In both cases, the bar is given an initial temperature of 0^{o}C and then heated accordingly. These problems are modeled using a single fiber heat transfer element and verified using a fine mesh of solid finite elements in ABAQUS. Various fiber meshes are considered for each case.

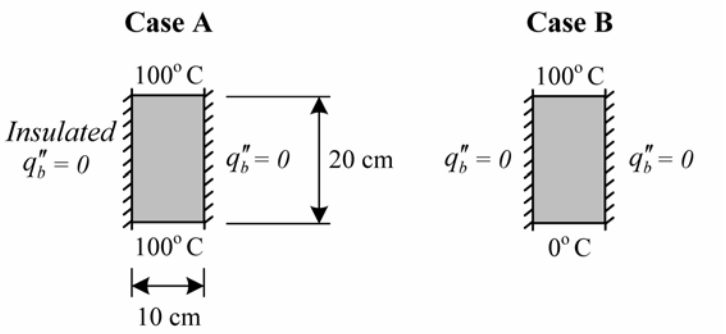

Fig. 4-5. Thermal boundary conditions for 1D heating of the bar's cross-section

For Case A, a temperature of 100^{o}C is maintained at the top and bottom of the bar while the sides of the bar are insulated. Under this heating, the temperature of the bar increases to a constant steady-state temperature of 100^{o}C. Case B is similar to Case A, except the temperature at the bottom of the bar is fixed at 0^{o}C. This heating results in a linear temperature gradient over the depth of the beam at the steady state. For both cases, two fiber meshes, shown in Fig. 4-6(a) and (b), are considered: 15 fibers in a 3x5 grid, and 45 fibers in a 5x9 grid.

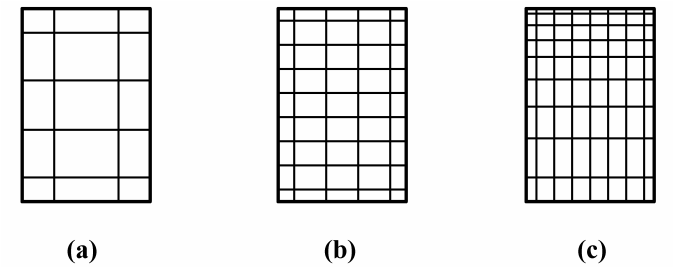

Fig. 4-6. Fiber meshes: (a) 15 fibers in a 3x5 grid, (b) 45 fibers in a 5x9 grid, and (c) 72 fibers in an 8x9 grid

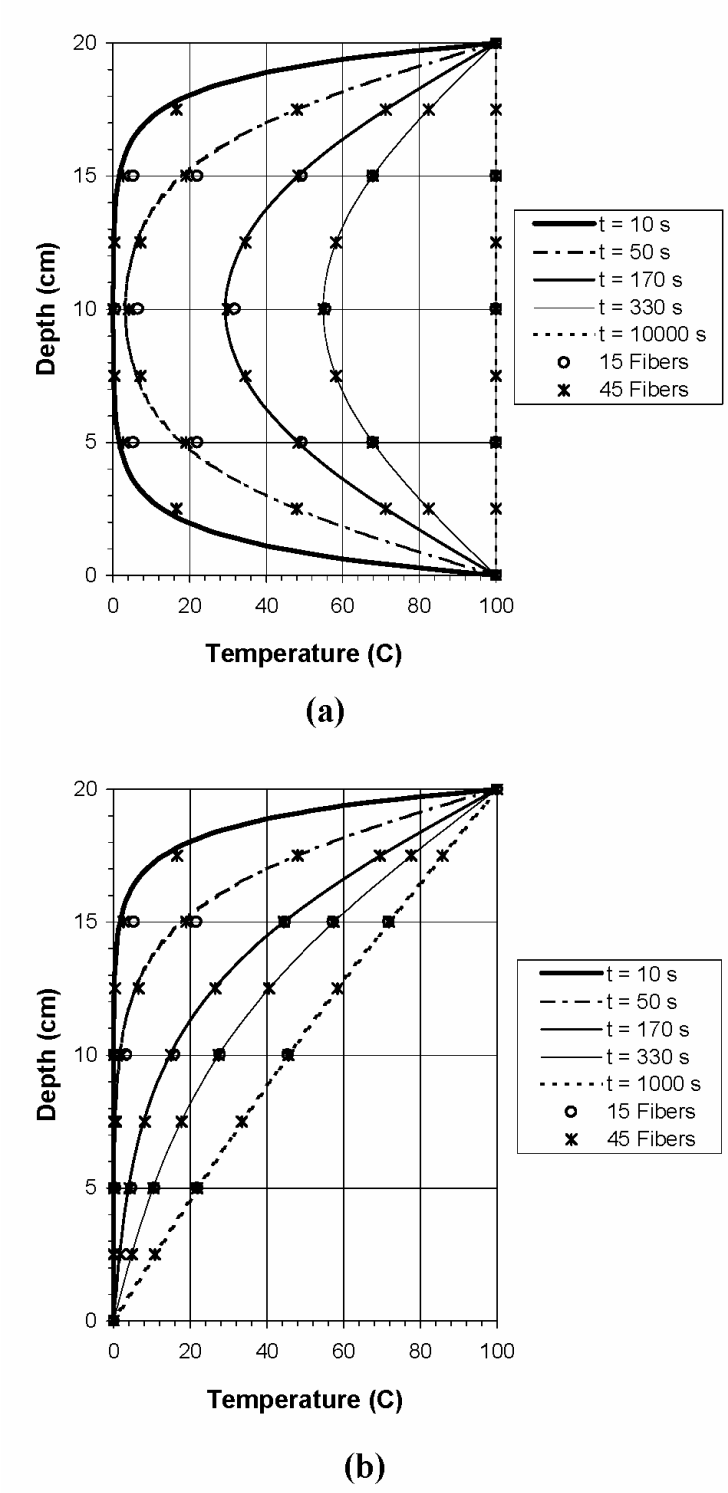

Fig. 4-7. Temperature over the depth of the bar at various times: (a) for Case A, and (b) for Case B. (Solid or dashed lines correspond to the converged finite element solution.)

Temperatures over the depth of the beam are plotted for various times in Fig. 4-7. The "exact" solution (obtained in ABAQUS using 2D solid finite elements) is represented by solid or dashed lines, while the results from the fiber heat transfer element are represented by data points. Note that good agreement is obtained for both cases. To better gauge the accuracy of the fiber element, the 2-norm error is calculated over the depth of the beam at various times. These errors are presented in Table 4-1. While both fiber meshes yield good agreement with the "exact" solution, greater accuracy is achieved using more fibers. Errors also tend to decrease as time progresses.

While it is acknowledged that this is not a good example to illustrate the efficiency of the proposed element, statistics were collected to show that even for such a simple example the proposed element performs well. For Cases A and B, heat transfer analyses are conducted in ABAQUS using traditional 1D, 2D, and 3D finite elements. Finite element meshes are selected to provide the same level of accuracy as the fiber heat transfer element. The number of degrees of freedom (DOFs) for each model and the total CPU time for each analysis are reported in Table 4-2. Note that, for Cases A and B, the times reported for the fiber heat transfer element correspond to analyses conducted using a single fiber element with a mesh of 45 fibers. In both Cases A and B, the fiber heat transfer element requires slightly more computational power than the 1D and 2D analyses. However, the fiber element offers significant time savings when compared to the full-blown 3D heat transfer analysis.

Table 4-1. 2-Norm Errors for Cases A and B at Various Times

	2-Norm Error (%)			
	Case A		**Case B**	
Time (sec)	**15 Fibers**	**45 Fibers**	**15 Fibers**	**45 Fibers**
10	3.70	3.83	3.63	3.67
50	4.57	1.49	3.95	1.23
170	1.74	0.50	1.30	0.39
330	0.33	0.08	0.45	0.13
$t \to \infty$	0.00	0.00	0.00	0.00

4.2.2 2D Heat Transfer over the Member's Cross-section

The element's ability to model 2D heat transfer over the member's cross-section is verified using the example shown in Fig. 4-8. For this case, the bar has an initial temperature of 0^{o}C. A temperature of 100^{o}C is instantaneously applied to the top of the

bar while the temperatures at the remaining sides are fixed at 0^{o}C. Like Cases A and B, the bar is insulated at the ends and heated uniformly along the length so that temperatures only vary over the member's cross-section. This example is modeled with a single fiber element and the steady-state solution is checked against the analytical solution provided by Incropera and DeWitt (2002). Two fiber meshes (shown in Fig. 4-6(b) and (c)) are considered: 45 fibers in a 5x9 grid, and 72 fibers in an 8x9 grid. Note that the mesh with 72 fibers is concentrated near the top of the bar in the region where the greatest temperature changes are expected.

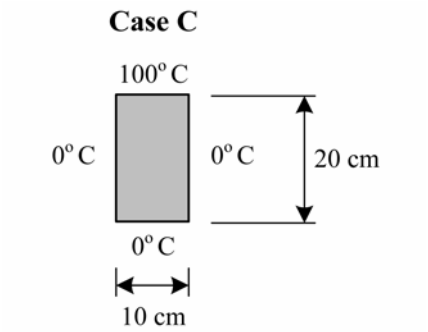

Fig. 4-8. Thermal boundary conditions for 2D heating of the bar's cross-section

Cross-sectional temperatures at steady state are shown in Fig. 4-9. Thermal contours for the "exact" analytical solution are plotted in Fig. 4-9(a), while results using the fiber element are shown in Fig. 4-9(b) and (c). Discrete fiber temperatures for the two fiber meshes are also shown in Fig. 4-9(d) and (e). Note that both fiber meshes yield a good approximation of the thermal response of the bar, although the finer mesh yields more accurate results.

Simulation times are shown in Table 4-2. For this case, 2D and 3D heat transfer analyses are conducted in ABAQUS using traditional finite elements. The time reported for the fiber heat transfer element represents the simulation time for an analysis using a single fiber heat transfer element with 72 fibers. Again, the fiber element requires slightly more computational power than the 2D analysis but only a fraction of the time needed to perform a full 3D analysis.

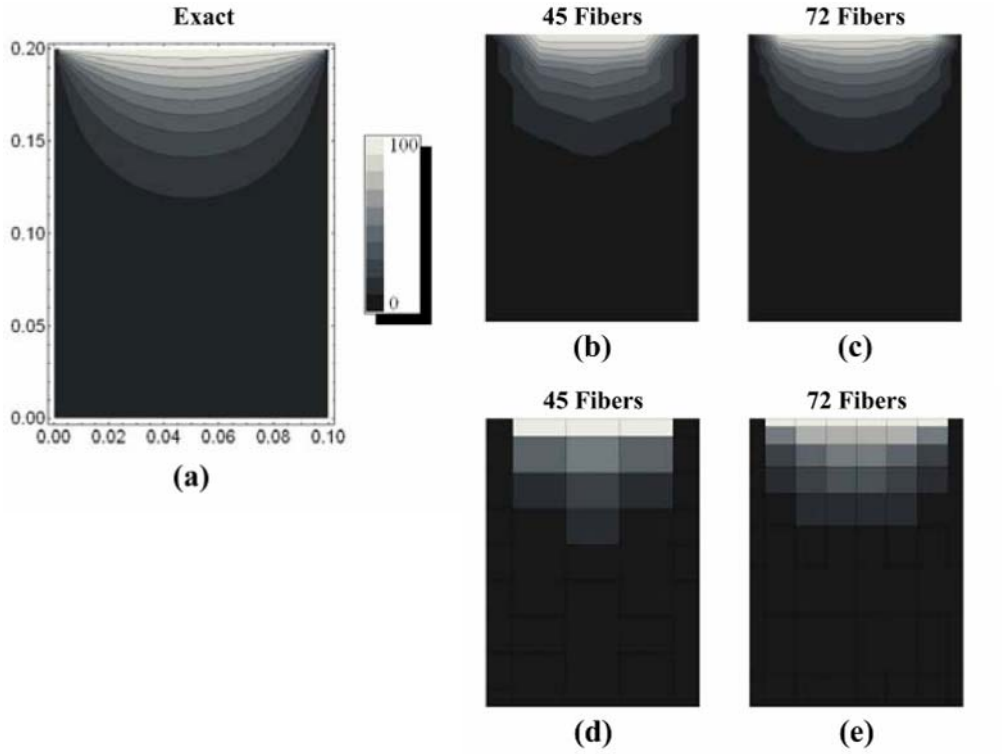

Fig. 4-9. Steady-state temperatures for Case C: (a)-(c) Thermal contours, and (d)-(e) discrete fiber temperatures

Table 4-2. Comparison of CPU Times for Cases A, B, and C

		Total CPU Time (s)		
Analysis	**No. of DOFs**	**Case A**	**Case B**	**Case C**
1D FEA	11	0.40	0.30	-----
2D FEA	60	0.40	0.40	0.40
3D FEA	2117	3.90	3.50	3.50
Fiber Element	**135 to 216**	**0.60**	**0.70**	**0.80**

4.2.3 Non-uniform Heating over Member's Length

To evaluate the fiber heat transfer element's ability to capture the thermal response in a structural member with non-uniform temperature distributions along the length and over the cross-section, the heating scheme shown in Fig. 4-10 is considered. In this case, the bar is heated by a distributed flux of 30 kW/m^2 that varies along the length in a stepwise manner. While a step flux is unlikely to be encountered in nature, this type of heating yields the most extreme thermal gradients over the length of the member (Franssen et al., 2007). The ends of the bar are insulated, and the remainder of the bar is cooled to 20^{o}C by a convective boundary condition. The sides of the bar are also insulated so that temperatures do not vary over the width of the bar. The bar has an initial

temperature of 20°C. Symmetry is utilized so that only the lower half of the bar is modeled with the fiber heat transfer element. Shown in Fig. 4-11, the fiber mesh consists of 55 fibers arranged in a 5x11 grid over the lower half of the bar. This problem is solved using two and four elements along the length of the bar.

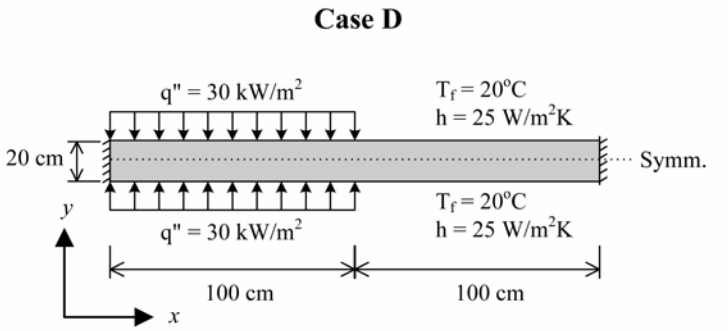

Fig. 4-10. Thermal boundary conditions for non-uniform heating along the length of the bar

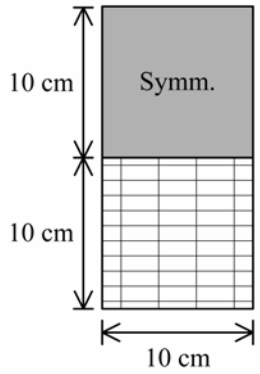

Fig. 4-11. Fiber mesh on lower half of bar: 55 fibers in a 5x11 grid

Surface temperatures over the length of the bar are plotted in Fig. 4-12 at various times. “Exact” solutions are represented by solid, bold lines, while results using the fiber heat transfer element are represented by solid or dashed lines marked with symbols. In general, results compare well with the “exact” solution. 2-Norm errors are calculated for the surface temperatures at various times and are presented in Table 4-3. While using two elements along the length results in somewhat significant errors (particularly at earlier times), excellent accuracy is achieved by using four fiber elements along the length.

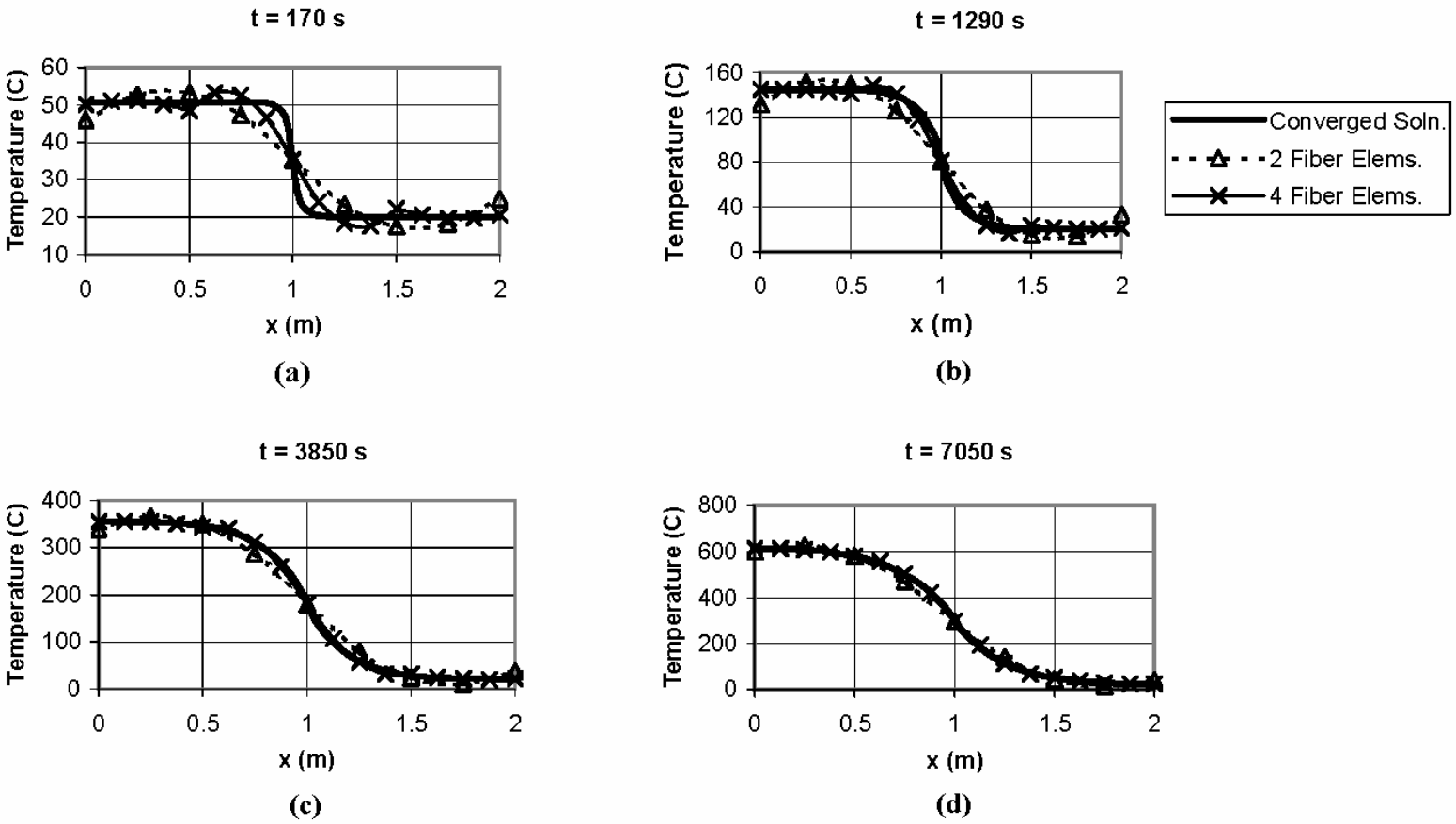

Fig. 4-12. Surface temperatures over the length for Case D at (a) 170 s, (b) 1750 s, (c) 3850 s, and (d) 7050 s.

Table 4-3. 2-Norm Errors for Case D at Various Times

	2-Norm Error (%)	
Time (s)	**2 Elements**	**4 Elements**
170	9.09	3.62
1750	8.98	1.64
3850	4.64	0.58
7050	2.47	0.36

Table 4-4. Comparison of CPU Times for Case D

Analysis	**No. of DOFs**	**Total CPU Time (s)**
2D FEA	645	1.50
3D FEA	3288	14.00
2 Fiber Elements	275	1.40
4 Fiber Elements	495	2.40

The efficiency of the fiber heat transfer element is demonstrated through a comparison of simulation times and number of degrees of freedom for various analyses. In Table 4-4, results from the fiber heat transfer element using two and four elements are shown as well as results from 2D and 3D heat transfer analyses conducted in ABAQUS. Note that, for this example, it is almost as efficient to use the fiber heat transfer element as to conduct a 2D finite element analysis. In a realistic fire situation, however, the temperatures will likely vary over the member's width as well, and so a 2D analysis would not suffice. When compared to the 3D analysis conducted in ABAQUS, the fiber heat transfer elements are much more efficient.

4.3 Application

To further illustrate the capabilities of the fiber heat transfer element, a more realistic application is considered. Wainman and Kirby (1988) provide the details of a series of experimental tests conducted on steel columns with blocked-in webs subjected to the standard ISO 834 fire (ISO, 1999). The experimental tests determined the fire resistance of four columns with varying cross-sectional dimensions and applied loads. The test set-up is illustrated in Fig. 4-13. As shown in Fig. 4-13, thermocouples were placed in the flanges and web of the steel section to measure the temperatures in the steel at various locations along the length of the column. Average furnace temperatures were reported throughout the duration of the test.

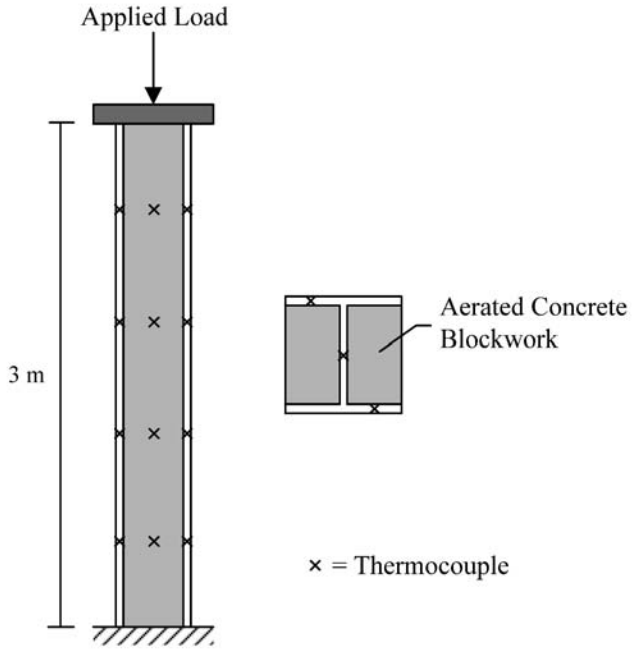

Fig. 4-13. Test setup for the steel columns with blocked-in webs (adapted from Wainman and Kirby, 1988)

The thermal response of one of the steel columns with blocked-in webs (i.e., test number TE 5154) is analyzed using a single fiber heat transfer element. Because the problem is symmetric, only one-fourth of the cross-section is modeled, as shown in Fig. 4-14. To simulate the fire behavior in the furnace, both convective and radiative boundary conditions are applied at the surface of the column. The convective heat transfer coefficient h is assumed to be 25 W/m^{2}K, and the emissivity ε is assumed to be 0.5 for steel and 0.8 for concrete. Rather than use the measured furnace temperatures in the analyses, the furnace temperatures are assumed to follow standard ISO 834 fire curve for simplicity. It is also assumed that the furnace temperatures do not vary over the length of the column. To account for temperature-dependent material properties, the Eurocode models for steel (EN 1993-1.2, 2005) and the concrete blockwork (EN 1996-1.2, 2005) are employed. As permitted by the Eurocode, the effects of moisture evaporation in the concrete blockwork are conservatively ignored.

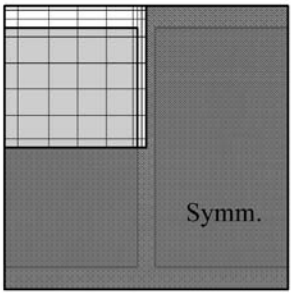

Fig. 4-14. Fiber mesh over one-fourth of the cross-section: 72 fibers in an 8x9 grid

The average flange and web temperatures in the steel are shown in Figure 4-15. The experimental values are represented with solid lines, while results obtained with the fiber heat transfer element are shown as dashed lines with data points. In general, the fiber heat transfer element tends to overestimate the temperatures in the steel. This is to be expected because the moisture evaporation in the concrete blockwork was ignored. Despite these errors, the fiber heat transfer element gives a reasonable prediction of the thermal response for this example.

4.4 Conclusions

This paper introduces a new type of heat transfer finite element that can be used to model the 3D thermal response in structural frames subjected to fire. Because it uses both finite element and finite difference approximations of the governing heat transfer equation, the fiber heat transfer element balances solution accuracy and computational efficiency in obtaining the transient thermal response of frames subjected to realistic (i.e., non-uniform) heating associated with fire. Although the element formulation is derived from a mixture of methods, the element equations are in a form that can readily be implemented into an existing finite element analysis program.

Because the fiber heat transfer element is purposely designed for compatibility with any fiber beam-column element, it offers a great simplification in performing sequentially-coupled analyses of frame structures in fire. By interpolating the temperatures along the length of the member using the element shape functions, the fiber heat transfer element allows the temperatures to be calculated directly at the Gauss points

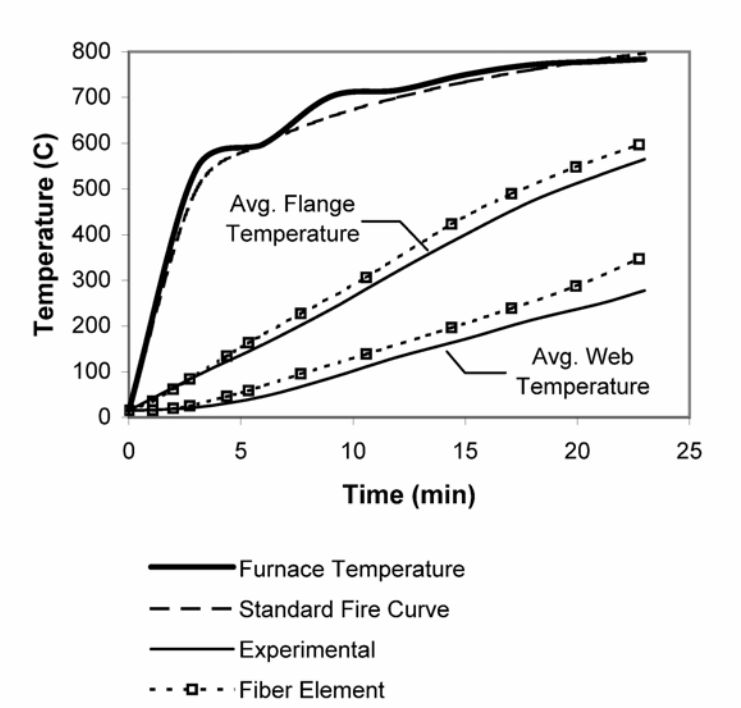

Fig. 4-15. Temperatures in the steel column with blocked-in web (Test No. TE 5154)

for the structural element. This is a task that cannot be readily accomplished when using 3D solid finite elements to perform the heat transfer analysis.

In this paper, the element formulation is verified by a number of analyses conducted on a rectangular steel bar subjected to various types of thermal loads. Results indicate that the element can accurately model temperature distributions in a member with a variety of thermal loads. The solution quickly converges to the exact solution with the use of more fibers over the cross-section and more elements along the length. With as few as four elements along the length, the fiber heat transfer element can provide an accurate prediction of the thermal response in members subjected to the most extreme case of non-uniform heating. Comparisons with traditional finite element analyses show that the fiber heat transfer element is comparable to 1D and 2D heat transfer analyses in terms of computational efficiency and offers significant time-savings when compared to full-blown 3D heat transfer analyses.

The full capacity of the fiber heat transfer element is demonstrated by considering the thermal response of a steel column with blocked-in web subjected to the standard ISO 834 fire. Results indicate that the fiber heat transfer element can effectively model the

thermal behavior in members comprising more than one material and with temperature-dependent material properties.

4.5 Notation

The following symbols are used in this paper:

A = area of fiber (i, j)

$[B]$ = first derivative of the shape function matrix with respect to x (i.e., $d[N]/dx$)

C = specific heat

$[c]$ = heat capacity matrix for the element

$[c_{i,j}]$ = heat capacity matrix for fiber (i, j)

h = heat transfer coefficient

h_r = radiation heat transfer coefficient

$[h_{i,j}]$ = convection heat transfer matrix for fiber (i, j)

i = integer representing the location of fiber (i, j) with respect to the local y-axis

i^+, i^-, $i^\pm$ = symbols denoting fiber boundaries between grid points in the y-direction (i.e., $i \pm ½$)

j = integer representing the location of fiber (i, j) with respect to the local z-axis

j^+, j^-, $j^\pm$ = symbols denoting fiber boundaries between grid points in the z-direction (i.e., $j \pm ½$)

k = thermal conductivity

$k_{i^\pm}$, $k_{j^\pm}$ = effective conductivities at the fiber interfaces

$[k]$ = conductivity matrix for the element

$[k_{i,j}]$ = conductivity matrix for fiber (i, j)

$[k_{i^-}]$ = AFC matrix for fiber (i, j): contribution of fiber $(i - 1, j)$

$[k_{i^+}]$ = AFC matrix for fiber (i, j): contribution of fiber $(i + 1, j)$

$[k_{j^-}]$ = AFC matrix for fiber (i, j): contribution of fiber $(i, j - 1)$

$[k_{j^+}]$ = AFC matrix for fiber (i, j): contribution of fiber $(i, j + 1)$

L = element length

$\bar{n}$ = unit vector normal to boundary surface S

$[N]$ = shape function matrix for fiber (i, j)

q_b'' = prescribed heat flux

Q = internal heat generation per unit volume

$\{r\}$ = array of thermal loads for the element

$\{r_{i,j}\}$ = array of thermal loads for fiber (i, j)

$\{r_h\}$ = thermal loads due to convective boundary conditions

$\{r_q\}$ = thermal loads due to prescribed fluxes

$\{r_Q\}$ = thermal loads due to internal heat generation

S = boundary surface

t = time

$T = T(x, y, z, t)$; temperature

$T_{i,j} = T_{i,j}(x, t)$; temperature of fiber (i, j)

T_{sur} = temperature of the surroundings (for radiation exchange)

T_∞ = fluid temperature

$\{T\}$ = array of nodal temperatures for the element

$\{\dot{T}\}$ = first derivative of nodal temperatures with respect to time (i.e., $\partial\{T\}/\partial t$)

$\{T_j\}$ = array of fiber temperatures at node j

$\{T_{i,j}\}$ = nodal temperatures for fiber (i, j)

V = volume of fiber (i, j)

$y_{i,j}$ = y-coordinate of fiber (i, j)

$z_{i,j}$ = z-coordinate of fiber (i, j)

Δy = height of fiber (i, j)

Δz = width of fiber (i, j)

ε = emissivity

ρ = mass density

σ = Stefan-Boltzmann constant (5.67×10^{-8} W/m$^2 \cdot$ K^4)

Chapter 5: "Modeling Structural Response in Fire using a Fiber-Based Approach"

Ann E. Jeffers and Elisa D. Sotelino

[A manuscript to be submitted for publication in the *Journal of Constructional Steel Research*]

Abstract

This paper presents a new approach to modeling the thermal-mechanical response of structural frames subjected to realistic fire conditions. The method involves the use of two finite elements: (1) a special-purpose fiber heat transfer element for analyzing the 3D thermal response of non-uniformly heated structural frames, and (2) a flexibility-based fiber beam-column finite element for simulating the force-deformation response of structural frames at elevated temperatures. The two elements have been implemented in ABAQUS (2007) using a user-defined element (UEL) subroutine and can be used collectively to perform sequentially coupled analyses of structural frames under fire conditions. Analyses of benchmark experimental tests on steel structures demonstrate that both elements individually and collectively provide excellent accuracy. Furthermore, the fiber-based approach offers a great simplification in transferring results from the thermal analysis to the structural analysis because the two elements have identical meshes.

5.1 Introduction

Existing methods for analyzing the response of structures under fire conditions range in complexity from simple design equations to advanced computational methods. Simplistic approaches may fail to capture important aspects of the response, while advanced numerical approaches can be computationally expensive, particularly when three-dimensional (3D) problems are considered. To achieve a balance between accuracy and computational efficiency, Jeffers and Sotelino (2009) developed a special-purpose fiber heat transfer element, which is shown in Fig. 5-1, to simulate the 3D thermal response of structural frames subjected to non-uniform thermal loads. Based on a combination of finite element and finite difference methods, the fiber heat transfer

element can account for 3D temperature differences as well as variations in material properties over the section. The element was formulated specifically for compatibility with any distributed plasticity frame finite element for performing sequentially coupled thermal-mechanical analyses of structural frames in fire. Analyses showed that the fiber heat transfer element can accurately and efficiently predict the thermal response of structures subjected to various types of heating.

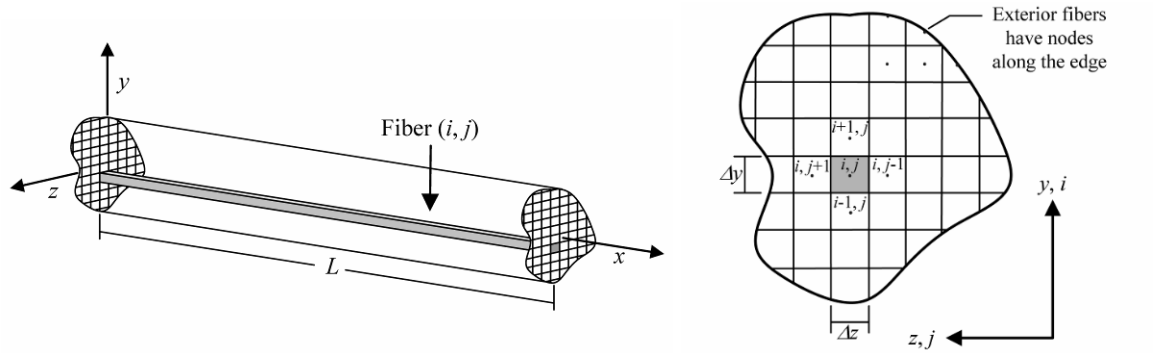

Fig. 5-1. The fiber heat transfer element (Jeffers and Sotelino, 2009)

This paper extends the work of Jeffers and Sotelino (2009) by using the fiber heat transfer element with a beam-column element to model the thermal and mechanical response of structures subjected to fire. Because the fiber heat transfer element is able to provide a large amount of data about the thermal response, it should ideally be used with a fiber beam-column element that is capable of extracting as much thermal data as possible from the heat transfer analysis. While the ABAQUS (2007) element library includes distributed plasticity elements that are able to model structural response at elevated temperatures, these elements are not recommended for use with the fiber heat transfer element because they are only capable of handling temperature data at a few points over the cross-section. S fiber beam-column element that is fully compatible with the fiber heat transfer element is described in this paper.

The fiber beam-column element presented here differs from existing elements for modeling structural response in fire in that it is based on the flexibility method of analysis. In the analysis of structures at room temperature, flexibility-based elements tend to improve computational efficiency because fewer elements are needed per member.

This paper investigates whether this feature holds true in the analysis of structures at elevated temperatures. The element presented here extends the formulation by Taucer et al. (1991) to include thermal effects, geometric nonlinearities, and residual stresses.

The full potential of the fiber-based approach is demonstrated herein by using the fiber heat transfer element with the flexibility-based fiber beam-column element to simulate the response of structures under realistic fire conditions. Analyses of benchmark experimental tests on steel structures are presented to demonstrate the capabilities of both fiber-based elements in modeling the thermal and mechanical response of structures in fire.

5.2 Literature Review

The plastic hinge and plastic zone (or distributed plasticity) methods have proven to be particularly effective at capturing the nonlinear response of structural frames under fire conditions. Both of these methods use frame elements to represent beams and columns. However, the two methods differ in the manner in which yielding is incorporated in the analysis. In the plastic hinge method, yielding is lumped in a plastic region of zero length. To account for gradual yielding of the section, the plastic hinge is given a nonlinear stiffness based on an approximation of the response beyond yield. In the plastic zone method, yielding is modeled by dividing the cross-section into a series of fibers and tracking the stresses within each of these fibers at specific control sections along the length of the member. While the plastic hinge elements tend to be more efficient, the distributed plasticity elements generally provide a more realistic representation of the structural response beyond yield. As a result, a number of distributed plasticity finite elements have been developed for modeling structural response under fire conditions (Tan et al., 2002; Cai et al., 2003, Liew and Chen, 2004; Di Capua and Mari, 2007; Kodur and Dwaikat, 2008).

Existing frame finite elements for modeling structural response in fire are limited to the stiffness method of analysis, in which the element equations are based on an assumption of the displacement field. Conventional displacement-based elements often experience loss of accuracy and efficiency for problems involving highly nonlinear structural behavior. As a result, recent efforts have focused on the development of

flexibility-based and mixed element formulations for modeling structural response at room temperature (Spaconi et al., 1996; Petrangeli and Ciampi, 1997; Neuenhofer and Filippou, 1997; Nukala and White, 2004; Adessi and Ciampi, 2007). In the flexibility-based elements, the force distribution, rather than the displacement field, is assumed through the selection of force interpolation functions. These force interpolation functions can be chosen such that equilibrium is strictly enforced throughout the element. The mixed element approach builds on the flexibility method such that the internal forces and deformations are interpolated separately. In a comparison by Alemdar and White (2005), the flexibility-based and mixed element formulations generally provided greater accuracy than the displacement-based elements in nonlinear structural problems at room temperature. Because the flexibility-based and mixed formulation elements have been successfully used to model nonlinear structural response at room temperature, it is of interest to investigate the possibility of using such elements to model structural response under fire conditions, a problem that involves geometric and material nonlinearities as well as temperature-dependent material properties and time-varying thermal loads.

5.3 Fiber-Based Approach

The fiber-based approach to modeling structural frames in fire involves two sequentially coupled analyses. First, the thermal response of the structure is evaluated by a heat transfer analysis conducted with the fiber heat transfer element, which is shown in Fig. 5-1. Using the temperatures from the heat transfer analysis as the input, the force-deformation response of the structure is then determined using the fiber-beam column element, which is shown in Fig. 5-2. The fiber-based approach is superior to traditional methods of analysis because it allows the 3D thermal response of structures to be evaluated in an efficient manner and simplifies the transfer of temperature data to the structural analysis because both elements have the same mesh. Jeffers and Sotelino (2009) provide a detailed formulation of the fiber heat transfer element. The flexibility-based fiber beam-column element is described in the following section.

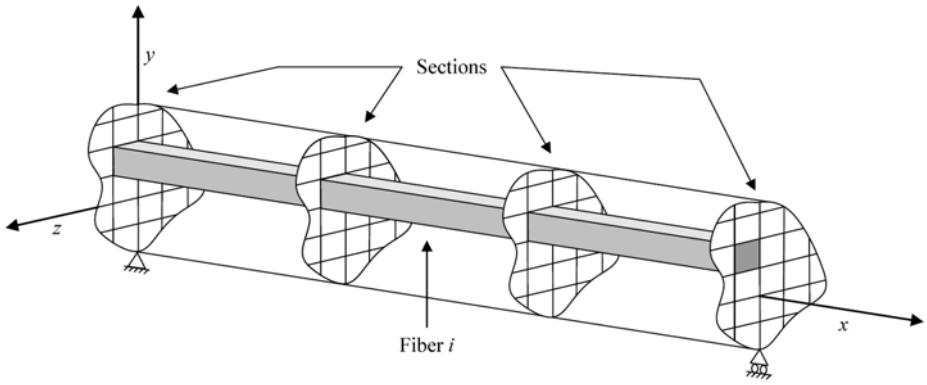

Fig. 5-2. The fiber beam-column element

5.3.1 Flexibility-Based Fiber Beam-Column Element

The fiber beam-column element shown in Fig. 5-2 is a distributed plasticity element that was originally formulated by Taucer et al. (1991) to simulate the response of reinforced concrete structures subjected to seismic loads. Based on the flexibility method of analysis, the element formulation involves an iterative state determination process in which the converged solution satisfies equilibrium, compatibility, and the material constitutive law within a prescribed tolerance. The element formulation is extended here to account for thermal effects associated with fire. Geometric nonlinearities are included using a total Lagrangian corotational transformation (Crisfield, 1991), in which natural deformations are handled separately from the rigid body displacements of the element. This paper considers a two-dimensional formulation of the element, but the formulation can easily be extended to three-dimensional space.

As illustrated in Fig. 5-3, the element degrees of freedom are defined at three levels: (1) the nodal forces $\{f\}$ and displacements $\{u\}$ at the element level, (2) the nodal forces $\{r\}$ and deformations $\{d\}$ within the corotational reference frame, and (3) the section forces $\{r_s(x)\}$ and deformations $\{d_s(x)\}$ within the corotational reference frame. It is assumed that deformations within the corotational reference frame are small. Large displacements are handled through geometric transformations of the corotational reference frame.

Because the element is flexibility-based, the section forces $\{r_s(x)\}$ (i.e., the axial force $N(x)$ and bending moment $M(x)$ along the element's length) are interpolated from the nodal forces $\{r\}$ using force interpolation functions, i.e.,

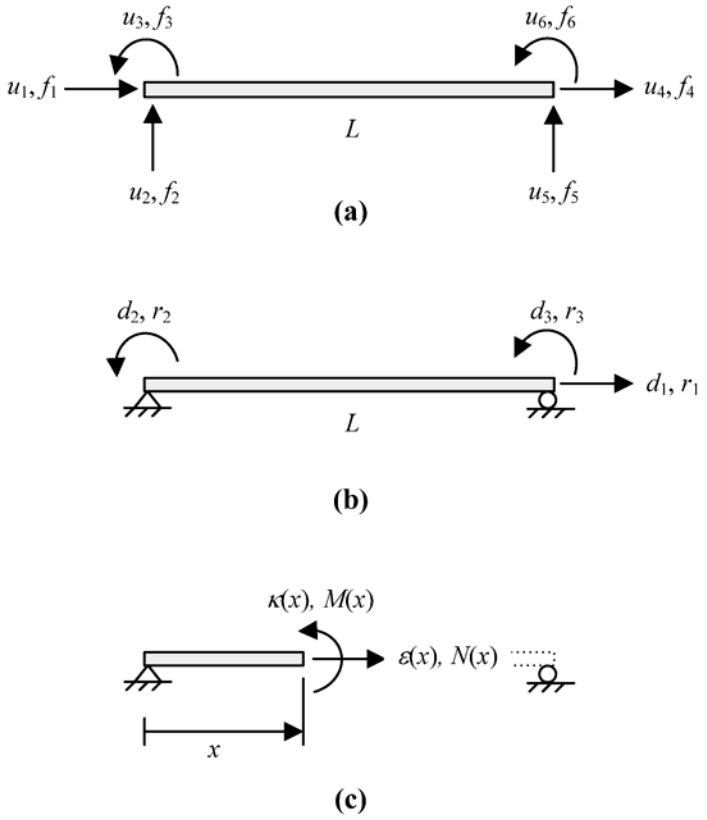

Fig. 5-3. Element degrees of freedom: (a) at the element level, (b) within corotational reference frame, and (c) at the section level

$$\{r_s(x)\} = [b(x)]\{r\}, \tag{1}$$

where $[b(x)]$ is the force interpolation function matrix. The force interpolation functions are chosen such that the axial force is constant along the length of the element and the bending moment varies linearly. This selection of interpolation functions ensures that equilibrium is satisfied along the element's length for the case when no element loads are applied.

The procedure for determining the element tangent stiffness matrix is described as follows. First, the section stiffness matrix $[k_s(x)]$ is determined by

$$[k_s(x)] = \begin{bmatrix} \sum_{i=1}^{n} E_i A_i & -\sum_{i=1}^{n} E_i A_i y_i \\ -\sum_{i=1}^{n} E_i A_i y_i & \sum_{i=1}^{n} E_i A_i y_i^{\,2} \end{bmatrix}, \tag{2}$$

where the subscript *i* indicates the fiber, *n* is the number of fibers in the cross-section, E_i is the tangent modulus of fiber *i* (determined from the appropriate uniaxial stress-strain relationship, which may be dependent on temperature), A_i is the area of fiber *i*, and y_i is the centroidal coordinate of fiber *i* with respect to the element's local coordinate axis. The section flexibility matrix $[f_s(x)]$ is then obtained by inverting the section stiffness matrix, i.e., $[f_s(x)] = [k_s(x)]^{-1}$. Applying the principle of virtual forces, the element flexibility matrix is obtained from

$$[f] = \int_0^L [b(x)]^T [f_s(x)][b(x)]dx. \tag{3}$$

Lastly, the element stiffness matrix $[k]$ is obtained by inverting the element flexibility matrix, i.e., $[k] = [f]^{-1}$ (Taucer et al., 1991).

While the flexibility-based fiber beam-column element offers the advantage of strictly enforcing equilibrium within the element, a challenge arises when the element is implemented into a finite element program that is based on the stiffness method of analysis because, without the availability of displacement interpolation functions, there is no direct way to back-calculate the internal element forces from the nodal displacements. To overcome this problem, Taucer et al. (1991) developed a nonlinear solution algorithm to recover the internal element forces from the nodal displacements. The process involves an iterative loop at the element level in which force unbalances yield correctional deformations. Displacement compatibility is enforced by integrating the section deformations over the length of the element to obtain the nodal deformations. Through iterations at the section level, the material constitutive law is satisfied within a prescribed tolerance. The algorithm, described in detail by Taucer et al. (1991), has been proven to be computationally stable for problems involving nonlinear material behavior. Once convergence is achieved, the element stiffness matrix $[k]$ and nodal force vector $\{r\}$ are assembled into the global system of equations.

To use the fiber beam-column element to model the response of structures in fire, the formulation must be extended to account for thermal effects and residual stresses due to differential cooling during fabrication. To achieve this, a new equation for computing the fiber strain is used. Based on the assumption that plane sections remain plane, the strain in fiber *i* is calculated within the solution algorithm as

$$\varepsilon_i(x) = \varepsilon(x) - y_i\kappa(x) - \varepsilon_{th}(x) + \varepsilon_{res}(x), \quad (4)$$

where $\varepsilon(x)$ is the axial strain in the member, $\kappa(x)$ is the curvature, $\varepsilon_{th}(x)$ is the strain due to thermal expansion (i.e., $\varepsilon_{th}(x) = \alpha_T \Delta T$, where α_T is the coefficient of thermal expansion for the material at temperature T, and ΔT is the change in temperature), and $\varepsilon_{res}(x)$ is the residual strain due to differential cooling during fabrication. Note that, because the element is based on the flexibility method, the thermal strains are applied directly at the section level rather than at the nodes (i.e., in the form of equivalent nodal forces).

5.4 Verification

The fiber heat transfer element and the fiber beam-column element are validated through analyses of benchmark experimental tests on steel structures subjected to elevated temperatures. Both fiber elements are implemented in ABAQUS (2007) using a user-defined element (UEL) subroutine. The linear residual stress pattern shown in Fig. 5-4 is used, for which the maximum residual stress is $0.5\sigma_y$ for d/b less than 1.2 and $0.3\sigma_y$ for d/b greater than 1.2 (Chan and Chan, 2001). The following examples involve cases of uniform and non-uniform heating of steel structures.

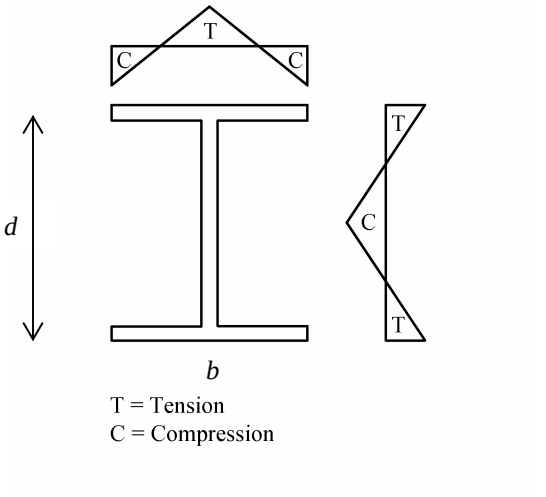

Fig. 5-4. Residual stress pattern

5.4.1 Uniformly Heated Steel Beams

Rubert and Schaumann (1986) conducted a series of experimental tests on simply supported steel I-beams subjected to uniform heating. As illustrated in Fig. 5-5, the test beams were loaded at mid-span and heated uniformly at a constant rate until failure. The mid-span deflection was measured at various temperatures. The tests considered the effects of heating rate and load ratio (i.e., the ratio of the applied load to the ultimate capacity of the beam at room temperature) on the fire resistance of steel beams. This problem has been analyzed numerically by Izzuddin et al. (2000), Chan and Chan (2001), Liew and Chen (2004), and Hojzan et al. (2007), among others.

The tests are modeled using two fiber beam-column elements, each with 77 fibers over the cross-section, as illustrated in Fig. 5-6. Because the beams were heated uniformly and because of the high thermal conductivity of the steel, temperatures within the steel are assumed to be constant and equal to the furnace temperatures (i.e., heat transfer analyses are not performed). Temperature-dependent material properties for steel

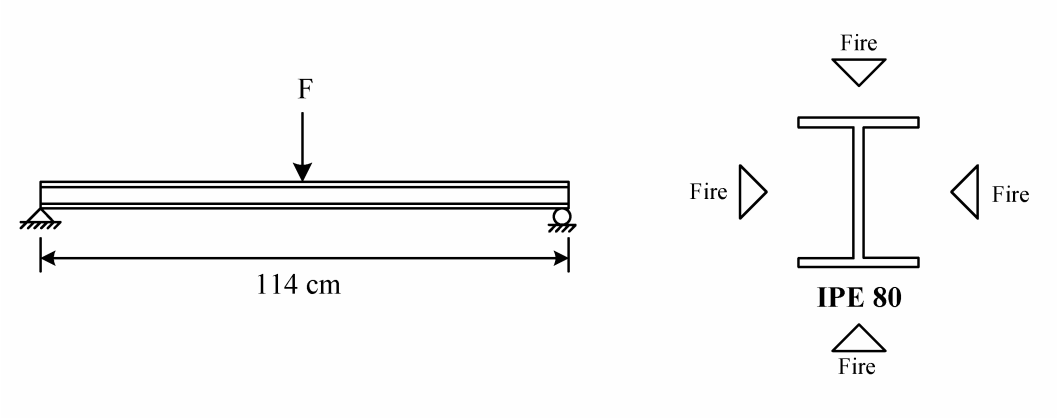

Fig. 5-5. Uniformly heated steel beam (adapted from Rubert and Schaumann, 1986)

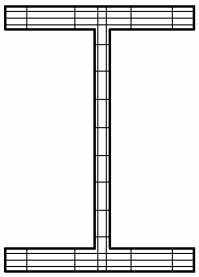

Fig. 5-6. Fiber mesh (77 fibers)

are obtained from the Eurocode (EN 1993-1.2). Note that the Eurocode model for steel is independent of heating rate (i.e., creep effects are accounted for implicitly) and so the effects of heating rate are not accounted for in these analyses. Four load ratios are considered: 0.20, 0.50, 0.70, and 0.85.

To evaluate the performance of the flexibility-based fiber element, this problem is also analyzed using B21 beam elements in ABAQUS. The B21 element is a 2-node distributed plasticity finite element that is based on the stiffness method. The B21 element is capable of modeling geometric and material nonlinearities, and allows temperature data to be specified at only three integration points over the depth of the beam. The Eurocode model for steel is defined in ABAQUS as metal plasticity with isotropic hardening. Residual stresses are not included in the B21 elements.

The mid-span deflection is plotted as a function of temperature in Fig. 5-7. Experimental values are represented by data points. Results using the fiber beam-column element are shown as solid lines, while results using the B21 elements are shown as dashed lines. In general, excellent accuracy is achieved with both the fiber-beam column element and the ABAQUS B21 element. Errors are most significant for the load ratio of 0.85, a finding that is consistent with analyses by others.

This problem was analyzed using only two fiber beam-column elements. However, Fig. 5-8 shows that at least eight B21 elements are required to achieve the same level of accuracy. This indicates that the flexibility-based element offers greater

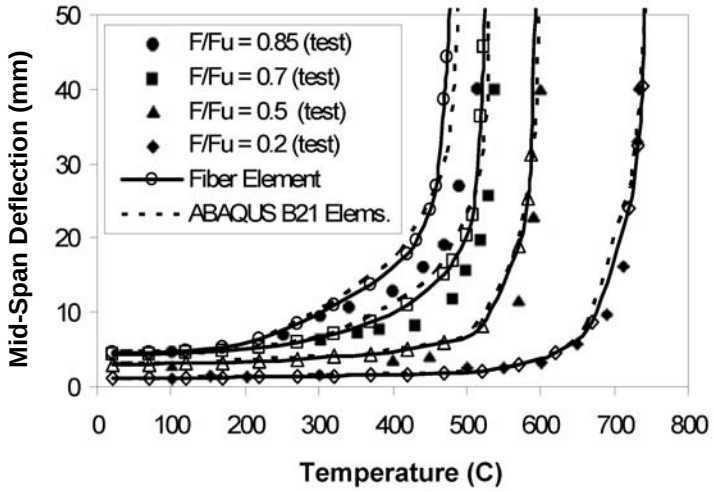

Fig. 5-7. Mid-span deflection for uniformly heated steel beams

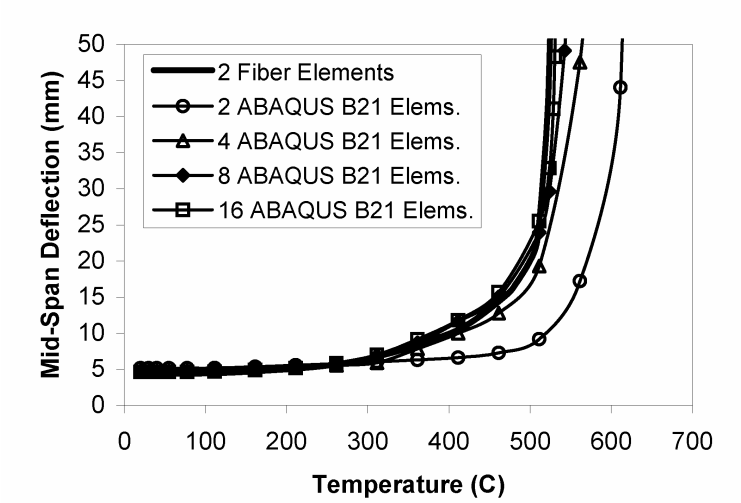

Fig. 5-8. Effects of mesh refinement on the convergence of the solution (load ratio = 0.7)

computational efficiency in modeling the response of structures under fire conditions because fewer elements can be used along the length of the member. This improved efficiency will become significant when simulations of large 3D structures are performed.

5.4.2 Uniformly Heated Steel Frames

Rubert and Schaumann (1986) also conducted a series of experimental tests on small-scale steel frames subjected to uniform heating. The frames were arranged in three configurations, as shown in Fig. 5-9. All members were made of IPE 80 sections with grade St 37 steel (σ_y = 240 N/mm^2). The test specimens were loaded and then heated uniformly at a constant rate until failure. The magnitudes of the applied loads F_1 and F_2 are shown in Table 5-1. Adequate bracing was provided to prevent out-of-plane deformations. In tests EGR 7 and 8, the beams were kept at room temperature while the columns were heated. In the ZSR tests, one bay of the frame was heated while the beam and column of the adjacent bay were kept at room temperature. Details about these tests are provided by Rubert (1984) and Rubert and Schaumann (1985, 1986). This problem has been analyzed numerically by Rubert and Schaumann (1986), Saab and Nethercot (1991), Izzuddin et al. (2000), and Chan and Chan (2001), among others.

The tests are modeled using the developed fiber beam-column elements with 77 fibers over the cross-section. As in the previous example, the steel temperatures are assumed to be constant and equal to the furnace temperature. Two elements are used for

each beam, while four elements are used for each column. Because it is assumed that deformations within the corotational reference frame are small, more elements are needed per column to accurately simulate the buckling response. The problem is also modeled using B21 elements in ABAQUS, in which eight elements are needed for each beam and column for convergence.

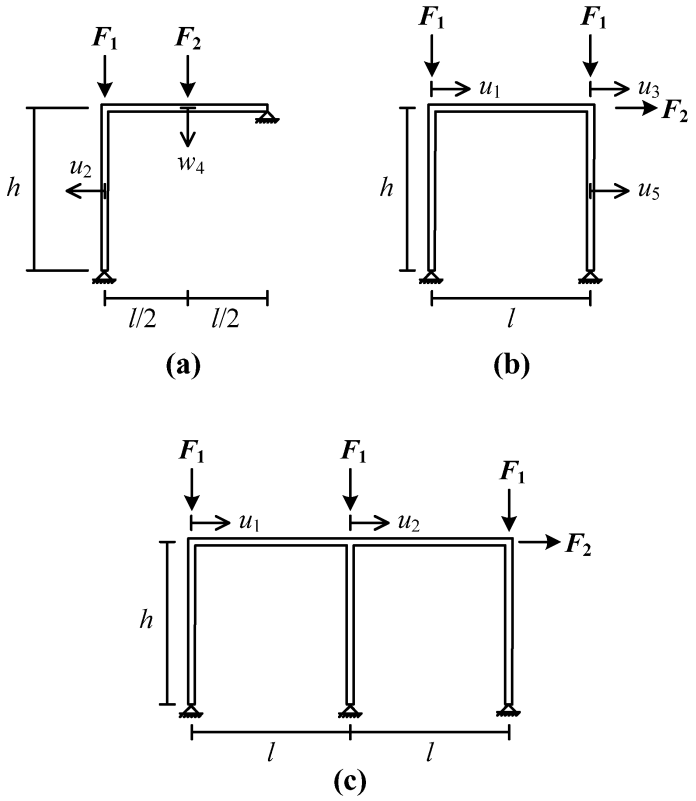

Fig. 5-9. Geometry for the uniformly heated steel frames: (a) EHR, (b) EGR, and (c) ZSR configurations (adapted from Rubert and Schaumann, 1986)

Preliminary analyses showed that the Eurocode model for steel provided overly conservative results, and so the material model proposed by Rubert and Schaumann (1986) is adopted here. A plot of the reduction factors $k_E = E_T / E_{20}$, $k_y = F_{y,T} / F_{y,20}$, and $k_p = F_{p,T} / F_{y,20}$ for the elastic modulus, yield strength, and proportional limit, respectively, at elevated temperatures shows similarities between the two models, as illustrated in Fig. 5-10. However, the Eurocode predicts a greater reduction in the proportional limit for temperatures between 300°C and 600°C and a more drastic decline

in stiffness at temperatures above 500^{o}C. Because the purpose of these analyses is to validate the element formulation, the Rubert and Schaumann (1986) model was selected. Critical temperature was defined as the temperature in the steel at failure in the experimental tests. For the analyses, the critical temperature is the temperature in the steel at which the analysis terminates. Some error in calculating the critical temperature is to be expected because failure is not clearly defined. The critical temperatures from the experimental tests are compared to results from the two analyses in Table 5-1. In general, results using the fiber element match up well with the experimental tests, with errors generally less than ten percent. Results from the fiber element are very close to those predicted by Izzuddin et al. (2000). Even with the use of more elements, analyses using the B21 elements tend to be substantially less accurate.

Displacements are plotted against temperature for frames EHR 3, EGR 1, and ZSR 1, respectively, in Figs. 5-11 to 5-13. In general, the fiber beam-column element accurately predicts the deformations, with agreement being particularly good for the ZSR 1 frame. Results using the B21 element in ABAQUS tend to be less accurate than the fiber element, with premature failure predicted for the EGR 1 and ZSR 1 frames.

Table 5-1. Uniformly heated steel frames (adapted from Rubert and Schaumann, 1986)

			Critical Temperature (C)			Error (%)		
System	F_1 (kN)	F_2 (kN)	Test	Fiber Elems.	ABAQUS Elems.	Fiber Elems.	ABAQUS Elems.	Comments
EHR 1	56	14	600	618	618	3.00	3.00	Fully heated, strong - axis bending
EHR 2	84	21	530	540	542	1.89	2.26	
EHR 3	112	28	475	448	455	-5.68	-4.21	
EHR 4	20	5	562	528	519	-6.05	-7.65	Fully heated, weak - axis bending
EHR 5	24	6	460	470	462	2.17	0.43	
EHR 6	27	6.7	523	417	415	-20.27	-20.65	
EGR 1b	65	2.5	533	492	455	-7.69	-14.63	Fully heated, strong - axis bending
EGR 1c	65	2.5	515	492	455	-4.47	-11.65	
EGR 2	40	1.6	612	595	574	-2.78	-6.21	
EGR 3	77	3.0	388	392	352	1.03	-9.28	
EGR 4	77	3.0	424	419	393	-1.18	-7.31	
EGR 5	88	3.4	335	296	282	-11.64	-15.82	
EGR 6	88	3.4	350	296	282	-15.43	-19.43	
EGR 7	68.5	2.6	454	428	399	-5.73	-12.11	Cold beam
EGR 8	77	3.0	464	428	326	-7.76	-29.74	
ZSR 1	74	2.85	547	511	500	-6.58	-8.59	Partial heating, strong - axis bending
ZSR 2	84.5	3.25	479	462	441	-3.55	-7.93	
ZSR 3	68.5	2.64	574	570	561	-0.70	-2.26	

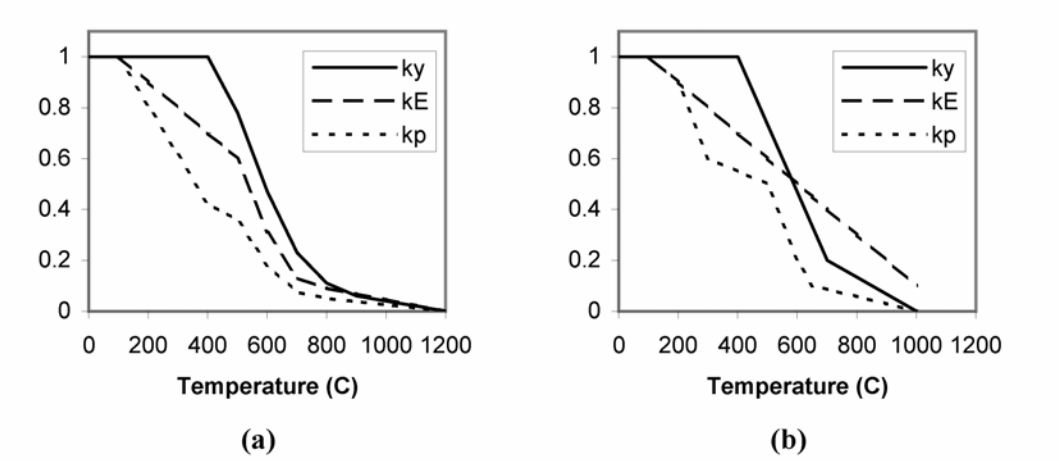

Fig. 5-10. Reduction factors for mechanical properties of steel: (a) Eurocode 3 (EN 1993-1.2, 2005), (b) Rubert and Schaumann (1986)

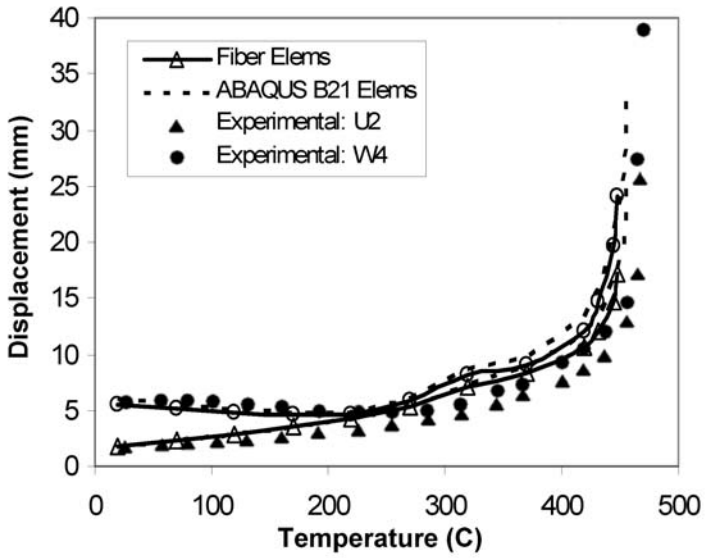

Fig. 5-11. Displacements u_2 and w_4 for frame EHR 3

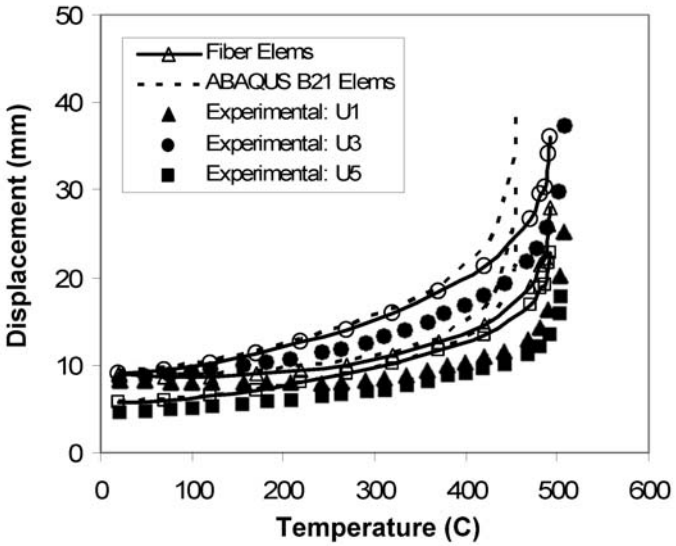

Fig. 5-12. Displacements u_1, u_3 and u_5 for frame EGR 1

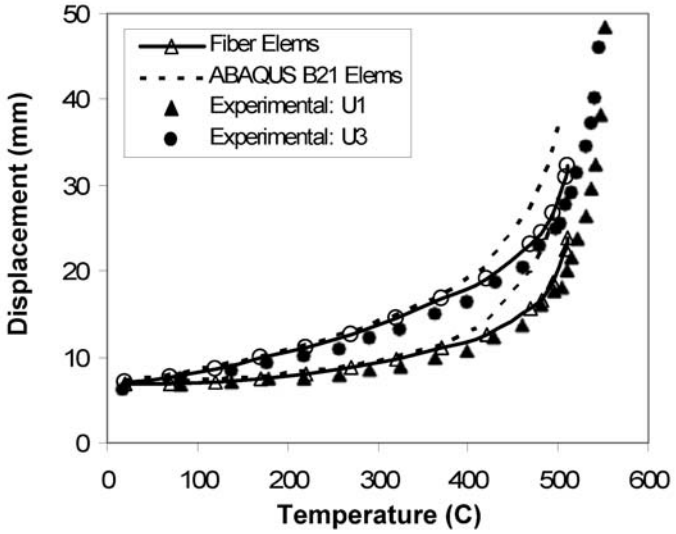

Fig. 5-13. Displacements u_1 and u_3 for frame ZSR 1

5.4.3 Standard Fire Tests on Steel Columns with Blocked-in Webs

Wainman and Kirby (1988) described a series of standard fire tests conducted on steel columns with blocked-in webs. The test setup is shown in Fig. 5-14. The columns were subjected to a constant axial load and then heated uniformly according to the standard ISO 834 fire (ISO, 1999). The concrete blockwork was intended to serve as fire protection to the steel and did not contribute to the structural performance. As illustrated in Fig. 5-14, thermocouples were placed in the flanges and web of the steel section at

various locations along the length of the column. Average furnace temperatures were reported throughout the duration of the tests. The vertical displacement at the top of each column was measured at various times.

Three of the columns (tests TE 4747, TE 5154, and TE 5236) are modeled using the fiber-based approach. The details of these three tests are described in Table 5-2. One-fourth of the cross-section is used to model the thermal response, as illustrated in Fig. 5-15. Note that the fiber mesh is denser in the steel region to provide greater accuracy in simulating the force-deformation response. The fire behavior in the furnace is modeled by applying both convective and radiative boundary conditions to the surface of the column. The convective heat transfer coefficient h is assumed to be 25 W/m^{2}K, and the emissivity ε is assumed to be 0.5 for the steel and 0.8 for the concrete. Instead of using the measured furnace temperatures in the analyses, the furnace temperature is assumed to follow the standard ISO 834 fire curve for simplicity. The Eurocode models for the thermal and mechanical properties of steel (EN 1993-1.2, 2005) and the thermal properties of the concrete blockwork (EN 1996-1.2, 2005) are employed. The effect of moisture content in the concrete blockwork is conservatively ignored. Note that

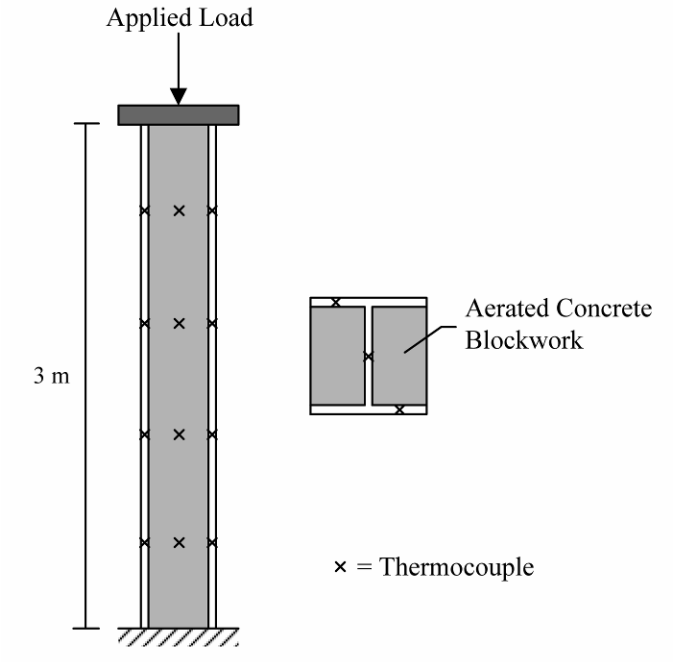

Fig. 5-14. Steel column with blocked-in web (adapted from Wainman and Kirby, 1988)

mechanical properties are not defined for the concrete blockwork because the steel is assumed to carry the entire load.

The average flange and web temperatures in the steel are shown in Fig. 5-16 for one of the columns (test TE 5154). Experimental values are represented by solid lines

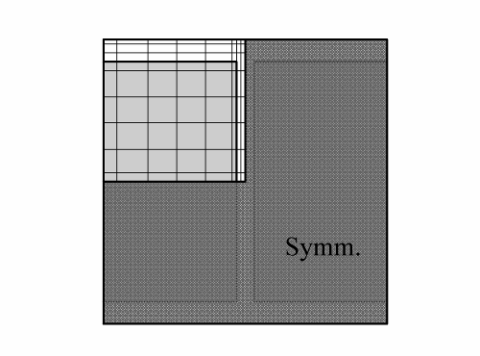

Fig. 5-15. Fiber mesh over one-fourth of the cross-section: 72 fibers in an 8x9 grid

Table 5-2. Steel columns with blocked-in webs (experimental data reported by Wainman and Kirby, 1988)

Test Number	Section	σ_y (N/mm^2)	Load (kN)	Fire Resistance (min)
TE 4747	203 x 203 x 52 UC	266	916	36
TE 5154	152 x 152 x 23 UC	280	381	23
TE 5236	203 x 203 x 46 UC	284	811	24

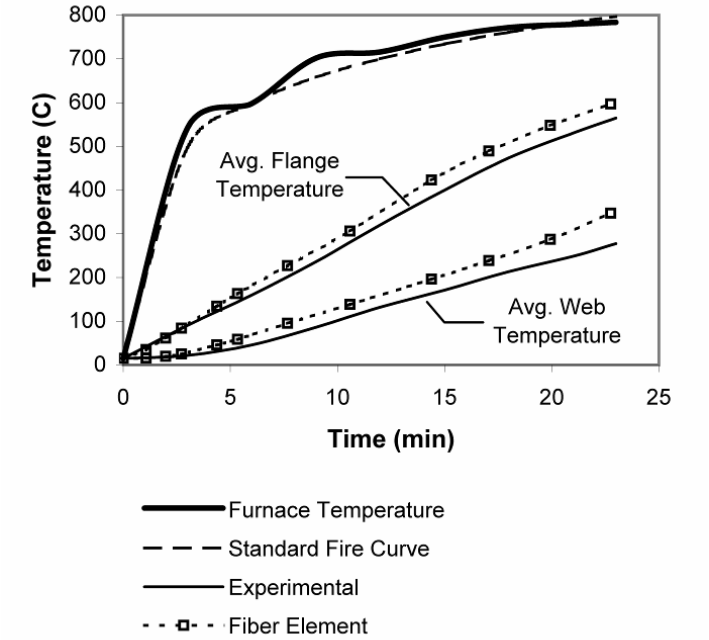

Fig. 5-16. Temperatures in the steel column with blocked-in web (Test No. TE 5154)

while results obtained with the fiber heat transfer element are represented by dashed lines with data points. The fiber heat transfer element tends to overestimate the temperatures in the steel. This is most likely because the effects of moisture evaporation in the concrete blockwork are ignored. Despite these errors, the fiber heat transfer element gives a good representation of the thermal response of the steel columns with blocked-in webs.

Using the calculated temperatures as the input, the structural analysis is then carried out using the fiber beam-column element. The entire cross-section is modeled, but it is assumed that the concrete blockwork does not carry any of the load. Eight elements are used along the length of the column. Axial displacements at the top of the column are shown in Fig. 5-17 as a function of the average flange temperature in the steel. While there are some differences between the experimental and calculated responses, the fiber beam- column element accurately predicts the fundamental behavior of the three columns, with failure occurring at approximately the same temperature for the analyses and the experimental tests. The differences in the response can be attributed to the various simplifying assumptions that were made.

5.4.4 Standard Fire Tests on Steel Beams with Non-Composite Concrete Slabs

Wainman and Kirby (1988, 1989) also described a series of standard fire tests on steel beams supporting non-composite concrete slabs subjected to the standard fire test. In addition to the self-weight of the beams, the beams were loaded at four points along the length, as shown in Fig. 5-18. The beams were heated on three sides, and so the temperatures in the steel varied non-uniformly over the depth. The concrete slabs were segmented to ensure that the beams carried the entire load in bending.

A total of thirteen tests are modeled using the fiber-based approach, the details of which are summarized in Table 5-3. Two different sized beams are considered: 254x146x43UB and 356x171x67UB. The beams were made of two different grades of steel (43A and 50B), and the tests considered various magnitudes of the applied loads.

In modeling the thermal response, it is assumed that the fire in the furnace applies both radiative and convective boundary conditions at the surface of the steel section. It is assumed that the coefficient h for convection heat transfer is 25 W/m^{2}K and the emissivity ε for steel is 0.2. Rather than explicitly model the concrete in the thermal

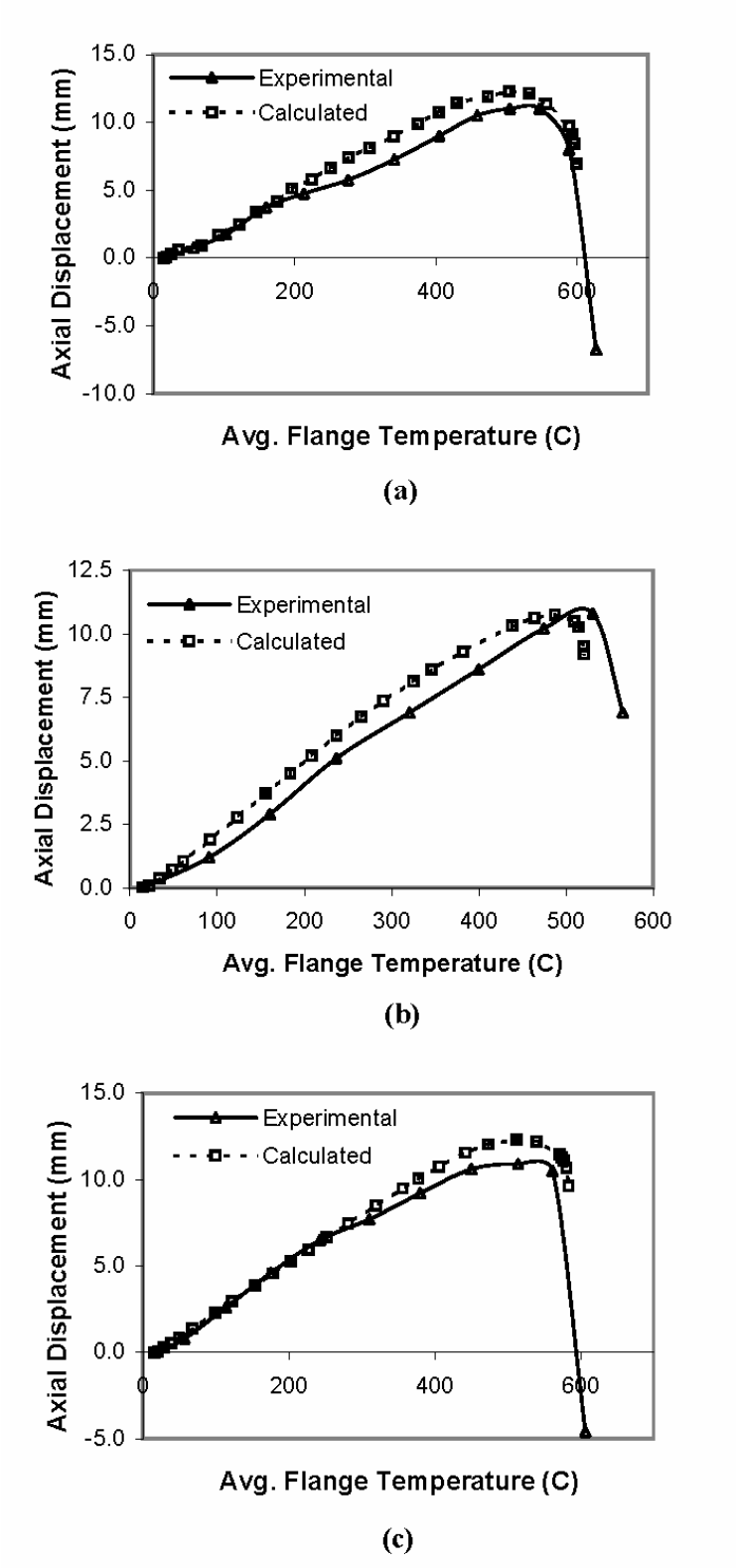

Fig. 5-17. Axial displacement at top of column: (a) TE 4747, (b) TE 5154, (c) TE 5236

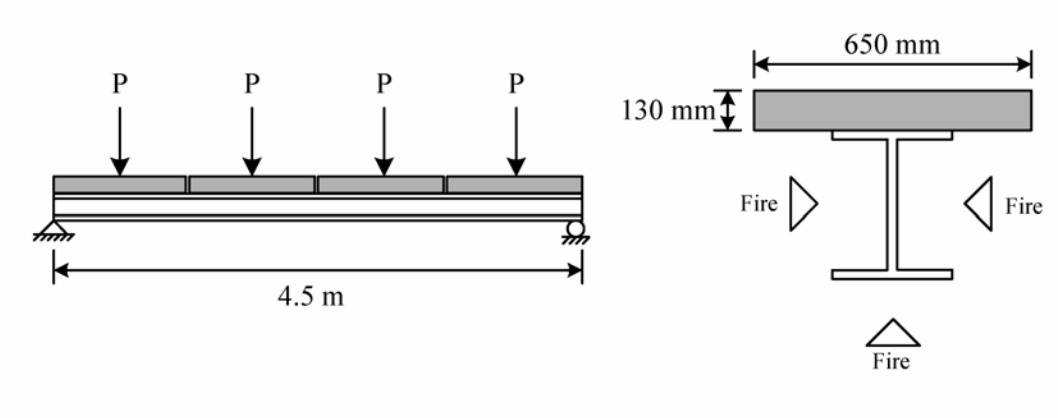

Fig. 5-18. Steel beam supporting non-composite concrete slab

Table 5-3. Steel beams with non-composite concrete slabs (experimental data reported by Wainman and Kirby, 1988, 1989)

Section	Steel Grade	Test No.	σ_y (N/mm^2)	Load (kN)	Fire Resistance (min)	Critical Temperature (C)		
						Exp.	Calc.	Error (%)
254 x 146 x 43 UB	43A	3	277	32.54	22	634	646	+1.97
	43A	10	304	33.38	21	655	654	-0.19
	43A	11	311	33.32	22	683	657	-3.83
	43A	14	297	15.83	27	745	720	-3.40
	50B	2	411	46.73	23	660	653	-1.10
	50B	4	408	33.92	30	701	684	-2.39
	50B	13	388	33.23	26	727	679	-6.59
356 x 171 x 67 UB	43A	5	280	72.90	27	647	666	+2.87
	43A	12	291	74.86	29	651	668	-1.87
	43A	89	292	75.24	20	630	668	+2.59
	43A	90	298	94.25	21	705	637	+1.05
	43A	91	296	50.01	23	714	718	+1.88
	50B	9	395	74.70	24.5	715	712	-0.25

analysis, the concrete is treated as a semi-infinite medium with constant temperature and included as a thermal boundary condition along the top flange of the beam. Thus, the heat flux q_c'' at the steel-concrete interface is calculated as (Incropera and DeWitt, 2002)

$$q_c'' = \frac{k_c(T_c - T_s)}{(\pi \alpha_c t)^{1/2}}, \tag{5}$$

where k_c is the thermal conductivity of concrete, T_c is the temperature of the concrete (which is assumed to remain at room temperature), T_s is the unknown surface temperature of the steel, α_c is the thermal diffusivity (i.e., $\alpha_c = k_c / \rho_c C_c$, where ρ_c and C_c are the density and specific heat of concrete), and t is time. The thermal properties for the concrete are assumed to be constant and independent of temperature (i.e., k_c = 1.3 W/m^{2}K and $\rho_c C_c = 2.3 \times 10^6$ J/m^{2}K). The boundary condition in Eq. (5) is implemented

in the fiber heat transfer element as a convective boundary condition, in which the convection heat transfer coefficient is $k_c/(\pi\alpha_c t)^{1/2}$ and the "fluid" temperature is T_c.

The thermal response is modeled using the fiber heat transfer element with 72 fibers over half of the cross-section, as shown in Fig. 5-19. Temperatures in the flanges and webs of the beams are shown in Figs. 5-20 and 5-21 for both beam sizes. The temperatures in the steel are plotted against the furnace temperature rather than time since the experimental furnace temperatures deviated somewhat from the standard fire curve. The temperature predictions demonstrate that the assumed boundary conditions are adequate and that the fiber heat transfer element accurately predicts the thermal response of the steel beams.

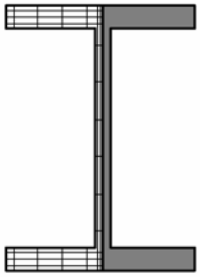

Fig. 5-19. Fiber mesh over half of cross-section (71 fibers)

The force-deformation response for each of the beams is modeled using eight fiber beam-column elements along the length. Distributed loads due to self-weight are applied as work-equivalent nodal forces. In the experimental tests, a maximum deflection of *L*/30 was permitted before the test was terminated. Thus, the critical temperature is defined here as the maximum temperature in the steel at which the deflection reaches *L*/30. Critical temperatures from the analyses are compared to the experimental values in Table 5-3. The analyses provide estimates of critical temperatures that are well within ten percent of the experimental values. To better illustrate the accuracy of the fiber-based approach, deformations are plotted against furnace temperatures for three of the 254x146x43UB (Grade 40A) beams with similar loading in Fig. 5-22(a) and two of the 356x171x67UB (Grade 40A) beams with similar loading in Fig. 5-22(b). In general, the fiber beam-column element accurately predicts the deformation throughout the duration of the test, with errors on the conservative side.

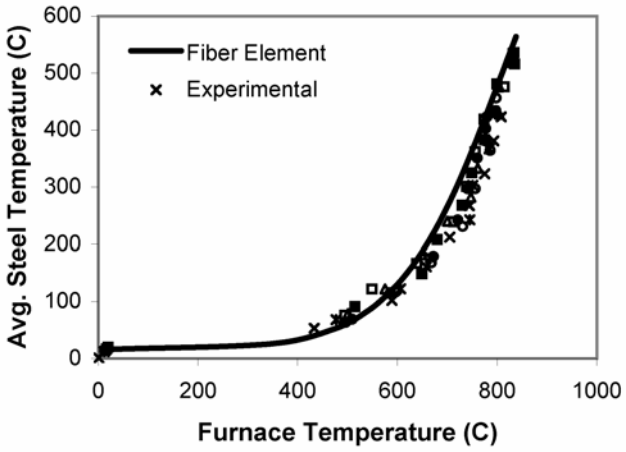

(a)

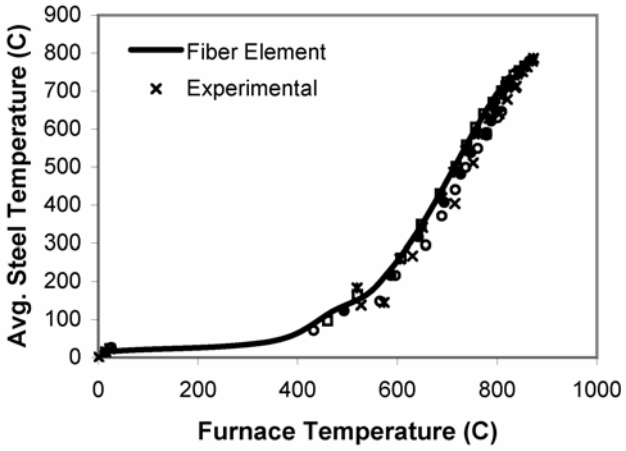

(b)

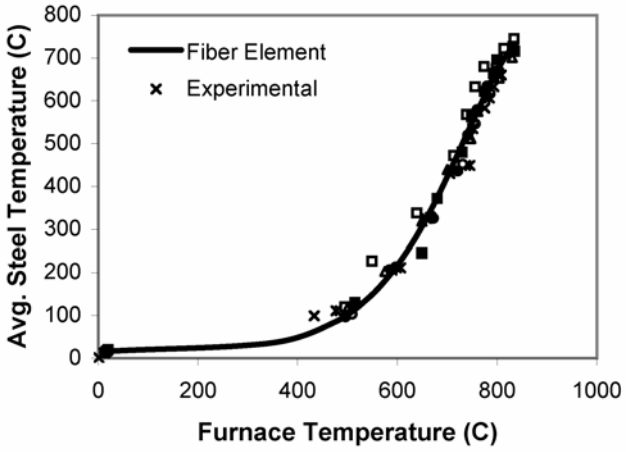

(c)

Fig. 5-20. Average steel temperatures for 254 x 146 x 43 UB beams: (a) upper flange, (b) web, and (c) lower flange

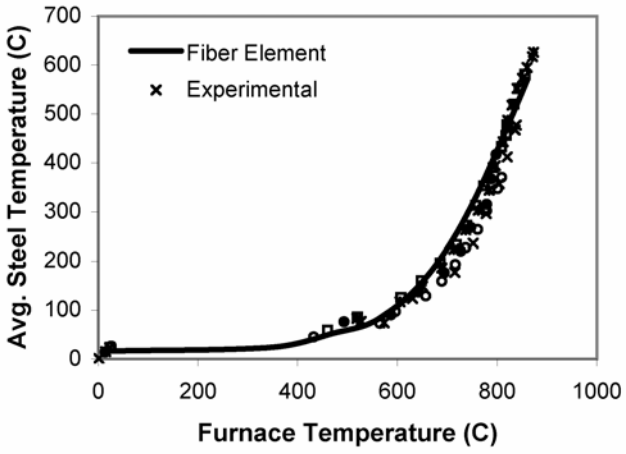

(a)

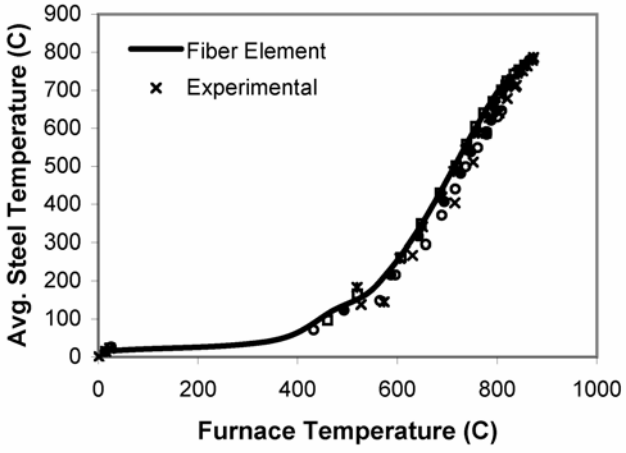

(b)

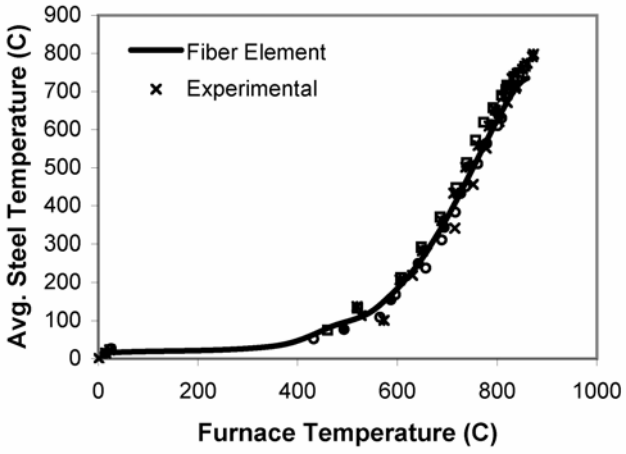

(c)

Fig. 5-21. Average steel temperatures for 356 x 171 x 67 UB beams: (a) upper flange, (b) web, and (c) lower flange

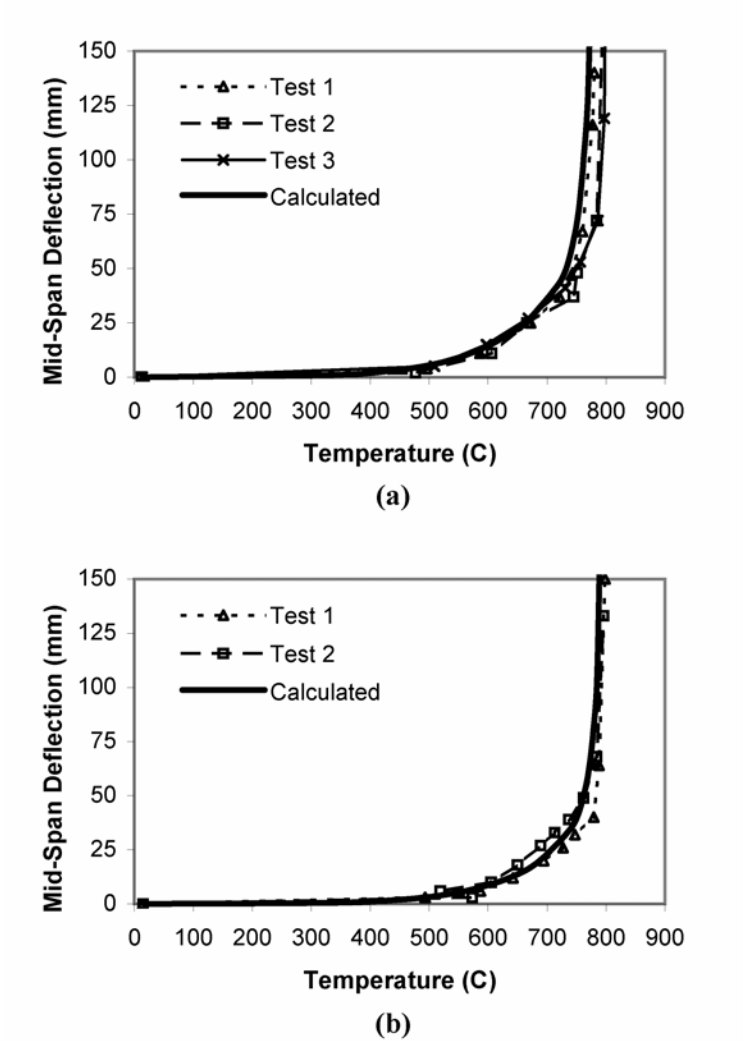

Fig. 5-22. Mid-span deflections for steel beams with non-composite concrete slab: (a) 254 x 146 x 43 UB cross-section, (b) 356 x 171 x 67 UB cross-section

5.5 Conclusions

This paper presents a new approach to modeling the response of structural frames subjected to fire. The approach involves the use of two fiber-based elements that can be used collectively to perform sequentially coupled analyses of structural frames subjected to any type of thermal loading. In addition to demonstrating the potential of the fiber-based approach, this paper also introduces a 2D flexibility-based fiber beam-column element for modeling structural response under fire conditions.

Analyses of benchmark experimental tests are presented to demonstrate the capabilities of this fiber-based approach. For uniformly heated steel structures,

comparisons are made between the flexibility-based fiber element and a stiffness-based beam element in ABAQUS. The flexibility-based element provides greater accuracy and requires fewer elements for convergence. Analyses of steel columns with blocked-in webs and non-composite steel beams with concrete slabs show that both fiber elements offer excellent accuracy in modeling the response of structures subjected to non-uniform heating. Future work will consider the response of structural systems with non-uniform heating over the length as well as over the cross-section.

Notation

A_i = area of fiber i

b = width of section

C_c = specific heat of concrete

$[b(x)]$ = force interpolation matrix

d = depth of the section

$\{d\}$ = nodal deformation vector within the corotational reference frame

$\{d_s(x)\}$ = section deformation vector

E_T = tangent modulus at temperature T

$F_{p,T}$ = proportional limit at temperature T

$F_{y,T}$ = yield strength at temperature T

$\{f\}$ = nodal force vector at the element level

$[f]$ = element flexibility matrix

$[f_s(x)]$ = section flexibility matrix

h = convection heat transfer coefficient

k_c = thermal conductivity of concrete

k_E = reduction factor for elastic modulus

k_p = reduction factor for proportional limit

k_y = reduction factor for yield strength

$[k]$ = element stiffness matrix

$[k_s(x)]$ = section stiffness matrix

L = element length

$M(x)$ = bending moment

n = number of fibers in the cross-section

$N(x)$ = axial force

q_c'' = heat flux at the steel-concrete interface

$\{r\}$ = nodal force vector within the corotational reference frame

$\{r_s(x)\}$ = section force vector

$\{u\}$ = nodal displacements at the element level

t = time

T = temperature

y_i = centroidal coordinate of fiber i with respect the element's local coordinate axis

α_c = thermal diffusivity of concrete

α_T = coefficient of thermal expansion at temperature T

ΔT = change in temperature

ε = effective emissivity

$\varepsilon(x)$ = axial strain

$\varepsilon_{res}(x)$ = residual strain in fiber i

$\varepsilon_{th}(x)$ = thermal strain in fiber i

$\kappa(x)$ = curvature

ρ_c = density of concrete

σ_y = yield strength

Chapter 6: "Analysis of Unprotected Steel Beams Subjected to Localized Fires"

Ann E. Jeffers and Elisa D. Sotelino

[A manuscript to be submitted for publication in the *Fire Safety Journal*]

Abstract

This paper takes a fundamental look at the effects of localized fires on the response of unprotected steel beams. Using a fire model for a localized fire impinging on an I-beam, the thermal and mechanical responses of various steel beams are analyzed by a fiber-based approach. A *t*-squared model is used to determine the heat release rate of the fire. The analyses consider the effects of fire growth rate and peak heat release rate on the response. Residual deformations upon cooling are also considered. Comparisons between the localized fire response and the response during standard fire tests are used to evaluate the standard fire test in terms of its ability to ensure structural integrity during realistic building fires. It is found that the concept of fire resistance (i.e., the time during which a member can endure the standard fire test) is very unreliable and generally unconservative for predicting the time at failure of a structure subjected to realistic fire conditions, because failure is primarily governed by the evolution of temperatures within the structure. The analyses also show that critical temperatures obtained from the standard fire test are conservative and thus offer a better means for predicting failure in steel structures within the context of the standard fire test.

6.1 Introduction

In recent years, a significant amount of experimental and analytical research has been conducted to investigate the response of structures under fire loading. Most of the research to date, however, is based on the standard fire test, in which isolated members and structural components are heated uniformly according to the standard fire curve. While the standard fire test has historically been the primary method for evaluating structural integrity under fire, the recent movement towards performance-based structural fire design has prompted a widespread effort to understand structural response under

more realistic fire conditions. As a result, much of the ongoing research dealing with structure-fire interaction focuses on the response of structural systems rather than isolated members, and investigates structural response under more realistic types of heating.

This paper is intended to broaden our understanding of structural response under realistic fire conditions by examining the response of unprotected steel beams subjected to localized fires. In the subsequent analyses, steel beams supporting non-composite concrete slabs are heated by localized fires with varying intensities and durations, as illustrated in Fig. 6-1. Using a fire model for a localized fire impinging on an I-beam (SFPE, 2004), the thermal response is evaluated using the fiber heat transfer element developed by Jeffers and Sotelino (2009). The force-deformation response is subsequently analyzed using the flexibility-based fiber beam-column element developed [in Chapter 5]. To evaluate the performance of the beams, results from the analyses are compared to standard fire tests of similar beams, which were published by Wainman and Kirby (1988, 1989) and have been analyzed [in Chapter 5].

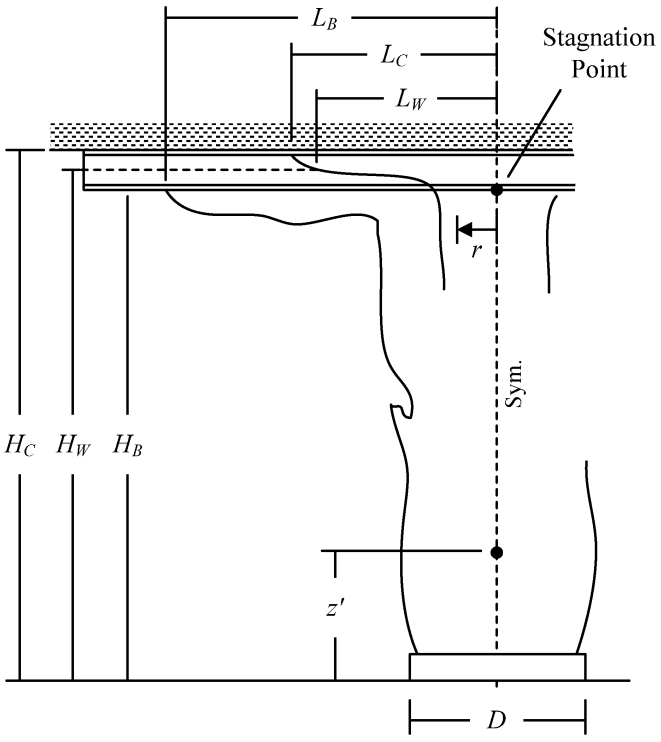

Fig. 6-1. Localized fire acting on a steel I-beam mounted below a ceiling (adapted from SFPE, 2004)

6.2 Literature Review

While most of the research to date has focused on the response of structures subjected to the standard fire, a limited amount of research has been conducted to investigate the effects of realistic fire behavior on structural response. For example, Cooke and Latham (1987) describe an experimental test on a steel frame subjected to a natural fire. The response of the steel frame was governed largely by thermal bowing in the beams and columns, which resulted from non-uniform heating over the member cross-sections. In addition to the Cooke and Latham (1987) test frame, a series of large-scale experimental tests was conducted on a multistory composite steel-framed building at the Cardington Laboratory in the United Kingdom (Wald et al., 2006). These tests and the subsequent analytical investigations have provided much insight into the response of structural systems subjected to natural fires. The tests are well-documented and their results have been published extensively. Although these efforts considered realistic fires, they were based on fully developed compartment fires, in which the gas temperatures are essentially uniform throughout the compartment.

While it is generally accepted that a fully developed compartment fire will be more damaging to the structure than a localized fire, there are instances in which it is desirable to investigate the effects of localized fires in structures. For example, parking structures and bridge structures are often damaged by localized fires caused by burning vehicles. Despite this fact, most of the work dealing with localized fires has focused on developing an understanding of the fire behavior rather than the structural response (Hasemi et al., 1995; Wakamatsu et al., 1996; Hamins et al., 2005). Research dealing with structural response under localized fires is limited to only a few analytical investigations (Franssen et al., 1998; Liew et al., 2002) involving specialized case studies. No known experimental work has been conducted to study structural response under localized fires.

Because knowledge of structural response under localized fire conditions is currently limited, this paper takes a fundamental look at the effects of localized fires on the response of steel beams. The following analyses investigate the effects of fire growth rate and peak heat release rate on the thermal and mechanical response of steel beams subjected to localized fires. The application considered here involves unprotected steel

beams in building structures subjected to localized fires that may be encountered during building construction. Comparisons between the localized fire response and the response during standard fire tests are used to evaluate the standard fire test in terms of its ability to ensure structural integrity during realistic building fires.

6.3 Description of the Fire Model

The Society of Fire Protection Engineers (SFPE, 2004) compiled the findings of experimental studies (i.e., Hasemi et al., 1995, Wakamatsu et al., 1996, and Myllymaki and Kokkala, 2000) that have been conducted to determine the thermal characteristics of a localized fire impinging on an I-beam that is mounted below a ceiling. In these studies, it was observed that the flame lengths along the lower flange, web, and upper flange vary and that a relationship exists between the flame length and the heat flux incident on the surface of the I-beam. Knowing the heat release rate $\dot{Q}$ of the fire and the vertical distances H_B, H_W, and H_C from the base of the fire to the bottom flange, center of the web, and ceiling, respectively, the flame lengths L_B, L_W, and L_C can be approximated as

$$L_B = H_B(2.3Q^{*\,0.3}_{H_B} - 1), \quad L_W = H_W(2.9Q^{*\,0.4}_{H_W} - 1), \quad \text{and} \quad L_C = H_C(2.9Q^{*\,0.4}_{H_C} - 1), \tag{1}$$

where $Q^*_{H_B}$, $Q^*_{H_W}$, and $Q^*_{H_C}$ are nondimensional quantities defined by

$$Q^*_{H_B} = \frac{\dot{Q}}{\rho_0 C_p T_0 \sqrt{g} H_B^{\,5/2}}, \qquad Q^*_{H_W} = \frac{\dot{Q}}{\rho_0 C_p T_0 \sqrt{g} H_W^{\,5/2}},$$
$$\text{and} \quad Q^*_{H_C} = \frac{\dot{Q}}{\rho_0 C_p T_0 \sqrt{g} H_C^{\,5/2}}. \tag{2}$$

Here, ρ_0 is the density of air at ambient (1.2 kg/m^3), C_p is the specific heat of air at ambient (1.0 kJ/kg K), T_0 is the temperature of air at ambient (293 K), and g is the gravitational acceleration (9.81 m/s^2).

A conservative estimate for the heat flux q'' (in kW/m^{2}K) can then be obtained from

$$\begin{aligned} q'' &= 120, && w \le 0.5 \\ q'' &= 682\exp(-3.4w), && w > 0.5 \end{aligned} \tag{3}$$

in which the nondimensional distance w is defined for the bottom flange, web, and top flange in the following equations:

Bottom Flange: $w = (r + H_B + z')/(L_B + H_B + z')$,

Web: $w = (r + H_W + z')/(L_W + H_W + z')$, (4)

Top Flange: $w = (r + H_C + z')/(L_C + H_C + z')$.

Here, r is the radial distance along the I-beam from the point of stagnation and z' is the virtual source correction, which is dependent on the equivalent diameter D of the fuel package and the heat release rate $\dot{Q}$ of the fire. Knowing the heat release rate of the fire, the diameter of the fuel package, and the vertical distance from the fuel package to the ceiling, the heat flux acting on the beam can be determined from Eqns. (1)-(4).

The heat release rate for a fire can be determined experimentally or calculated according to a parametric fire curve. In the following analyses, a t-squared fire curve is adopted. As illustrated in Fig. 6-2, three phases of fire development are represented: growth, steady burning, and decay. In the growth phase of the fire, the heat release rate is calculated as

$$\dot{Q} = (t/k)^2, \quad (5)$$

where t is time and k is a constant that accounts for the growth rate of the fire (Buchanan, 2001). The fire grows until a peak heat release rate of $\dot{Q}_p$ is reached. It is assumed that the fire burns at this rate until 70 percent of the total energy in the fuel has been expended, after which the fire decays linearly. A similar fire model was used by Cadorin et al. (2003) for evaluating heat release rates in compartment fires.

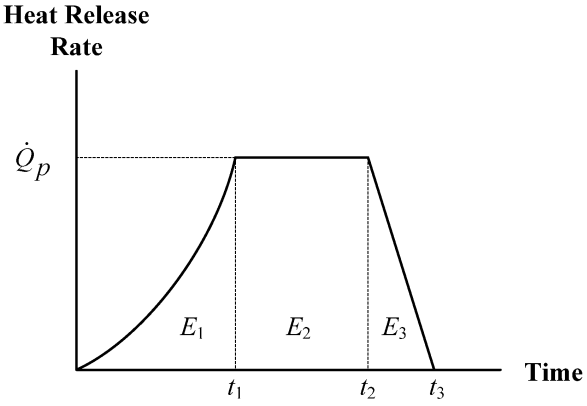

Fig. 6-2. t-Squared model for determining heat release rate

The energy released by the fire can be found by integrating the heat release rate with respect to time. For a fire with total energy E_T, energies E_1, E_2, and E_3, shown in Fig. 6-2, can be determined by examining the area under the heat release rate curve, i.e.,

$$E_1 = t_1 \dot{Q}_p / 3, \qquad E_2 = 0.70 E_T - E_1, \qquad \text{and } E_3 = 0.30E. \tag{6}$$

In addition, times t_1, t_2, and t_3 can be found by

$$t_1 = k\sqrt{\dot{Q}_p}, \qquad t_2 = t_1 + \frac{E_2}{\dot{Q}_p}, \qquad \text{and } t_3 = t_2 + \frac{E_3}{0.5\dot{Q}_p}. \tag{7}$$

Equations (5)-(7) can be used collectively to determine the heat release rate of a fire at any time *t*.

A comparison between a realistic fire and the *t*-squared fire is shown in Fig. 6-3. The experimental data shown in Fig. 6-3 was obtained from a free-burning stack of wood pallets. The test was conducted at the Building Fire Research Laboratory at the National Institute of Standards and Technology (NIST, 1999). Estimating the total energy at 1000 MJ and assuming that the fire growth rate is moderately slow (i.e., k = 450), a *t*-squared approximation is constructed. A reasonable approximation of the realistic fire behavior is provided by the *t*-squared fire, as illustrated in Fig. 6-3.

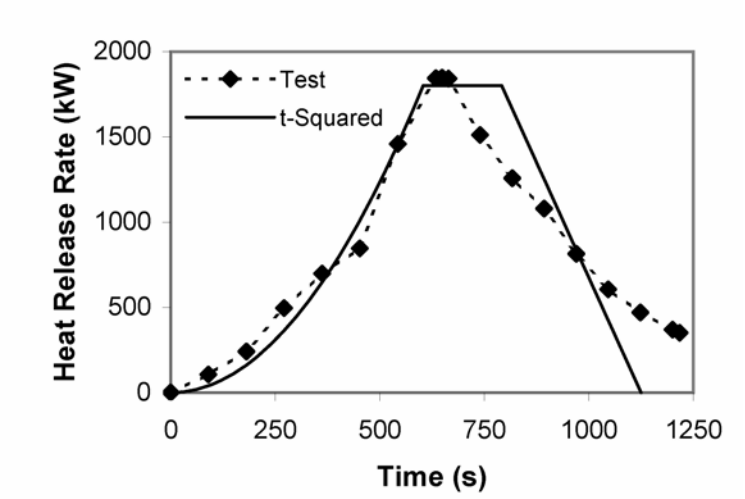

Fig. 6-3. Comparison between a real fire (NIST, 1999) and the *t*-squared fire

6.4 Analysis of Beams Subjected to Localized Fires

6.4.1 Parameters for the Fire Analyses

The following analyses consider the response of unprotected steel beams subjected to localized fires with varying intensity and duration. While it is common practice to apply fire protection to all exposed structural steel in a building to achieve the adequate fire resistance, there are times during building construction in which the steel is unprotected. In addition, passive and active fire protection systems (e.g., sprinkler systems) are typically not operational during early phases of construction, and so a steel-framed structure is particularly susceptible to fire damage during construction (Buchanan, 2001). Unprotected steel beams are also encountered in other types of structures, such as bridges.

Wainman and Kirby (1988, 1989) describe a series of standard fire tests that were carried out on unprotected steel beams supporting non-composite concrete slabs. The experimental tests considered beams of different sizes with varying magnitudes of applied load. While a thirty-minute fire resistance rating could not be achieved, the unprotected beams were able to maintain structural integrity for periods exceeding 20 minutes. Analyses [in Chapter 5] show that the thermal and mechanical response of these beams can be predicted with excellent accuracy using the fiber-based approach.
Two different sized beams are considered here: 254x146x43UB and 356x171x67UB. The geometry and loading for the beams are taken from tests 3, 10, and 11 for the 254x146x43UB beam, and tests 5, 12, and 89 for the 356x171x67UB beam (Wainman and Kirby, 1988, 1989). As illustrated in Fig. 6-4, each of the beams is simply-supported, and is loaded at four points along the length. The concrete slab is assumed to act non-compositely with the steel beam and therefore does not carry any of the load in bending. The beams are made of grade 43A steel, which is assumed to have a yield strength of 305 N/mm^2 at room temperature.

To simulate different types of fire behavior, the heat release rate curve is adjusted by varying the peak heat release rate of the fuel and the fire growth constant. For example, Fig. 6-5 shows the heat release rate curves for slow-growth and fast-growth fires with varying heat release rates. In the following analyses, peak heat release rates are varied between 1000 kW and 2000 kW. Slow-growth fires are modeled by setting k at

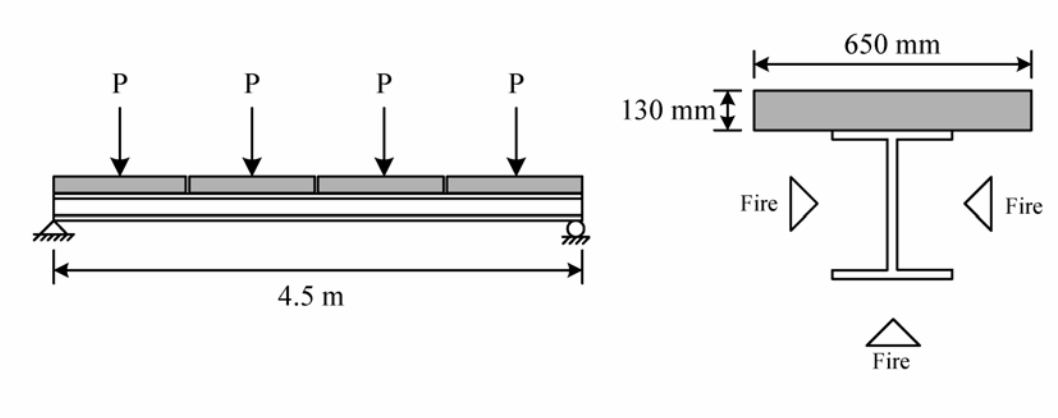

Fig. 6-4. Unprotected steel beam with non-composite concrete slab

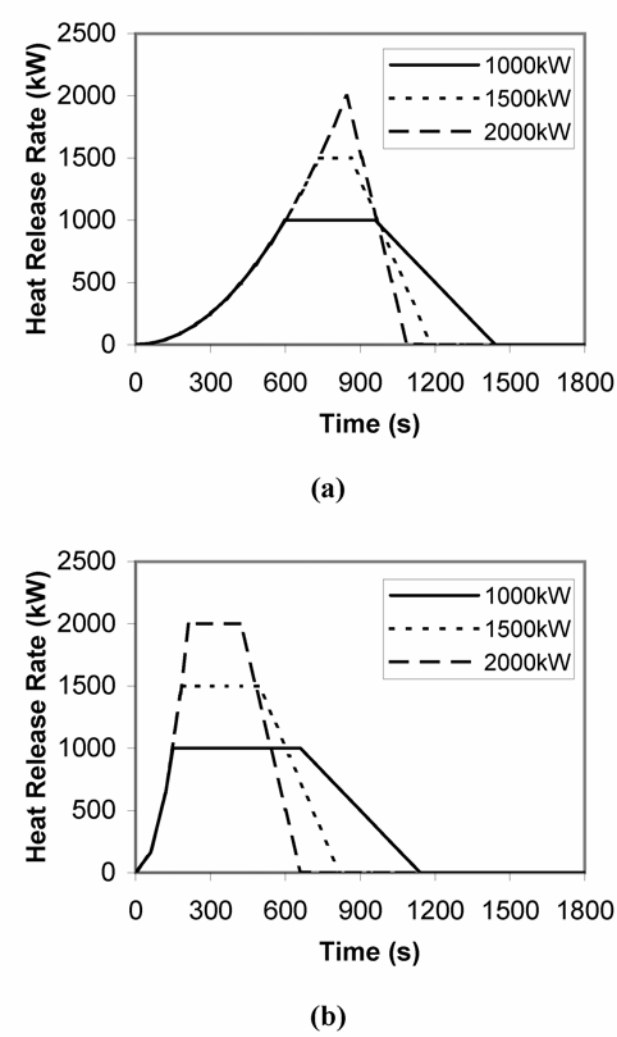

Fig. 6-5. Heat release rate curves: (a) slow-growth fires (k = 600), and (b) fast-growth fires (k = 150)

600, while fast-growth fires are modeled by setting k at 150. For all analyses, the fuel package is assumed to have a total energy of 800 MJ, which is equivalent to 50 kg of wood with a net calorific value of 16 MJ/kg (Buchanan, 2001). The diameter of the fuel package is assumed to be 1.128 m. A ceiling height H_C of 2.5 m is used to ensure that the flames act directly on the steel beam.

6.4.2 Analysis of the Thermal Response

The thermal boundary conditions for the steel beam are described as follows. The beam is heated by the surface flux q'', which is calculated according to Eq. 3. Note that the flanges and web are subjected to different magnitudes of heat flux. Furthermore, the magnitude of the heat flux varies along the length of the beam, with the center of the beam being subjected to the most intense heating. While the heat flux along the length of the beam varies exponentially, the heat flux is assumed to vary linearly along the length of an element. Consequently, eight fiber heat transfer elements are used along the length of the beam to provide sufficient accuracy in modeling the thermal problem. In addition to the surface flux, the beam loses heat to the surroundings by radiation and loses heat to the concrete slab by conduction. For the radiative boundary condition, an emissivity of 0.85 is assumed to account for soot formation on the surface of the beam (Staggs and Phylaktou, 2008). The presence of a hot gas layer is ignored (SFPE, 2004), and the surroundings are assumed to remain at the initial ambient temperature of 20 C.

By treating the concrete as a semi-infinite medium with constant thermal properties, the heat transfer at the steel-concrete interface can effectively be included as a convective boundary condition, in which the convection heat transfer coefficient is $k_c/(\pi\alpha_c t)^{1/2}$ and the "fluid" temperature is the temperature of the concrete T_c [refer to Chapter 5]. Here, k_c, ρ_c, and C_c are the conductivity, density, and specific heat of concrete, respectively (i.e., k_c = 1.3 W/m^{2}K and $\rho_c C_c = 2.3\times10^6$ J/m^{2}K); α_c is the thermal diffusivity of concrete (i.e., $\alpha_c = k_c/\rho_c C_c$); and t is time. This method for including heat flow to the concrete is much more efficient than explicitly including the concrete in the heat transfer analysis, and analyses [in Chapter 5] show that this method for including the concrete provides sufficient accuracy.

The full three-dimensional thermal response is modeled for each fire using eight fiber heat elements along the length. Symmetry is utilized such that only half of the cross-section is analyzed. Temperature-dependent material properties for steel are taken from the Eurocode (EN 1993-1.2, 2005).

6.4.3 Analysis of the Mechanical Response

The force-deformation response of the structure is modeled using eight flexibility-based fiber beam-column elements [from Chapter 5] along the length of the beam. Because the fiber heat transfer element is used for the thermal analysis, the three-dimensional temperature data can be transferred directly from the heat transfer analysis to the structural analysis. The Eurocode model for steel (EN 1993-1.2, 2005) is used to account for temperature-dependent material properties. Because the fire model used here includes the cooling phase, the material model needs to be adjusted to account for the effects of cooling.

The effects of strain reversal during the cooling phase have been investigated by a number of researchers including Franssen (1990), Bailey et al. (1996), El-Rimawi et al. (1996), and Wang et al. (2008). Because this paper considers the response of statically determinate beams under monotonic loading, the effects of cooling are included using the simple unloading curve shown in Fig. 6-6, which is based on the bilinear model proposed by El-Rimawi et al. (1996). Essentially, as the temperature decreases from T_1 to T_2, the material unloads fully at temperature T_1 (from points *A* to *B*) and reloads at temperature T_2 (from points *B* to *C*). The slope of the unloading/reloading curve is linear and equal to

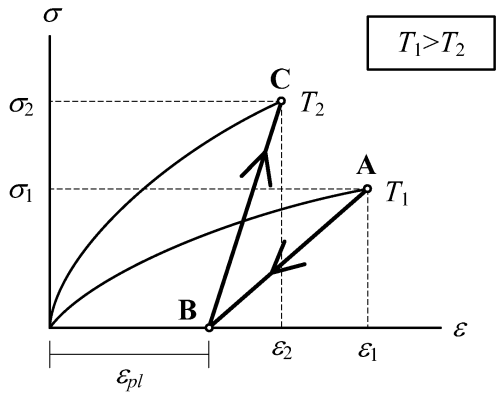

Fig. 6-6. Model for unloading during cooling

the initial tangent slope of the stress-strain curve at temperature *T*. It is assumed that the irrecoverable plastic strain ε_{pl} remains unchanged as temperature changes.

6.5 Results

A summary of the results is presented in Table 6-1 for the slow-growth fires and Table 6-2 for the fast-growth fires. These tables list the various fire intensities and durations that are considered for each beam. Note that the slow-growth fires last for longer periods of time than the fast-growth fires. In addition, the maximum temperatures in the steel are slightly greater for the fast-growth fires.

A comparison of the temperatures in the steel at mid-span are shown in Fig. 6-7 for the 1000 kW fires and 2000 kW fires acting on the 254x146x43UB beam. In all cases, the temperatures in the top flange are significantly less than the temperatures in the web and bottom flange because of the thermal interaction between the top flange and cooler concrete

Table 6-1. Slow-growth fires (k = 600)

Beam	Peak Heat Release Rate (kW)	Fire Duration (min)	Max. Steel Temperature (C)	Max. Deformation (mm)	Time of Max. Deformation (min)	Residual Deformation (mm)
254x146x43UB	1000	24.0	620	43.3	18.0	15.8
	1250	21.3	669	64.4	17.0	34.5
	1500	19.7	706	177.5	16.0	145.2
	2000	18.1	725*	> 250 mm	14.4	–
356x171x67UB	1500	19.7	699	52.1	17.0	29.8
	1750	18.7	722	123.1	16.0	99.1
	2000	18.1	732	201.5	16.0	176.3

*Maximum temperature in the steel at failure

Table 6-2. Fast-growth fires (k = 150)

Beam	Peak Heat Release Rate (kW)	Fire Duration (min)	Max. Steel Temperature (C)	Max. Deformation (mm)	Time of Max. Deformation (min)	Residual Deformation (mm)
254x146x43UB	1000	19.0	623	45.6	13.0	16.8
	1250	15.7	677	73.3	11.0	41.6
	1500	13.6	719	244.9	10.0	210.3
	2000	11.0	740*	> 250 mm	6.6	–
356x171x67UB	1500	13.6	711	64.3	10.0	40.6
	1750	12.1	736	179.2	10.0	153.7
	2000	11.0	747*	> 250 mm	7.9	–

*Maximum temperature in the steel at failure

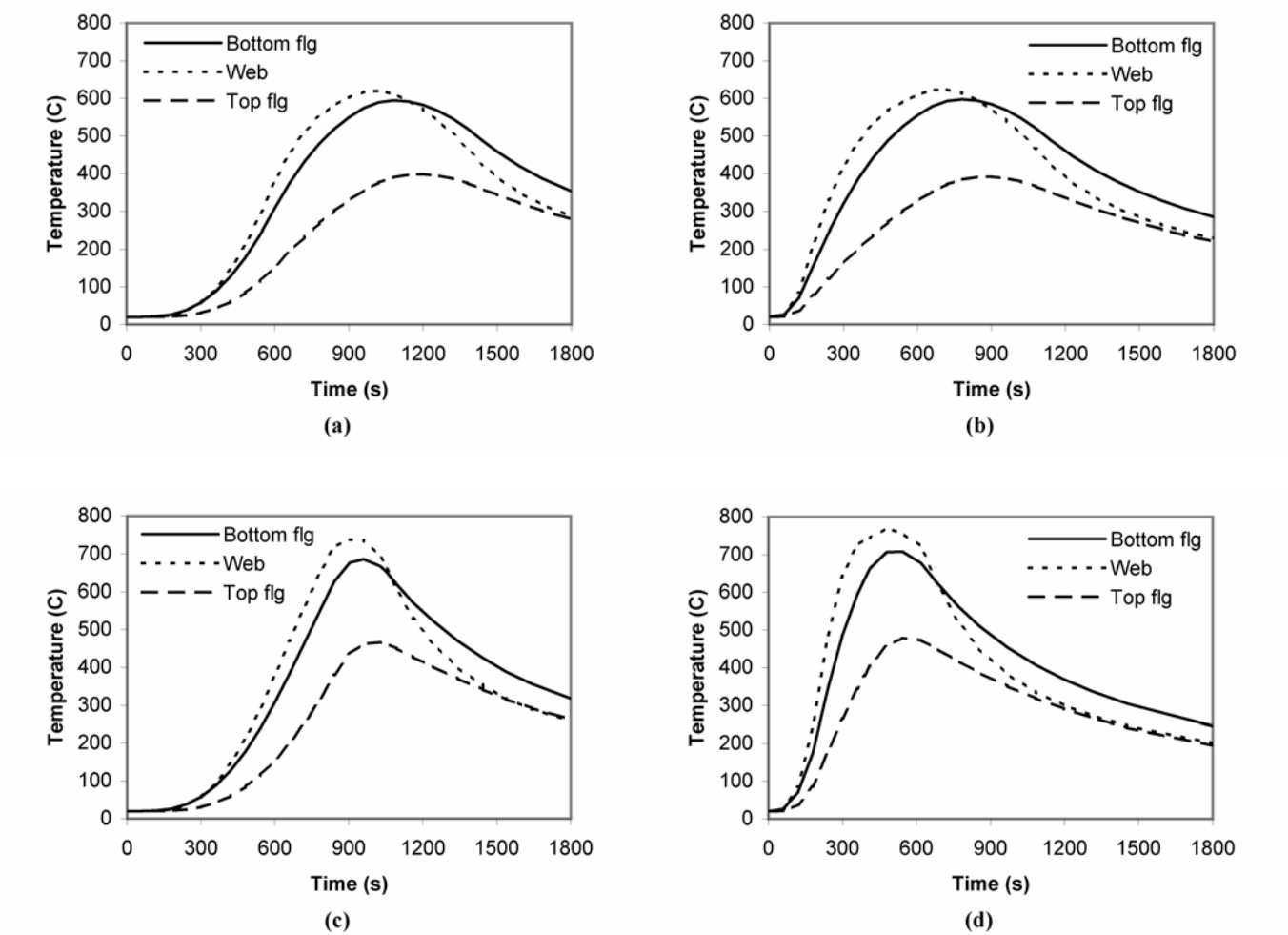

Fig. 6-7. Temperatures in the 254x146x43UB steel beam due to various fires: (a) 1000 kW fire (slow-growth), (b) 1000 kW fire (fast-growth), (c) 2000 kW fire (slow-growth), (d) 2000kW fire (fast-growth)

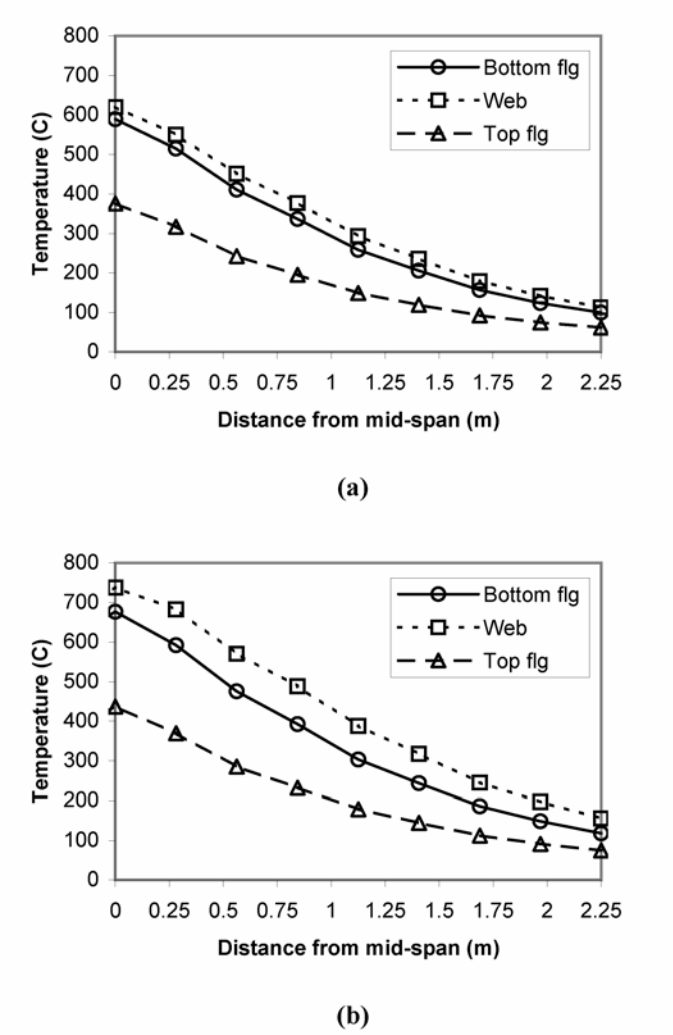

Fig. 6-8. Temperatures along the length of the 254x146x43UB steel beam: (a) 1000 kW fire, and (b) 2000 kW fire

slab. The web heats up and cools down slightly faster than the bottom flange because the web thickness is somewhat less than the flange thickness. The fast-growth fires reach peak temperatures at earlier times, and the maximum temperatures in the steel are slightly higher during the fast-growth fires. While all four fires in Fig. 6-7 have the same fuel load, the 2000 kW fires produce significantly higher temperatures in the steel than the 1000 kW fires.

The bottom flange temperatures during the 2000 kW slow-growth and fast-growth fires are compared to the temperature evolution in the steel during the standard fire test in Fig. 6-9. The steel tends to heat up much more quickly under the localized fires

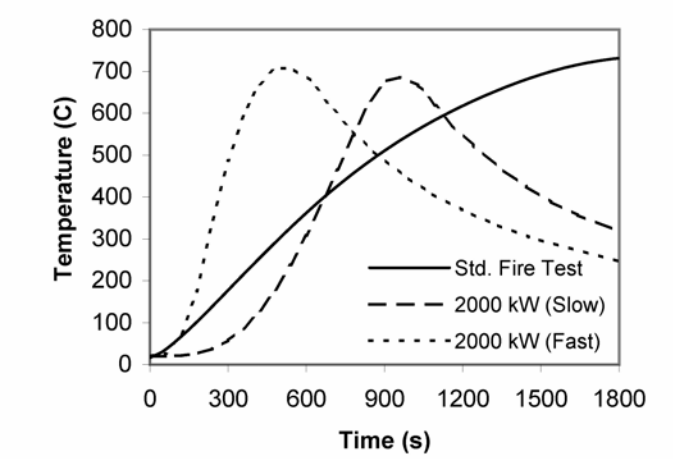

Fig. 6-9. Comparison of bottom flange temperatures for different fires

than during the standard fire test. Thus, the beam reaches its maximum temperature at an earlier time.

The mid-span deflections in the 254x146x43UB beam are shown in Fig. 6-10 for various fires. Under the 2000 kW fires, displacements exceed 250 mm and the beam fails. For the other fires, the displacement increases until the peak temperature is reached, after which the beam begins to cool and displacements decrease. A permanent residual displacement remains in the beam after cooling because the beam is subjected to loading beyond the elastic range. The maximum displacement, the maximum temperature in the steel, the time at which the maximum displacement is attained, and the residual displacements are shown in Tables 6-1 and 6-2 for various cases. Note that beams subjected to the fast-growth fires tend to experience larger displacements than beams subjected to the slow-growth fires. In addition, the maximum displacements occur at significantly earlier times and residual displacements are larger for the fast-growth fires.

As can be observed in Fig. 6-10, the maximum displacements occur at significantly earlier times than predicted by the standard fire test. This suggests that failure depends more on the temperature evolution in the steel than the duration of fire exposure. In terms of a realistic building fire, early failure could have grave consequences, since less time is allowed for evacuation.

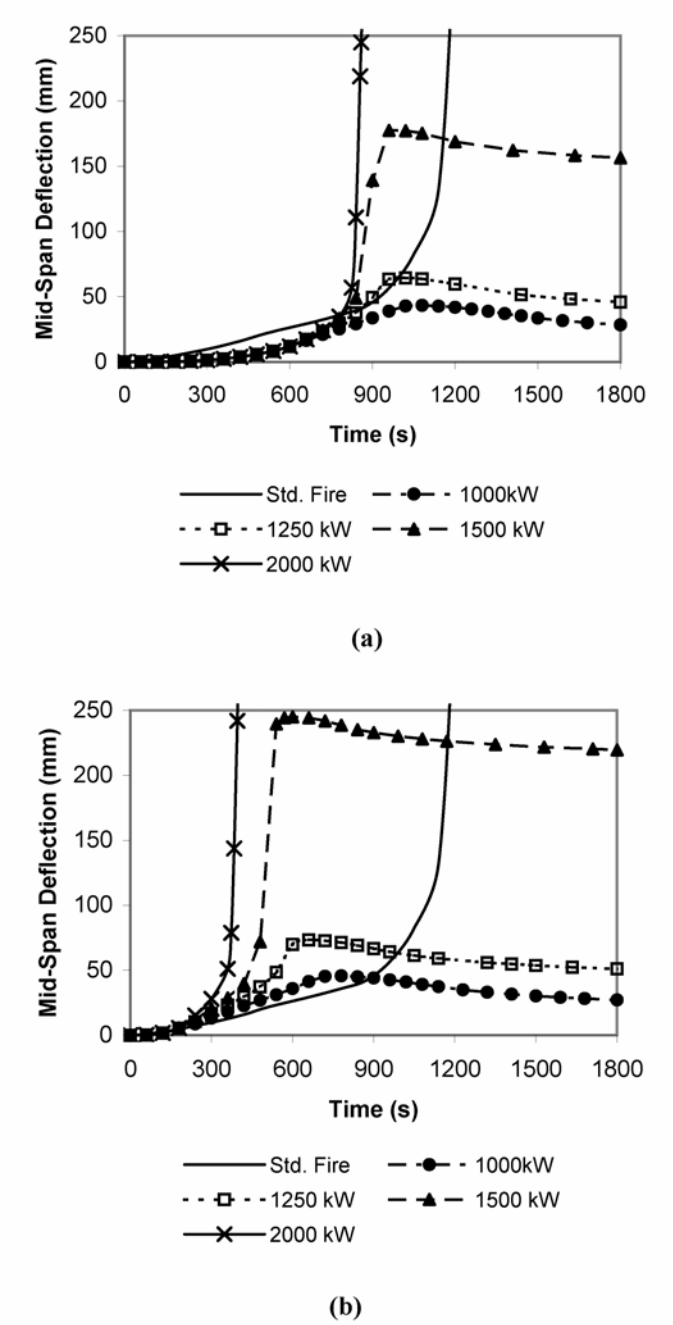

Fig. 6-10. Displacements vs. time for the 254x146x43UB steel beam subjected to various fires: (a) slow-growth fires, and (b) fast-growth fires

A plot of deformation vs. temperature in the bottom flange is shown in Fig. 6-11 for the 254x146x43UB beam. The residual deformation due to heating and cooling is more apparent in this figure. While there are slight discrepancies in the heating and cooling curves for various fires, it appears that a critical temperature exists at which deformations

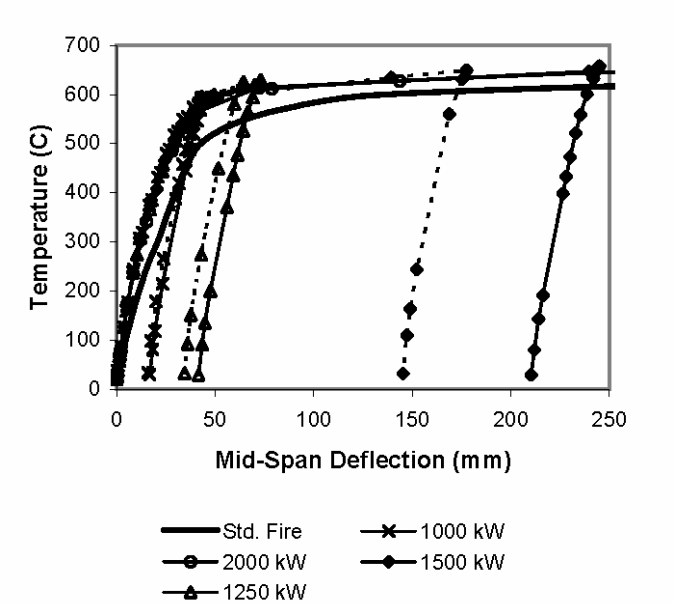

Fig. 6-11. Displacements vs. temperature in the bottom flange for the 254x146x43UB steel beam subjected to various fires (dashed lines represent slow-growth fires, solid lines represent fast-growth fires)

increase at a rapid rate. When compared to the response during the standard fire test, the beam subjected to localized fire is able to withstand somewhat higher maximum temperatures, most likely because it is not heated uniformly.

Results for the 356x171x67UB beam are shown in Fig. 6-12 and 6-13 and in Tables 6-1 and 6-2. Because the 356x171x67UB beam is somewhat larger than the 254x146x43UB beam, it has a greater capacity to withstand the fire loads. For example, Tables 6-1 and 6-2 show that the maximum steel temperatures and mid-span deflections are smaller during the 1500 kW and 2000 kW fires for the 356x171x67UB beam. This is also apparent in Figs. 6-12 and 6-13. Comparisons to the standard fire test yield the same conclusions as previously, i.e., that the standard fire test is unconservative in predicting the time at failure, yet slightly conservative in predicting the critical temperature of the beam.

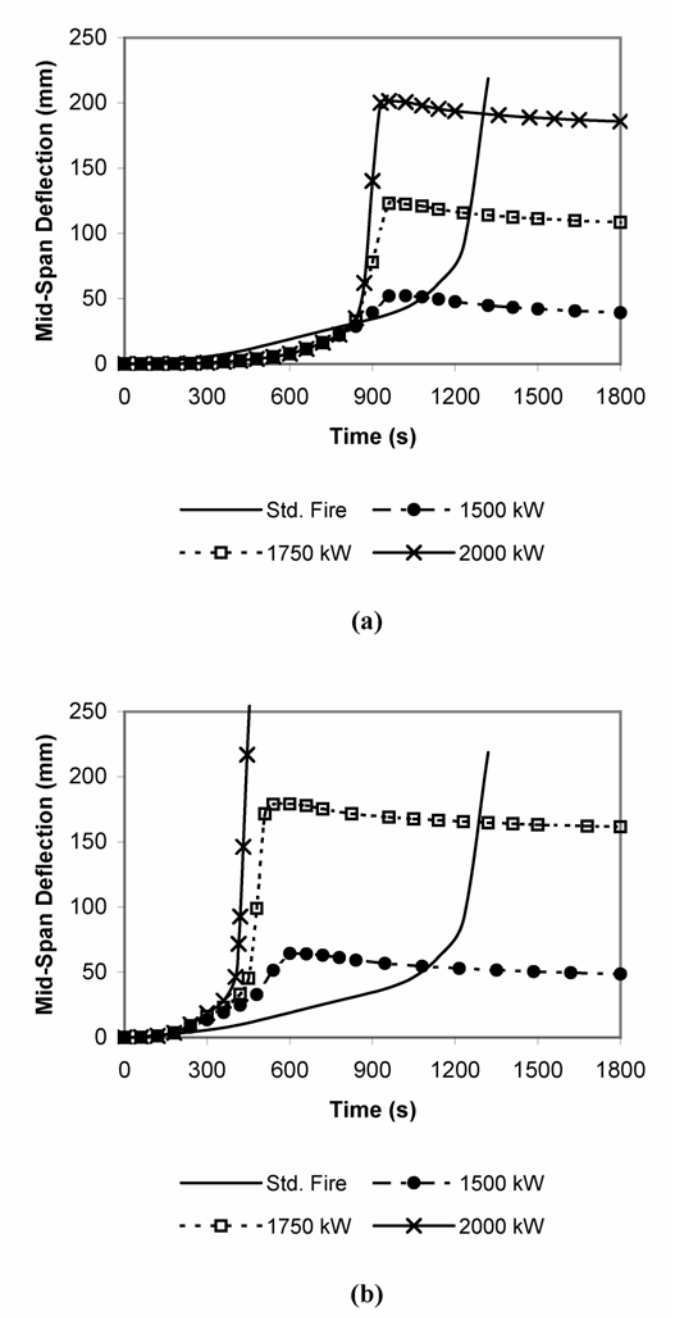

Fig. 6-12. Displacements vs. time for the 356x171x67UB steel beam subjected to various fires: (a) slow-growth fires, and (b) fast-growth fires

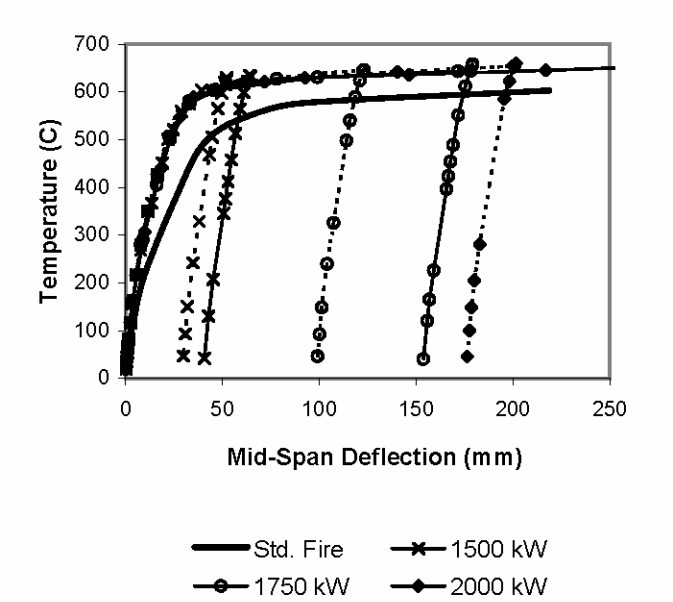

Fig. 6-13. Displacements vs. temperature in the bottom flange for the 356x171x67UB steel beam subjected to various fires (dashed lines represent slow-growth fires, solid lines represent fast-growth fires)

6.6 Conclusions

The response of unprotected steel beams subjected to localized fires is investigated in this paper. The analyses considered realistic fire models in which the three phases of fire development (i.e., growth, burning, and decay) are represented. Parameters for the analyses were selected to simulate localized fires that may be caused during building construction. Two different sized beams were considered, and results were compared to analyses of standard fire tests. It is found that the concept of fire resistance, as defined for standard fire test, is unconservative for predicting an actual time of failure in steel beams, because failure is dependent on the actual temperature evolution within the structure. The analyses described herein demonstrate that the concept of critical temperature (i.e., the maximum temperature in the steel at failure) may be a more accurate measure for predicting the failure of steel structures subjected to fire within the scope of the standard fire test. Note that these conclusions are drawn from comparisons to standard fire tests conducted in Europe, in which the structures were loaded and heated until failure.

The response due to localized fires differs from that of uniformly heated beams in that the structure exhibits greater stiffness at a given temperature and the temperature at failure is slightly higher. However, the importance of considering realistic fire behavior is highlighted by the fact that the standard fire produces a slower rise in temperature than the more realistic fires considered here. In addition, the standard fire fails to capture the cooling phase of the fire, which becomes significant when the structure is restrained and strain reversal occurs. The simply-supported beams analyzed here do not consider the effects of restraint during cooling, although residual deformations during the cooling phase were evaluated.

Notation

C_c = specific heat of concrete

C_p = specific heat of air at ambient (1.0 kJ/kg K)

D = diameter of the fuel package

E_1, E_2, E_3 = areas under the heat release rate curve

E_T = total energy

g = gravitational acceleration (9.81 m/s^2)

H_B = vertical distance from the base of the fire to the bottom flange

H_C = vertical distance from the base of the fire to the top flange

H_W = vertical distance from the base of the fire to the center of the web

k = growth rate constant

k_c = thermal conductivity of concrete

L_B = flame tip length along the bottom flange

L_C = flame tip length along the top flange

L_W = flame tip length along the web

q'' = heat flux

$\dot{Q}$ = heat release rate

$\dot{Q}_p$ = peak heat release rate

Q^* = dimensionless parameter

r = radial distance from the center of beam

t = time

T = temperature

T_0 = temperature of air at ambient (293 K)

w = non-dimensional distance

z' = virtual source correction

α_c = thermal diffusivity of concrete

ρ_0 = density of air at ambient (1.2 kg/m^3)

ρ_c = density of concrete

Chapter 7: Summary, Conclusions, and Future Work

Because experimental fire tests are very costly, the need for accurate and efficient computational tools to simulate structural response in fire cannot be overstated. While the problem has received significant attention in recent years, much work can still be done in the development of methods for structural fire analysis. Consequently, this research has focused on the development two new finite elements, a fiber heat transfer element and a flexibility-based fiber beam-column element, which can be used collectively to accurately and efficiently simulate the thermal and mechanical response of structural frames. The analytical investigations described herein have demonstrated that the proposed fiber-based approach offers significant advantages over existing methods of analysis and thus warrants further development.

This chapter provides a summary of the work described herein. The first section in this chapter gives an overview of the methodology used in the development of the two fiber-based elements and a summary of key findings. The second section in this chapter describes the limitations of the proposed approach and directions for future research.

7.1 Summary and Conclusions

The fiber heat transfer element introduced in Chapter 4 is a new type of heat transfer element for modeling the 3D thermal response of structural frames. Starting with the governing conduction heat transfer equation, a combination of finite element and finite difference approximations was made. The end result is an accurate and highly efficient heat transfer element that is fully compatible with any fiber-based (i.e., distributed plasticity) beam-column element for performing sequentially coupled analyses of structural frames under fire. Analyses of structures subjected to various types of thermal loads indicate that the fiber heat transfer element offers excellent accuracy. Comparisons to 3D heat transfer analyses using solid finite elements show that the fiber heat transfer element also offers substantial time savings. Furthermore, the element facilitates the transfer of temperature data from the thermal analysis to the structural analysis since the element uses a fiber mesh.

Chapter 5 considers the application of the flexibility method of analysis as a means for improving computational efficiency in the analysis of structural frames in fire. The flexibility-based fiber beam-column element extends the element formulation by Taucer et al. (1991) to account for thermal effects, geometric nonlinearities, and residual stresses. Comparisons with a stiffness-based element in ABAQUS demonstrate that the flexibility-based element offers significant advantages since fewer elements are needed per member. Analyses of benchmark experimental tests also demonstrate that the flexibility-based element provides excellent accuracy.

In addition to introducing the flexibility-based fiber beam-column element, Chapter 5 also showcases the proposed fiber-based approach, in which the fiber heat transfer element and the fiber beam-column element are used collectively to perform sequentially-coupled analyses of structural frames subjected to realistic fire conditions. Analyses of structures with non-uniform heating (e.g., steel columns with blocked-in webs and steel beams supporting non-composite concrete slabs) demonstrate that the fiber-based approach offers significant advantages over existing methods of analysis, since it allows the response of structures subjected to realistic thermal loads to be evaluated easily and efficiently. Furthermore, the method offers improved accuracy since it involves an accurate representation of the thermal response.

In Chapter 6, the fiber-based approach is used to investigate the response of unprotected steel beams subjected to localized fires. The thermal analyses highlight key differences between the standard fire test and the response of structures subjected to realistic fires. In particular, the maximum temperatures in the steel occurred at much earlier times than during the standard fire test, especially during the fast growth fires. Analyses of the structural response demonstrate that the standard fire test is unconservative for predicting a time of failure, since failure is governed by the evolution of temperatures within the steel beams rather than the time of exposure. While the testing standards explicitly state that “fire resistance” in no way guarantees that the structure will withstand a realistic fire for a given period of time, the notion of “fire resistance” is misleading and offers a false sense of security. On the other hand, the idea of critical temperature (i.e., the temperature in the member at the time of failure) appears to be a more reliable measure for predicting the failure of structural members.

7.2 Limitations and Future Work

This document considers a 2D formulation of the flexibility-based fiber beam-column element. In its current form, large displacements are taken into account using geometric transformations of the corotational reference frame. It is assumed that displacements within the corotational reference frame are small. Improved efficiency could be achieved by extending the formulation to allow for large deformations within the corotational reference frame. The flexibility-based fiber beam-column element also lacks the ability to account for localized failures such as local buckling in steel sections. Future work is needed to develop a method for including localized failures in distributed plasticity elements at elevated temperatures. Additional work can also be done to extend the element formulation to three-dimensional space, so that problems involving biaxial bending, lateral-torsional buckling, etc. can be explored.

Analyses thus far have focused primarily on the response of individual structural members and small-scale structural frames. Future work should investigate the response of large-scale structural systems subjected to realistic fires. The fiber-based elements introduced here can also be combined with layered shell elements to investigate the response of composite floor systems subjected to realistic fires. Experimental investigations at the Cardington Laboratory (Wald et al., 2006) should form the basis of this type of work. In addition, this research has focused primarily on the response of steel structures. Future work can adapt the fiber-based approach to modeling the response of reinforced concrete and steel-concrete composite structures.

Lastly, both fiber elements were implemented in ABAQUS using a user-defined element subroutine. While this approach allowed us to explore the new element formulations, we encountered some limitations in working with the rigid structure of ABAQUS. For example, we were limited in the number of temperature degrees of freedom that could be specified for the fiber heat transfer element. These limitations were of little consequence for the relatively simple analyses here, but would need to be dealt with if larger and more complex problems are to be considered.

References

ABAQUS, Version 6.7 (2007). Dassault Systemes.

Adessi, D., and Ciampi, V. (2007). "A Regularized Force-Based Beam Element with a Damage-Plastic Section Constitutive Law," *International Journal for Numerical Methods in Engineering*, 70, 610-629.

Alemdar, B. N., and White, D. W. (2005). "Displacement, Flexibility, and Mixed Beam-Column Finite Element Formulations for Distributed Plasticity Analysis," *Journal of Structural Engineering*, 131, 1811-1819.

ASTM (1999). "Standard Test Methods for Fire Tests of Building Construction and Materials," *E119*, American Society for Testing and Materials, West Conshohocken, PA.

Bailey, C. G. (1998). "Development of Computer Software to Simulate the Structural Behavior of Steel-Framed Buildings in Fire," *Computers and Structures*, 67, 421-438.

Bailey, C. G. (2004a). "Membrane Action of Slab/Beam Composite Floor Systems in Fire," *Engineering Structures*, 26, 1691-1703.

Bailey, C.G. (2004b). "Structural Fire Design: Core or Specialist Subject?" *The Structural Engineer*, 82, 32-38.

Bailey, C.G. (2006). "Advances in Fire Engineering Design of Steel Structures," *Structures and Buildings*, 159, 21-35.

Bailey, C. G., Burgess, I. W., and Plank, R. J. (1996). "Analyses of the Effects of Cooling and Fire Spread on Steel-framed Buildings," *Fire Safety Journal*, 26, 273-293.

Becker, R. (2002a). "Effects of Heat Sinks on Evolution of Longitudinal Temperature Distributions in Steel Structures," *Fire Safety Journal*, 37, 1-20.

Becker, R. (2002b). "Structural Behavior of Simple Steel Structures with Non-Uniform Longitudinal Temperature Distributions under Fire Conditions," *Fire Safety Journal*, 37, 495-515.

Beyler, C., Beitel, J., Iwankiw, N., and Lattimer, B. (2007). *Fire Resistance Testing for Performance-based Fire Design of Buildings*, The Fire Protection Research Foundation, Quincy, MA.

Buchanan, A. H. (2001). *Structural Design for Fire Safety*, John Wiley & Sons, England.

Bukowski, R. W. (2003). "Prediction of the Structural Fire Performance of Buildings," *Fire and Materials*, Interscience Communications Ltd., San Francisco, CA.

Burgess, I. W., El-Rimawi, J. A., and Plank, R. J. (1990). "Analysis of Beams with Non-Uniform Temperature Profile Due to Fire Exposure," *Journal of Constructional Steel Research*, 16, 169-192.

Cabrita Neves, I., Valente, J. C., and Correia Rodrigues, J. P. (2002). "Thermal Restraint and Fire Resistance of Columns," *Fire Safety Journal*, 37, 753-771.

Cadorin, J.-F., Pintea, D., Dotreppe, J.-C., and Franssen, J.-M. (2003). "A Tool to Design Steel Elements Submitted to Compartment Fires—OZone V2. Part 2: Methodology and Application," *Fire Safety Journal*, 38, 429-451.

Cai, J., Burgess, I.W., and Plank, R.J. (2002). "Modelling of Asymmetric Cross-Section Members for Fire Conditions," *Journal of Constructional Steel Research*, 58, 389-412.

Cai, J., Burgess, I., and Plank, R. (2003). "A Generalised Steel/Reinforced Concrete Beam-Columns Element Model for Fire Conditions," *Engineering Structures*, 25, 817-833.

Chan, S. L., and Chan, B. H. M. (2001). "Refined Plastic Hinge Analysis of Steel Frames under Fire," *Steel and Composite Structures*, 1, 111-130.

Cook, R. D., Malkus, D .S., and Plesha, M. E. (1989). *Concepts and Applications of Finite Element Analysis*, 3rd Ed., John Wiley and Sons, New York.

Cooke, G. M. E., and Latham, D. J. (1987). "The Inherent Fire Resistance of a Loaded Steel Framework," *Steel Construction Today*, 1, 49-58.

Crisfield, M. A. (1991). *Non-Linear Finite Element Analysis of Solids and Structures*, Vol. 1, Wiley, New York.

Culver, C. (1972). "Steel Column Buckling under Thermal Gradients," *Journal of the Structural Division*, 92, 1853–1865.

Di Capua, D., and Mari, A. R. (2007). "Nonlinear Analysis of Reinforced Concrete Cross-Sections Exposed to Fire," *Fire Safety Journal*, 42, 139-149.

El-Rimawi, J. A., Burgess, I. W., and Plank, R. J. (1995). "The Analysis of Semi-Rigid Frames in Fire—A Secant Approach," *Journal of Constructional Steel Research*, 33, 125-146.

El-Rimawi, J. A., Burgess, I. W., and Plank, R. J. (1996). "The Treatment of Strain Reversal in Structural Members during the Cooling Phase of a Fire," *Journal of Constructional Steel Research*, 37, 115-135.

EN 1991-2.2: Eurocode 1: Basis of Design and Actions on Structures, Part 2-2: Actions on Structures—Actions on Structures Exposed to Fire. (2005). British Standards Institution, London.

EN 1993-1.2: Eurocode 3: Design of Steel Structures, Part 1-2: General Rules—Structural Fire Design. (2005). British Standards Institution, London.

EN 1996-1.2: Eurocode 6: Design of Masonry Structures, Part 1-2: General Rules—Structural Fire Design. (2005). British Standards Institution, London.

Franssen, J.-M. (1990). "The Unloading of Building Materials Submitted to Fire," *Fire Safety Journal*, 16, 213-227.

Franssen, J.-M. (2005). "SAFIR: A Thermal/Structural Program for Modeling Structures under Fire," *Engineering Journal*, 42, 143-158.

Franssen, J.-M., Cajot, L.-G., and Schleich, J.-B. (1998). "Natural Fires in Large Compartments: Effects Caused on the Structure by Localized Fires in Large Compartments," *Proceedings of the Eurofire '98 Conference*, Belgium.

Franssen, J.-M., Cooke, G. M. E., and Latham, D. J. (1995). "Numerical Simulation of a Full Scale Fire Test on a Loaded Steel Framework," *Journal of Constructional Steel Research*, 35, 377-408.

Franssen, J.-M., Pintea, D., and Dotreppe, J.-C. (2007). "Considering the Effects of Localised Fires in the Numerical Analysis of a Building Structure," *Fire Safety Journal*, 42, 473-481.

Gewain, R. G., Iwankiw, N. R., and Alfawakhiri, F. (2003). *Facts for Steel Buildings: Fire*, American Institute of Steel Construction, United States.

Ghojel, J. I. (1998). "A New Approach to Modeling Heat Transfer in Compartment Fires," *Fire Safety Journal*, 31, 227-237.

Ghojel, J. I., and Wong, M. B. (2005). "Three-Sided Heating of I-Beams in Composite Construction Exposed to Fire." *Journal of Constructional Steel Research*, 61, 834-844.

Hamins, A., McGrattan, K., Prasad, K., Maranghides, A., and McAllister, T. (2005). "Experiments and Modeling of Unprotected Structural Steel Elements Exposed to a Fire," *Proceedings of the Eighth International Symposium on Fire Safety Science*, 189-200.

Hasemi, Y., et al. (1995). "Fire Safety of Building Components Exposed to a Localized Fire – Scope and Experiments on Ceiling/Beam System Exposed to a Localized Fire," *Proceedings of the First ASIAFLAM Conference*, Hong Kong.

Hozjan, T., Turk, G., and Srpcic, S. (2007). "Fire Analysis of Steel Frames with the Use of Artificial Neural Networks," *Journal of Constructional Steel Research*, 63, 1396-1403.

Huang, Z., Burgess, I. W., and Plank, R. J. (2000). "Three-Dimensional Analysis of Composite Steel-Framed Buildings in Fire," *Journal of Structural Engineering*, 126, 389-397.

Huang, Z. F., and Tan, K. H. (2003). "Analytical Fire Resistance of Axially Restrained Steel Columns," *Journal of Structural Engineering*, 129, 1531-1537.

IBC (2003). *International Building Code*, International Code Council, Falls Church, VA.

Incropera, F. P., and DeWitt, D. P. (2002). *Fundamentals of Heat and Mass Transfer*, 5th Ed., John Wiley and Sons, New York.

ISO (1999). "Fire-Resistance Tests – Elements of Building Construction," *International Standard 834*.

Iu, C. K., and Chan, S. L. (2004). "A Simulation-Based Large Deflection and Inelastic Analysis of Steel Frames under Fire," *Journal of Constructional Steel Research*, 60, 1495-1524.

Iu, C. K., Chan, S. L., and Zha, X. X. (2007). "Material Yielding by Both Axial and Bending Spring Stiffness at Elevated Temperature," *Journal of Constructional Steel Research*, 63, 677-685.

Izzuddin, B. A., Song, L., Elnashai, A. S., and Dowling, P. J. (2000). "An Integrated Adaptive Environment for Fire and Explosion Analysis of Steel Frames—Part II: Verification and Application," *Journal of Constructional Steel Research*, 53, 87-111.

Jaluria, Y., and Torrance, K. E. (2003). *Computational Heat Transfer*, 2nd Ed., Taylor and Francis, New York.

Jeffers, A. E., and Sotelino, E. D. (2009). "A Fiber Heat Transfer Element for Modeling the Thermal Response of Structures in Fire," to appear in the *Journal of Structural Engineering*.

Jiang, X. M., Chen, H., and Liew, J. Y. R. (2002). "Spread-of-Plasticity Analysis of Three-Dimensional Steel Frames," *Journal of Constructional Steel Research*, 58, 193-212.

Johann, M. A., Albano, L. D., Fitzgerald, R. W., and Meacham, B. J. (2006). "Performance-Based Structural Fire Safety," *Journal of Performance of Constructed Facilities*, 20, 45-53.

Kodur, V. K. R., and Dwaikat, M. (2008). "A Numerical Model for Predicting the Fire Resistance of Reinforced Concrete Beams," *Cement and Concrete Composites*, 30, 431-443.

Kruppa, J. (1981/82). "Some Results on the Fire Behaviour of External Steel Columns," *Fire Safety Journal*, 4, 247-257.

Kythe, P.K., and Schäferkotter, M.R. (2005). *Handbook of Computational Methods for Integration*, Chapman and Hall/CRC Press, Boca Raton, Florida.

Lamont, S., Usmani, A. S., and Gillie, M. (2004). "Behavior of a Small Composite Steel Frame Structure in a 'Long-Cool' and a 'Short-Hot' Fire," *Fire Safety Journal*, 39, 327-357.

Landesmann, A., de M. Batista, E., and Drummond, Alves, J. L. (2005). "Implementation of Advanced Analysis Method for Steel-Framed Structures under Fire Conditions," *Fire Safety Journal*, 40, 339-366.

Liew, J. Y. R., and Chen, H. (2004). "Explosion and Fire Analysis of Steel Frames Using Fiber Element Approach," *Journal of Structural Engineering*, 130, 991-1000.

Liew, J. Y. R., Tang, L. K., and Choo, Y. S. (2002). "Advanced Analysis for Performance-Based Design of Steel Structures Exposed to Fires," *Journal of Structural Engineering*, 128, 1584-1593.

Liew, J. Y. R., Tang, L. K., Holmaas, T., and Choo, Y. S. (1998). "Advanced Analysis for the Assessment of Steel Frames in Fire," *Journal of Constructional Steel Research*, 47, 19-45.

Liu, T. C. H. (1996). "Finite Element Modelling of Behaviours of Steel Beams and Connections in Fire," *Journal of Constructional Steel Research*, 36, 181-199.

Magnusson, S. E., and Thelandersson, S. (1970). "Temperature-Time Curves of Complete Process of Fire Development," *Acta Polytechnica Scandinavica*, Civil Engineering and Building Construction Series, 65.

McGuire, W., Gallagher, R.H., and Ziemian, R.D. (2000). *Matrix Structural Analysis*, 2nd Ed., John Wiley and Sons, New York.

Meacham, B. J. (1998). "Assessment of the Technological Requirements for the Realization of Performance-based Fire Safety Design in the United States-Phase 1: Fundamental Requirements," *Second International Conference on Fire Research and Engineering*, Society of Fire Protection Engineers, Gaithersburg, MD.

Milke, J. A. (1999). "Analytical Methods to Evaluate Fire Resistance of Structural Members," *Journal of Structural Engineering*, 125, 1179-1187.

Myllymaki, J., and M. Kokkala (2000). “Thermal Exposure to a High Welded I-Beam above a Pool Fire,” *First International Workshop on Structures in Fires*, Copenhagen.

Najjar, S. R., and Burgess, I. W. (1996). “A Nonlinear Analysis for Three-Dimensional Steel Frames in Fire Conditions,” *Engineering Structures*, 18, 77-89.

National Institute of Standards and Technology (NIST) (1999). “NIST FASTData Fire Test Database,” *NIST Standard Reference Database 75*, CD-ROM, Jan. 1999 Release, Gaithersburg, MD.

Neuenhofer, A., and Filippou, F. C. (1997). “Evaluation of Nonlinear Frame Finite-Element Model,” *Journal of Structural Engineering*, 123, 958-966.

Neuenhofer, A., and Filippou, F. C. (1998). “Geometrically Nonlinear Flexibility-Based Frame Finite Element,” *Journal of Structural Engineering*, 124, 704-711.

Newman, G. (1999). “The Cardington Fire Tests,” *Proceedings of the North American Steel Construction Conference*, American Institute of Steel Construction, New Orleans, LA.

Nukala, P. K., and White, D. (2004). “A Mixed Element Formulation for Three-Dimensional Nonlinear Analysis of Steel Frames,” *Computer Methods in Applied Mechanics and Engineering*, 193, 2507-2545.

Ossenbruggen, P., Aggarwal, V., and Culver, C. (1973). “Steel Column Failure under Thermal Gradients by Member,” *Journal of the Structural Division*, 99, 727-739.

Petrangeli, M., and Ciampi, V. (1997). “Equilibrium Based Iterative Solutions for the Non-Linear Beam Problem,” *International Journal for Numerical Methods in Engineering*, 40, 423–437.

Poh, K. W., and Bennetts, I. D. (1995). “Behavior of Steel Columns at Elevated Temperatures,” *Journal of Structural Engineering*, 121, 676-684.

Prasad, K., and Baum, H. R. (2005). “Coupled Fire Dynamics and Thermal Response of Complex Building Structures,” *Proceedings of the Combustion Institute*, 30, 2255-2262.

Rubert, A. (1984). Experimentelle Untersuchungen zum Brandverhalten kompletter, ebener Rahmensysteme aus Baustahl, *Forschungsbericht zur Teilaktivität 3.2 des Vorhabens Bau 6004/P86, Teil I (Bericht), Teil II (Dokumentation)*, Studiengesellschaft für Anwendungstechnik von Eisen und Stahl e.V., Düsseldorf, durchgeführt im Krupp Forschungsinstitut, Essen.

Rubert, A., and Schaumann, P. (1985). Tragverhalten stählerner Rahmensysteme bei Brandbeanspruchung, *Stahlbau*, 54, 280-287.

Rubert, A., and Schaumann, P. (1986). “Structural Steel and Plane Frame Assemblies under Fire Action,” *Fire Safety Journal*, 10, 173-184.

Saab, H. A., and Nethercot, D. A. (1991). “Modelling Steel Frame Behaviour under Fire Conditions,” *Engineering Structures*, 13, 371-382.

SFPE (2004). *The SFPE Task Group on Fire Exposure to Structural Elements*, Society of Fire Protection Engineers, USA.

Song, L., Izzuddin, B. A., Elnashai, A. S., and Dowling, P. J. (2000). “An Integrated Adaptive Environment for Fire and Explosion Analysis of Steel Frames—Part I: Analytical Models,” *Journal of Constructional Steel Research*, 53, 63-85.

Souza Junior, V., and Creus, G. J. (2007). “Simplified Elastoplastic Analysis of General Frames on Fire,” *Engineering Structures*, 29, 511-518.

Spacone, E., Ciampi, V., and Filippou, F. C. (1996). “Mixed Formulation of Nonlinear Beam Finite Element,” *Computers and Structures*, 58, 71-83.

Staggs, J. E. J., and Phylaktou, H. N. (2008). “The Effects of Emissivity on the Performance of Steel in Furnace Tests,” *Fire Safety Journal*, 43, 1-10.

Tan, K. H., Ting, S. K., and Huang, Z. F. (2002). “Visco-Elasto-Plastic Analysis of Steel Frames in Fire,” *Journal of Structural Engineering*, 128, 105-114.

Tan, K. H., and Yuan, W. F. (2008). “Buckling of Elastically Restrained Steel Columns under Longitudinal Non-Uniform Temperature Distribution,” *Journal of Constructional Steel Research*, 64, 51-61.

Taucer, F.F., Spacone, E., and Fillipou, F.C. (1991). “A Fiber Beam-Column Element for Seismic Response Analysis of Reinforced Concrete Structures,” Report No. UCB/EERC-91/17, University of California, Berkeley.

Thompson, B. P., and Bank, L. C. (2007). “Risk Perception in Performance-Based Building Design and Applications to Terrorism-Resistant Design.” *Journal of Performance of Constructed Facilities*, 21, 61-69.

Toh, W. S., Fung, T. C., and Tan, K. H. (2001). “Fire Resistance of Steel Frames Using Classical and Numerical Methods,” *Journal of Structural Engineering*, 127, 829-838.

Wald, F., Simoes da Silva, L., Moore, D. B., Lennon, T., Chladna, M., Santiago, A., Benes, M., and Borges, L. (2006). “Experimental Behaviour of a Steel Structure under Natural Fire,” *Fire Safety Journal*, 41, 509-522.

Wainman, D. E., and Kirby, B. R. (1988). *Compendium of UK Standard Fire Test Data: Unprotected Structural Steel - 1*, Report No. RS/RSC/S10328/1/87/B, British Steel Corporation, England.

Wainman, D. E., and Kirby, B. R. (1989). *Compendium of UK Standard Fire Test Data: Unprotected Structural Steel - 2*, Report No. RS/RSC/S10328/1/87/B, British Steel Corporation, England.

Wakamatsu, T., Hasemi, Y., Yokobayashi, Y., and Ptchelintsev, A. V. (1996). "Experimental Study on the Heating Mechanism of a Steel Beam under Ceiling Exposed to a Localized Fire," *Proceedings from INTERFLAM '96*, Interscience, 509-518.

Wang, P., Guoqiang, L., and Guo, S. (2008). "Effects of the Cooling Phase of a Fire on Steel Structures," *Fire Safety Journal*, 43, 451-458.

Witteveen, J., and Twilt, L. (1981/82). "A Critical View on the Results of Standard Fire Resistance Tests on Steel Columns," *Fire Safety Journal*, 4, 259-270.

Wong, M. B. (2001a). "Elastic and Plastic Methods for Numerical Modelling of Steel Structures Subject to Fire," *Journal of Constructional Steel Research*, 57, 1-14.

Wong, M. B. (2001b). "Plastic Frame Analysis under Fire Conditions," *Journal of Structural Engineering*, 127, 290-295.